



The
University
Of
Sheffield.

**NON-LINEAR SYSTEM IDENTIFICATION AND CONTROL
OF SOLVENT-BASED POST-COMBUSTION CO₂ CAPTURE
PROCESS**

By:

Toluleke E Akinola

Supervisor: Prof Meihong Wang

A thesis submitted in partial fulfilment of the requirement for the degree of
Doctor of Philosophy

Department of Chemical and Biological Engineering
Faculty of Engineering
The University of Sheffield

September 2019

Acknowledgement

I will like to express my tremendous gratitude to Professor Meihong Wang, my research supervisor, for his guidance, patience, motivational role and contribution to the successful completion of my thesis. Also, I would like to say a big thank you to Dr Eni Oko, my second supervisor, for his massive support, critical and insightful comments on my research work and also putting the drive to always put out the best quality of research work. Special thanks to the various collaborators, Dr Hualiang Wei and Dr Yuanlin Gu for your contributions toward the published Journal paper.

I would like to appreciate my friends and colleagues in the Process & Energy Systems Engineering Group, both at the University of Sheffield and University of Hull. I cherished the discussions, which provided various avenues to develop my critical thinking and problem-solving skills.

To everyone at Shekinah Glory E-group fellowship, I am grateful for the friendship, companionship, care and prayers throughout the period of my study. I cherish every single one of you.

Finally, I will like to give a special thanks to my family. My parents, Mr and Mrs Akinola for their continual support and belief in me. I really appreciate the love and by his grace, you all shall live to enjoy the fruits of all the labour on me. Special shout out to my siblings Ibukun, Seyi, Pelumi and Favour for their support from Nigeria throughout my stay

Financial support from EU FP7 Marie Curie International Research Staff Exchange Scheme (IRSES) for me to visit Tsinghua University, China in 2017 is gratefully acknowledged.

Abstract

Solvent-based post-combustion capture (PCC) is a well-developed technology for CO₂ capture from power plants and industry. A reliable model that captures the dynamics of the solvent-based capture process is essential to implement suitable control system design. Typically, first principles models are used, however, they usually require comprehensive knowledge and in-depth understanding of the process. In addition, the high computational time required and high complexity of the first principles models makes it unsuitable for control system design implementation. This thesis is aimed at the development of a reliable dynamic model via system identification technique as well as a suitable process control strategy for the solvent-based post-combustion CO₂ capture process.

The nonlinear autoregressive with exogenous (NARX) inputs model is employed to represent the relationship between the input variables and output variables as two multiple-input single-output (MISO) sub-systems. The forward regression with orthogonal least squares (FROLS) algorithm is implemented to select an accurate model structure that best describes the dynamics within the process. The prediction performance of the identified NARX models is promising and shows that the models capture the underlying dynamics of the CO₂ capture process.

The model obtained was adopted for various process control system design of the solvent-based PCC process (conventional PI, MPC, and NMPC). For the conventional PI controller design, multivariable control analysis was carried out to determine a suitable control structure. Control performance evaluation of the control schemes reveals that the NMPC scheme was suitable to control the solvent-based PCC process

at flexible operations. Findings obtained from the thesis underlines the advancement in dynamic modelling and control implementation of solvent-based PCC process.

Keywords: *Solvent-based post-combustion capture; chemical absorption; System Identification; NARX; FROLS-ERR, control structure configuration, conventional PI, MPC, NMPC*

Peer-reviewed Publications and Presentations

Part of this thesis has been published in the peer-reviewed journal:

- **Akinola, T. E.**, Oko, E., Gu, Y., Wei, H.-L., & Wang, M. (2019). Non-linear system identification of solvent-based post-combustion CO₂ capture process. *Fuel*, 239, 1213–1223.

The author contributed to the publication of the Journal paper:

- **Akinola, T. E.**, Oko, E., & Wang, M. (2019). Study of CO₂ removal in natural gas process using mixture of ionic liquid and MEA through process simulation. *Fuel*, 236, 135–146.

The author also contributed to the conference proceedings:

- Oko, E., **Akinola, T. E.**, Cheng, C.-H., Wang, M., Chen, J., & Ramshaw, C. (2019). Experimental study of CO₂ solubility in high concentration MEA solution for intensified solvent-based carbon capture. In *MATEC Web of Conferences* (Vol. 272, p. 1004). EDP Sciences.

Conference Presentation:

- **Akinola, T. E.**, Oko, E., & Wang, M. (2017). Study of CO₂ removal in natural gas process using mixture of ionic liquid and MEA through process simulation. *15th International Conference on Carbon Dioxide Utilization (ICCDU XV)*, Shanghai Tech University, Shanghai, China, 17th-21st, July 2017
- **Akinola, T. E.**, Oko, E., Gu, Y., Wei, H.-L., & Wang, M. (2018). Non-linear system identification of solvent-based post-combustion CO₂ capture process. *Postgraduate Research Conference*. The University of Sheffield, Sheffield, United Kingdom, 6, June 2017

Table of Contents

| | |
|---|-------|
| Acknowledgement | i |
| Abstract | ii |
| Peer-reviewed Publications and Presentations | iv |
| Table of Contents | v |
| List of Figures | xi |
| List of Tables | xv |
| Nomenclatures | xviii |
| Abbreviations | xx |
| 1 Introduction | 1 |
| 1.1 Background..... | 1 |
| 1.1.1 Energy Demand, Climate change and CCUS..... | 1 |
| 1.1.2 Post-combustion CO ₂ capture process..... | 4 |
| 1.1.2.1 Adsorption..... | 5 |
| 1.1.2.2 Cryogenic separation | 6 |
| 1.1.2.3 Membrane separation | 6 |
| 1.1.2.4 Physical Absorption..... | 7 |
| 1.1.2.5 Chemical Absorption..... | 7 |
| 1.2 Motivations for this study | 10 |
| 1.3 Aim and Objectives of this study..... | 11 |
| 1.4 Novel Contribution of the Thesis | 12 |
| 1.5 Scope of this study..... | 13 |
| 1.6 Research methodology and tools used for the study | 14 |

| | | |
|-----------|---|----|
| 1.6.1 | Research methodology..... | 14 |
| 1.6.2 | Software tools used for the study | 14 |
| 1.6.2.1 | gPROMS® | 14 |
| 1.6.2.2 | Matlab® Toolbox/ Simulink® | 15 |
| 1.7 | Outline of the Thesis | 15 |
| 2 | Literature review..... | 17 |
| 2.1 | Introduction | 17 |
| 2.2 | Review of Pilot plants and commercially deployed plants..... | 17 |
| 2.2.1 | Review of solvent-based post-combustion CO ₂ capture pilot plants..... | 17 |
| 2.2.2 | Commercial deployment of solvent-based PCC plant | 20 |
| 2.2.3 | Summary | 21 |
| 2.3 | Model Development of the solvent-based post-combustion CO ₂ capture process..... | 22 |
| 2.3.1 | First principles modelling approach | 22 |
| 2.3.1.1 | Current status on steady-state modelling of post-combustion capture plant..... | 24 |
| 2.3.1.2 | Current status of dynamic modelling of solvent-based post-combustion capture plant | 26 |
| 2.3.2 | Data-driven modelling approach- System identification (SI) | 30 |
| 2.3.2.1 | Linear SI..... | 31 |
| 2.3.2.2 | Nonlinear SI | 32 |
| 2.3.2.2.1 | NARMAX | 33 |

| | | |
|-------------|---|----|
| 2.3.2.2.1.1 | Multiple-input multiple-output (MIMO) system | 35 |
| 2.3.2.2.1.2 | NARMAX SI Approach | 36 |
| 2.3.2.3 | Current status on SI of PCC process plant | 42 |
| 2.3.3 | Summary | 45 |
| 2.4 | Process Control System Design for PCC Plant: Multivariable System..... | 46 |
| 2.4.1 | Control structure configuration..... | 48 |
| 2.4.1.1 | Mathematical oriented approach | 48 |
| 2.4.1.1.1 | Niederlinski Index (NI) and Morari Index of Integral controllability (MIC) | 48 |
| 2.4.1.2 | Process Oriented approach | 49 |
| 2.4.2 | Type of Control | 49 |
| 2.4.2.1 | Traditional PID control..... | 49 |
| 2.4.2.2 | Model Predictive Control | 50 |
| 2.4.3 | Current Status on Control system design on solvent-based PCC process..... | 51 |
| 2.5 | Summary..... | 55 |
| 3 | Non-linear SI of solvent-based post-combustion CO ₂ capture process..... | 58 |
| 3.1 | Introduction | 58 |
| 3.2 | The first principles dynamic model for solvent-based PCC process | 59 |
| 3.3 | Process data acquisition | 60 |
| 3.3.1 | Selection of Input and Output Variables | 60 |

| | | |
|-------|---|----|
| 3.3.2 | Input signal design and Data Collection | 62 |
| 3.4 | SI | 65 |
| 3.4.1 | NARX SI using FROLS..... | 65 |
| 3.4.2 | Model term candidate development..... | 67 |
| 3.5 | Performance Evaluation..... | 68 |
| 3.5.1 | Sub-model 1 | 68 |
| 3.5.2 | Sub-model 2 | 75 |
| 3.5.3 | Statistical Analysis..... | 80 |
| 3.6 | Process dynamics analysis | 81 |
| 3.6.1 | Increase in flue gas flowrate to the absorption column..... | 81 |
| 3.6.2 | Increase in lean solvent (MEA) flow rate | 82 |
| 3.6.3 | Increase in steam flowrate to the reboiler | 84 |
| 3.7 | Summary..... | 85 |
| 4 | Multivariable PI control Design on the solvent-based post-combustion CO ₂ capture process..... | 86 |
| 4.1 | Introduction | 86 |
| 4.2 | State-space realisation of the solvent-based PCC model | 86 |
| 4.2.1 | Model Reduction..... | 88 |
| 4.2.2 | Classical state-space realisation | 93 |
| 4.3 | Multivariable Control structure design and analysis | 95 |
| 4.3.1 | RGA analysis..... | 96 |

| | | |
|---------|--|-----|
| 4.3.2 | Process-oriented approach..... | 98 |
| 4.4 | Controller design..... | 100 |
| 4.5 | Decentralised Control Performance Evaluation | 100 |
| 4.5.1 | Disturbance rejection (scenario 1) | 102 |
| 4.5.2 | Set-point tracking (Scenarios 2 &3) | 104 |
| 4.5.2.1 | Scenario 2 | 104 |
| 4.5.2.2 | Scenario 3..... | 105 |
| 4.6 | Summary..... | 106 |
| 5 | Linear model predictive control design and implementation on the solvent-based PCC process | 108 |
| 5.1 | Introduction | 108 |
| 5.2 | Model Linearization | 109 |
| 5.3 | Multivariable MPC Control scheme design | 111 |
| 5.3.1 | MPC tuning design and Implementation | 112 |
| 5.4 | Performance Evaluation..... | 115 |
| 5.4.1 | Scenario 1 | 117 |
| 5.4.2 | Scenario 2 | 118 |
| 5.4.3 | Scenario 3 | 120 |
| 5.5 | Summary..... | 123 |
| 6 | Nonlinear model predictive control design for the solvent-based PCC process..... | 124 |
| 6.1 | Introduction | 124 |

| | | |
|-------|---|-----|
| 6.2 | Nonlinear model predictive control (NMPC) formulation | 125 |
| 6.3 | Performance Evaluation..... | 129 |
| 6.3.1 | Scenario 1 | 129 |
| 6.3.2 | Scenario 2 | 132 |
| 6.4 | Summary..... | 135 |
| 7 | Conclusion and Recommendation | 136 |
| 7.1 | Conclusion | 136 |
| 7.1.1 | Nonlinear SI of the solvent-based PCC process..... | 137 |
| 7.1.2 | Multivariable conventional PI control scheme | 137 |
| 7.1.3 | MPC scheme | 138 |
| 7.1.4 | NMPC scheme | 138 |
| 7.2 | Recommendation for future study | 139 |
| | References..... | 141 |

List of Figures

| | |
|--|----|
| Figure 1-1 World electricity consumption by various countries from 2000 -2018 (Enerdata, 2019) | 1 |
| Figure 1-2 World CO ₂ emission from fuel combustion by sectors in 2016 (Coent, 2017). Note: this shows allocation of electricity and heat end-use sectors..... | 2 |
| Figure 1-3 Global average atmospheric CO ₂ from 1994-2019 (Lindsey, 2019)..... | 3 |
| Figure 1-4 technology options to reduce CO ₂ emission in power generation (Huaman & Jun, 2014)..... | 4 |
| Figure 1-5 Schematic diagram of a power plant with post-combustion CO ₂ capture (Wang <i>et al.</i> , 2017)..... | 5 |
| Figure 1-6 Process flow diagram of the chemical absorption plant (Lawal <i>et al.</i> , 2010) | 9 |
| Figure 1-7 scope of the study..... | 13 |
| Figure 1-8 Overview of Research methodology (in the Figure, 'DM' refers to 'Dynamic Modelling'; 'SI' refers to 'system identification'; 'CD' refers to-control design..... | 14 |
| Figure 2-1 Representation of the level of complexity when modelling solvent-based PCC (Lawal <i>et al.</i> , 2009) | 24 |
| Figure 2-2 SI approach (Solomatine & Ostfeld, 2008)..... | 31 |
| Figure 2-3 Control Hierarchy system in a chemical plant (Skogestad, 2004) | 47 |
| Figure 3-1 Multiple Input Single Output MEA based PCC Model | 62 |
| Figure 3-2 Input-output data obtained from an MEA-based PCC model developed in gPROMS; CO ₂ -CL: CO ₂ Capture level; T _{reb} : reboiler temperature | 64 |

Figure 3-3 Power spectrum distribution across frequency range on each input variable 65

Figure 3-4 Comparison of the model predictions (OSA and MSP(10)) and measurements over the test data for sub-model 1 using M1u. Note: MSP(10) indicates 10-step ahead prediction..... 71

Figure 3-5 Comparison of the model predictions (OSA and MSP) and measurements over the test data for sub-model 1 using M11. Note: MSP(10) indicates 10-step ahead prediction..... 72

Figure 3-6 Comparison of the model predictions (OSA and MSP) and measurements over the test data for sub-model 1 using M0u. Note: MSP(10) indicates 10-step ahead prediction..... 73

Figure 3-7 Comparison of the model predictions (OSA and MSP) and measurements over the test data for sub-model 1 using M01. Note: MSP(10) indicates 10-step ahead prediction..... 74

Figure 3-8 Comparison of the model predictions (OSA and MSP) and measurements over the test data for sub-model 2 using M1u. Note: MSP(10) indicates 10-step ahead prediction..... 76

Figure 3-9 Comparison of the model predictions (OSA and MSP) and measurements over the test data for sub-model 2 using M11. Note: MSP(10) indicates 10-step ahead prediction..... 77

Figure 3-10 Comparison of the model predictions (OSA and MSP) and measurements over the test data for sub-model 2 using M0u. Note: MSP(10) indicates 10-step ahead prediction..... 78

| | |
|--|-----|
| Figure 3-11 Comparison of the model predictions (OSA and MSP) and measurements over the test data for sub-model 2 using M01. Note: MSP(10) indicates 10-step ahead prediction..... | 79 |
| Figure 3-12 Output response to flue gas flowrate (kg/s) increase to the absorber: gPROMS model | 82 |
| Figure 3-13 Output responses to a 10% step increase of lean solvent (MEA) flowrate (kg/s) to the absorber | 83 |
| Figure 3-14 Output responses to a 10% step increase in steam flowrate (kg/s) | 84 |
| Figure 4-1 Output responses to step-change implemented on each input variable: for each input variables a step change of +10% was introduced one at a time. | 95 |
| Figure 4-2 Solvent-based PCC model on Simlink® environment..... | 99 |
| Figure 4-3 Design and implementation of PI controller on the PCC model; FGF-flue gas flowrate ; LSF- lean solvent flowrate; SF- steam flowrate; CO ₂ -CL – CO ₂ capture level ; T _{reb} – Reboiler temperature..... | 101 |
| Figure 4-4 Close-loop capture model response, to a 10% step change in flue gas flowrate..... | 103 |
| Figure 4-5 Closed-loop output responses to an increase in CO ₂ -CL (%) | 105 |
| Figure 4-6 Closed-loop output responses to an increase in reboiler temperature (T _{reb}) | 106 |
| Figure 5-1 Step response plot of the discrete linear state-space model..... | 110 |
| Figure 5-2 Implementation of MPC control strategy on the solvent-based PCC (identified) model; FGF-flue gas flowrate ; LSF- lean solvent flowrate; SF- steam | |

| | |
|---|-----|
| flowrate; CO ₂ -CL – CO ₂ capture level ; T _{reb} – Reboiler temperature; DV- disturbance variables; MV-manipulated variables; CV-controlled variables..... | 113 |
| Figure 5-3 Closed-loop performance to a 20% ramp change in flue gas flowrate for 3hr (10800s). LMPC – linear model predictive control; conv PI – conventional PI control; SP – set point; DV – disturbance variable | 116 |
| Figure 5-4 Closed-loop performance to a decrease in CO ₂ -CL for 3hr (10800s). LMPC – linear model predictive control; conv PI – conventional PI control; SP – set point; DV – disturbance variable | 119 |
| Figure 5-5 Closed-loop performance to a variation in CO ₂ -CL for 24hr (86400s). LMPC – linear model predictive control; conv PI – conventional PI control; SP – set point; DV – disturbance variable | 122 |
| Figure 6-1 Schematic diagram of NMPC scheme on the solvent-based PCC model; FGF-flue gas flowrate ; LSF- lean solvent flowrate; SF- steam flowrate; CO ₂ -CL – CO ₂ capture level ; T _{reb} – Reboiler temperature; DV- disturbance variables; MV-manipulated variables; CV-controlled variables. | 127 |
| Figure 6-2 Closed-loop performance to a variation in flue gas flowrate for 24hr (86400s). LMPC – linear model predictive control; conv PI – conventional PI control; NMPC – nonlinear MPC; SP – set point; DV – disturbance variable | 130 |
| Figure 6-3 NMPC closed-loop performance to a variation in CO ₂ -CL and flue gas flowrate for 24hr (86400s). LMPC – linear model predictive control; conv PI – conventional PI control; NMPC – nonlinear MPC; SP – set point; DV – disturbance variable..... | 134 |

List of Tables

| | |
|---|----|
| Table 2-1 Summary of operational solvent-based PCC Pilot plant integrated into a power plant..... | 19 |
| Table 2-2 Specifications of both Boundary Dam and Petra Nova CCS project (Mantripragada <i>et al.</i> , 2019) | 20 |
| Table 3-1 CF and PIPS for each input variable | 63 |
| Table 3-2 Identified model (M1 _u) structures from D1 _u for sub-model 1 using FROLS algorithm | 70 |
| Table 3-3 Identified model (M11) structures from D11 for sub-model 1 using FROLS algorithm | 71 |
| Table 3-4 Identified model (M0 _u) structures from D0 _u for sub-model 1 using FROLS algorithm | 72 |
| Table 3-5 Identified model (M01) structures from D01 for sub-model 1 using FROLS algorithm | 74 |
| Table 3-6 VAF (and PE) for the Identified sub-model 1 (OSA and MSP) | 75 |
| Table 3-7 Identified model (M1 _u) structures from D1 _u for sub-model 2 using FROLS algorithm | 75 |
| Table 3-8 Identified model (M11) structures from D11 for sub-model 2 using FROLS algorithm | 76 |
| Table 3-9 Identified model (M0 _u) structures from D0 _u for sub-model 2 using FROLS algorithm | 77 |

| | |
|---|-----|
| Table 3-10 Identified model (M01) structures from D01 for sub-model 2 using FROLS algorithm | 78 |
| Table 3-11 VAF (and PE) for the Identified sub-model 1 (OSA and MSP) | 79 |
| Table 3-12 Statistical performance of the Identified NARX model..... | 81 |
| Table 4-1 re-evaluated parameters for the observable i/o map representation of CO ₂ capture model | 93 |
| Table 4-2 RGA at different steady-state condition; FGF: flue gas flowrate; LSF: lean solvent flowrate; SF: steam flowrate | 97 |
| Table 4-3 NI and MIC values for the RGA pairings; SSC-steady state condition | 98 |
| Table 4-4 Conventional PI Control Parameters for each loop pairing | 100 |
| Table 4-5 Performance evaluation of the conventional PI control scheme..... | 104 |
| Table 5-1 Linearization operating point | 109 |
| Table 5-2 Nominal operating condition..... | 114 |
| Table 5-3 Process constraints..... | 114 |
| Table 5-4 MPC control scheme-tuning parameters..... | 115 |
| Table 5-5 summary of the closed-loop control performance evaluation for control schemes (MPC vs PI)..... | 118 |
| Table 5-6 sum of squared deviation of MVs for each control scheme (MPC vs PI).. | 120 |
| Table 6-1 Nominal operating condition..... | 128 |
| Table 6-2 Process constraints..... | 128 |
| Table 6-3 NMPC formulation parameters..... | 129 |

Table 6-4 Summary of the closed-loop control performance evaluation for control schemes (NMPC vs MPC vs PI) 132

Nomenclatures

| | |
|------------|--|
| D | Dictionary |
| $e(t)$ | Noise sequence |
| $f(\cdot)$ | Nonlinear function |
| F | Mass flowrate (kg/s) |
| K_c | Proportional gain |
| N | Number of samples in a training data set |
| n | Effective number of model terms |
| n_{CO_2} | Mass fraction of CO ₂ in the flue gas |
| n_e | Maximum lag for the system noise |
| n_u | Maximum lag for the system input |
| n_y | Maximum lag for the system output |
| Q_r | Reboiler duty (MJ) |
| r | Number of input variables |
| RE | Regeneration energy (MJ/kg_{CO_2}) |
| s | Number of output variables |
| SSE | sum of squares error |
| SST | The total sum of squares |
| $u(t)$ | System input |
| u_1 | Flue gas flowrate (measured input) (kg/s) |

| | |
|----------------------------|--|
| u_2 | Lean MEA flowrate (measured input) (kg/s) |
| u_3 | steam flowrate (measured input) (kg/s) |
| VAF | Model prediction efficiency (%) |
| $x_{sj}(t)$ | Regressors vector |
| $y(t)$ | System output |
| $y_{measure}$ | Measured output |
| $y_{predict}$ | Model prediction output |
| $y_s(t)$ | Response signal (output) |
| y_1 | CO ₂ Capture level |
| y_2 | Reboiler temperature |
| Greek letter | |
| Φ | Parameter vector |
| φ_{sj} | Parameter Estimate |
| ξ | Modelling error vector |
| $\lambda_{G_p^+}(0)$ | Vector of the eigenvalues |
| τ_I | Integral time constant |
| τ_D | Derivative time constant |
| Superscript | |
| ABS_{in} | Absorber inlet |
| ABS_{out} | Absorber outlet |
| Subscript | |
| FG | Flue gas |
| $CO_2_regen_vap_outlet$ | CO ₂ mass flowrate at the regenerator vapour outlet |

Abbreviations

| | |
|-----------------|---|
| APC | Advanced process control |
| AR | Auto-regressive |
| ARX | Auto-regressive with exogenous input |
| ARMAX | Auto-regressive moving average with exogenous input |
| BIC | Bayesian information criterion |
| CAP | Chilled ammonia process |
| CCS | Carbon Capture and Storage |
| CCUS | Carbon capture, utilisation and storage |
| CERTs | Carbon emission reduction targets |
| CL | capture level |
| CO ₂ | Carbon dioxide |
| DEA | Diethanolamine |
| E-NRTL | Electrolyte Non-Random Two Liquids |
| EOR | Enhanced oil recovery |
| ERR | Error reduction ratio |
| ESA | Electrical swing adsorption |
| FGD | Flue Gas Desulphurization |
| FOPDT | First order plus dead time |
| FROLS | Forward regression orthogonal least square |
| GBN | Generalized binary noise |

| | |
|--------|---|
| IEA | International Energy Agency |
| IP | Intermediate pressure |
| ITC | International Test Centre |
| LP | Low pressure |
| MDEA | Methyldiethanolamine |
| MEA | Monoethanolamine |
| MIMO | Multiple input multiple output |
| MISO | Multiple input single output |
| MOFs | Meta-organic frameworks |
| MPC | Model predictive control |
| MSP | multi-step prediction output |
| NARMAX | Nonlinear auto-regressive moving average with exogenous |
| NARX | Non-linear auto-regressive with exogenous input |
| NGCC | Natural gas combined cycle |
| NMPC | Nonlinear model predictive control |
| OLS | Orthogonal least squares |
| OSA | One-step ahead |
| PCC | Post-combustion capture |
| PE | Prediction efficiency |
| PID | Proportional Integral Derivative |

| | |
|------|--------------------------------------|
| PRBS | Pseudo random binary sequence |
| PSA | Pressure swing adsorption |
| PZ | Piperazine |
| RBF | Radial basis function |
| R&D | Research and development |
| RGA | Relative gain array |
| SAFT | Statistical Association Fluid Theory |
| SCR | Selective Catalytic Reduction |
| SRP | Separation Research Program |
| SI | System identification |
| SISO | Single-input single-output |
| SNCR | Selective Non-Catalytic Reduction |
| SSE | Sum of squares error |
| SST | Total sum of squares |
| TSA | Temperature swing adsorption |
| VLE | Vapour-liquid equilibrium |

1 Introduction

This chapter introduces the study on the system identification and process control of the solvent-based post-combustion CO₂ capture process. Sections 1.1 and 1.2 describe the background and motivation of the study. Section 1.3 presents the aim and objectives of this thesis. The novel contributions, scope of study and research methodology are detailed in Sections 1.4, 1.5 and 1.6 respectively. Section 1.7 presents the outline of the thesis.

1.1 Background

1.1.1 Energy Demand, Climate change and CCUS

The increased world population and economic activities around the world have led to an increased global energy demand. This has resulted in increased electricity consumed in 2018 as shown in Figure 1-1. Although, renewable energy is predicted to become dominant in global energy mix (Mac Dowell & Staffell, 2015), fossil fuels still contributes the largest share in meeting global energy demands.

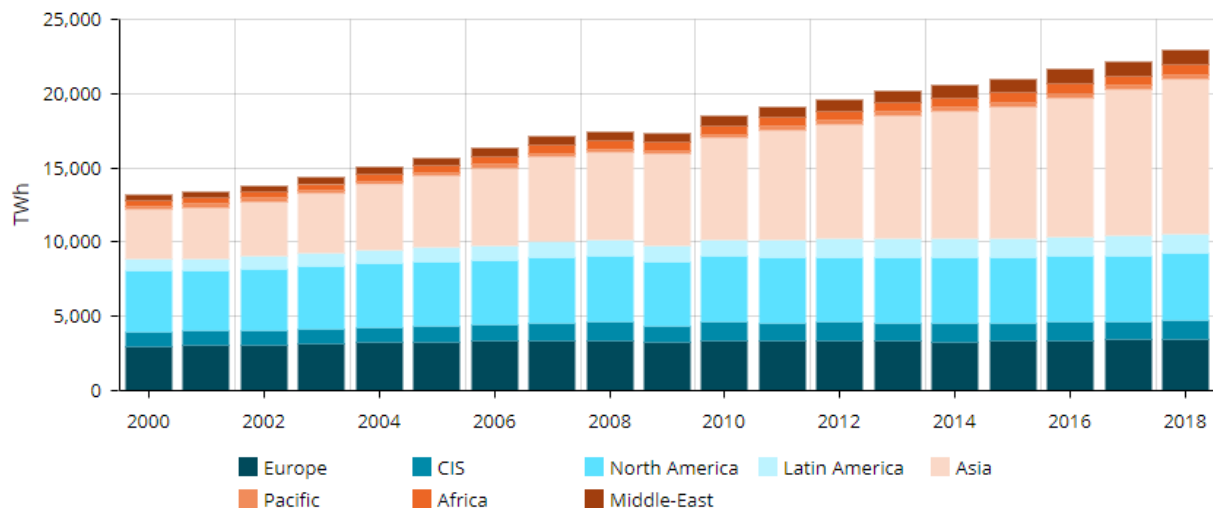


Figure 1-1 World electricity consumption by various countries from 2000 -2018 (Enerdata, 2019)

Fossil fuel combustion for electricity and heat generation is the biggest culprit for anthropogenic CO₂ emission (Figure 1-2) which is regarded as a major contributor to global warming (Lawal *et al.*, 2010; Huaman & Jun, 2014; Coent, 2017). Atmospheric CO₂ levels, which stands currently at about 407.4ppm, could reach catastrophic level by 2100 if present trends in emission continues unabated as shown in Figure 1-3 (Lindsey, 2019). The consequences could range from rise in global average temperature to a series of severe impact on agriculture, water security and sea level (Huaman & Jun, 2014).

There is now a global commitment to reduce CO₂ emission. At the COP21 in 2015, 196 countries historically agreed to support role out of CO₂ abatement technologies to keep global temperature rise below 2°C above pre-industrial levels and to pursue efforts to limit the temperature rise further to 1.5°C.

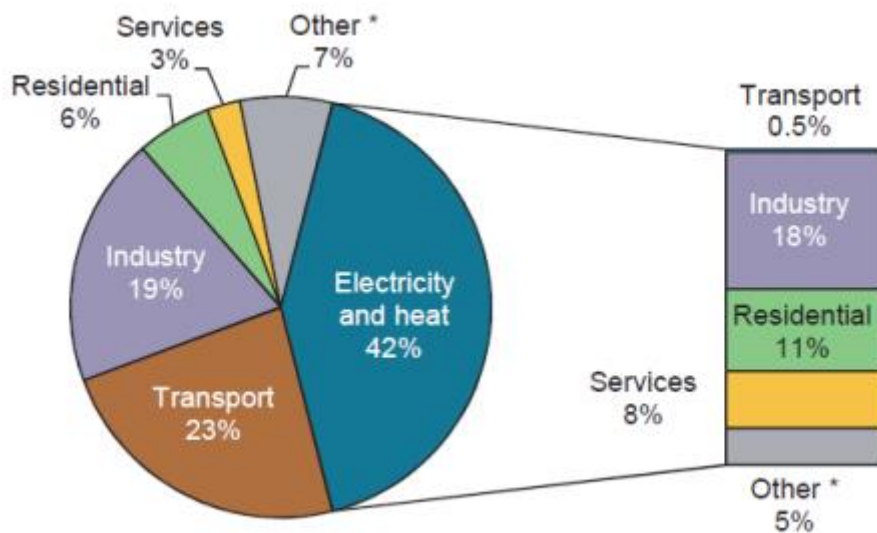


Figure 1-2 World CO₂ emission from fuel combustion by sectors in 2016 (Coent, 2017). Note: this shows allocation of electricity and heat end-use sectors.

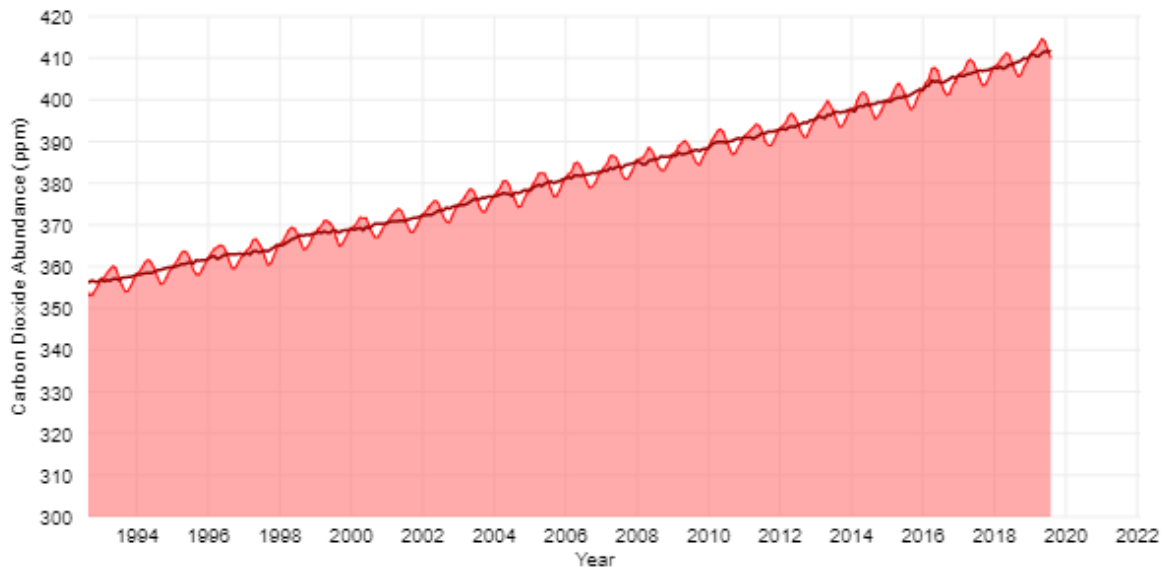


Figure 1-3 Global average atmospheric CO₂ from 1994-2019 (Lindsey, 2019)

The IEA in its BLUE Map scenario proposed a portfolio of technologies for reducing CO₂ emission from the power sector shown in Figure 1-4 (Huaman & Jun, 2014). Carbon capture, CO₂ utilisation and storage (CCUS) is considered the most strategic technology for sustainably and economically meeting carbon emission reduction targets (CERTs) for 2050 (Huaman & Jun, 2014; GCCS, 2017). The global Institute of CCS in a new report confirm that the PARIS agreement cannot be met in a cost effective manner without CCUS (Global CCS institute, 2017).

CCUS mainly involves separation of CO₂, the transportation, utilisation and storage (Wang *et al.*, 2011). CO₂ is first separated from effluent gases generated from industrial energy processes through one of the three approaches: post-combustion capture, pre-combustion capture and oxy-fuel process (Wang *et al.*, 2011). The captured CO₂ is then transferred to either a plant where CO₂ is converted to other products or a stored underground in geological formations (Zhu, 2019).

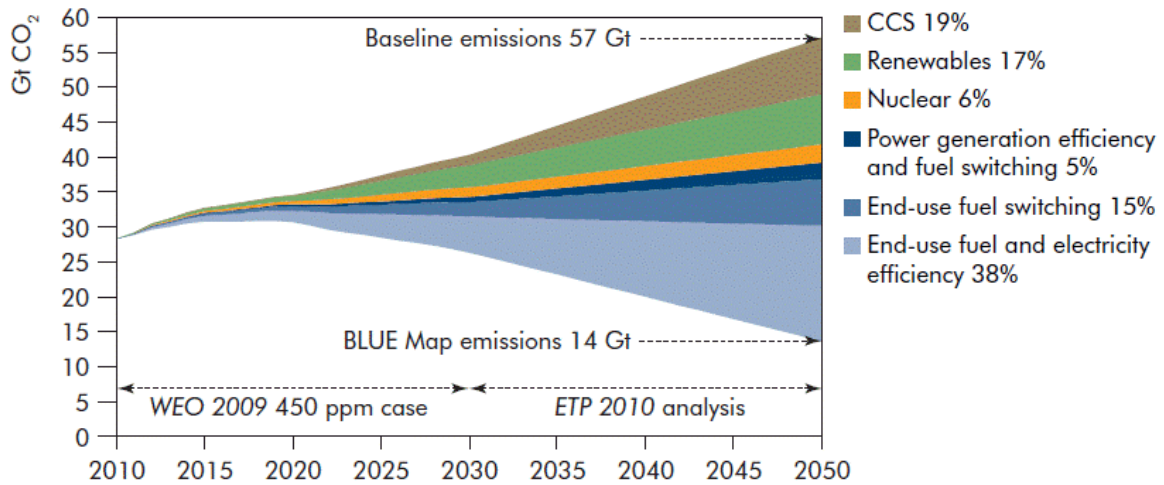


Figure 1-4 technology options to reduce CO₂ emission in power generation (Huaman & Jun, 2014)

The post-combustion capture (PCC) technology is the most matured of the capture technologies (Bui *et al.*, 2014). This is attributed to their suitability to be retrofitted to existing power plants and their capacity to treat flue gas with low CO₂ partial pressure, (Lawal *et al.*, 2010). The PCC technology is the focus of this thesis and therefore will be discussed in further details below.

1.1.2 Post-combustion CO₂ capture process

The PCC process removes CO₂ in flue gases emanating from fossil fuel combustion (Leung *et al.*, 2014). This process is placed after the removal of contaminants in the flue gas such as NO_x, SO_x and particulate matters as shown in Figure 1-5.

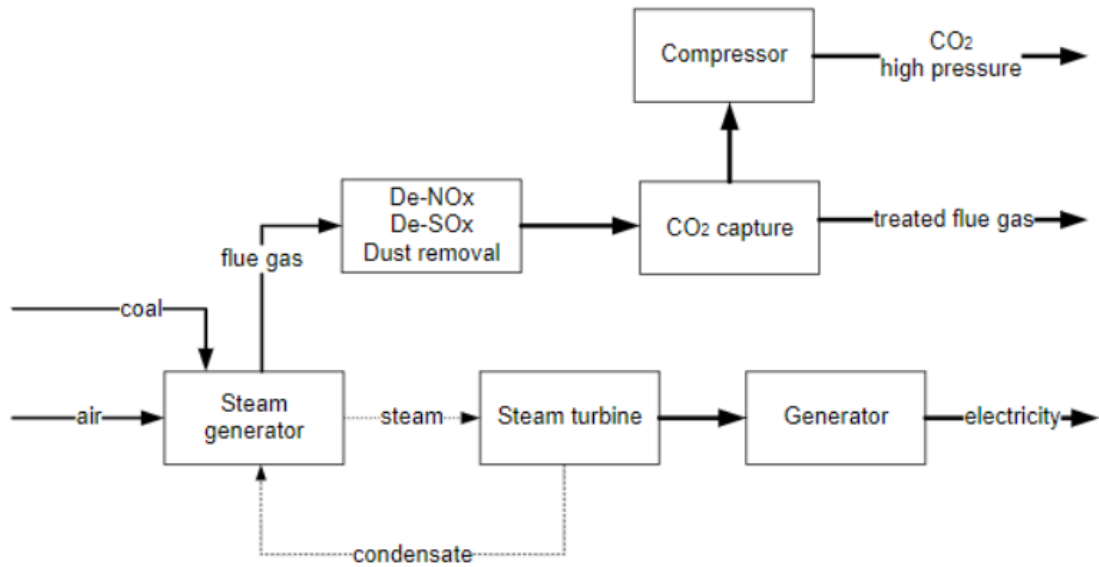


Figure 1-5 Schematic diagram of a power plant with post-combustion CO₂ capture (Wang *et al.*, 2017)

The PCC process employs several separation technologies for CO₂ capture namely: (a) Adsorption; (b) Absorption; (c) Cryogenic separation and (d) Membrane separation.

1.1.2.1 Adsorption

The adsorption process involves selective separation of CO₂ using a solid sorbent material (Harker *et al.*, 2002; Wang *et al.*, 2011; Lee & Park, 2015). The sorbent material can be regenerated either through temperature swing (TSA) (Tlili *et al.*, 2009; Pirngruber *et al.*, 2013), pressure swing adsorption (PSA) (Ishibashi *et al.*, 1996; Hasan *et al.*, 2012), electrical swing adsorption (ESA) (Grande & Rodrigues, 2008) or a combination of the technologies.

Although the adsorption enthalpy for this technology is generally low leading to low regeneration energy requirement, the CO₂ selectivity and adsorptive capacity are low (Álvarez-Gutiérrez *et al.*, 2017; Yu *et al.*, 2017). This has limited their application on a commercial scale to treat a large amount of flue gas, despite its maturity in the chemical industry (Samanta *et al.*, 2012).

1.1.2.2 Cryogenic separation

In the cryogenic separation process, the flue gas firstly goes through a condensing heat exchanger where it is cooled and dried. The dry flue gas is then compressed via a compressor. The flue gas is further cooled to a temperature (between -120°C to -135°C) slightly above the point where CO_2 forms a solid, which is separated via a solid-gas separator. The solid CO_2 is reheated and pressurized via a pump to a safe location (Burt *et al.*, 2010). The cryogenic separation process has advantages of no chemical absorbents or adsorbents as well as no large pressure difference needed and a high CO_2 purity can be achieved. However, the cryogenic separation process is considered expensive and also not realistic technology for PCC due to the high refrigeration cost (Annaland *et al.*, 2015). Thus, this has made the technology not commercially viable.

1.1.2.3 Membrane separation

This is a technology, which involves the selective separation of specific components from a gas stream (Olajire, 2010). In a solvent-based PCC process, the membrane technology utilizes a membrane contactor to separate CO_2 from flue gas. The membrane contactor contains membranes, which are semi-permeable barriers that enable separation of specific components via various mechanisms (Zhao *et al.*, 2016). The membrane mainly filters CO_2 gas component from the flue gas.

The membrane technology is seen to be a more promising technology than the conventional absorption technology for CO_2 capture (Mansourizadeh & Ismail, 2009; Zhang *et al.*, 2015), but it has mostly been demonstrated at laboratory scale (Zhao *et al.*, 2016). This is due to critical challenges from plugging by impurities and membrane wetting which affects the mass transfer and consequently the CO_2 capture performance (Zhao *et al.*, 2016).

1.1.2.4 Physical Absorption

In physical absorption process, a solvent absorbs CO₂ physically according to Henry's law (Olajire, 2010; Wang *et al.*, 2011). Physical solvents use organic solvents absorbs acid gas components physically rather than reacting chemically (Olajire, 2010). CO₂ removal by physical absorption is based on the solubility of CO₂ in the solvents, which depends on the partial pressure and temperature of the feed gas (Olajire, 2010; Wang *et al.*, 2011). The physical absorption occurs at higher CO₂ partial pressure and low temperature and thus not suitable for a post-combustion capture system (Wang *et al.*, 2011). The solvent is regenerated by either heat application or pressure reduction. The energy requirement for regeneration is low due to the weak interaction between CO₂ and the absorbent (Olajire, 2010). Commercial physical solvents include Selexol (dimethyl ether of polyethylene glycol), Rectisol (methanol), propylene carbonate and N-methyl-2-pyrrolidone gas (Olajire, 2010; Wang *et al.*, 2011).

1.1.2.5 Chemical Absorption

The chemical absorption process is a technology widely applied in natural gas and chemical industries, where CO₂ partial pressure is low in the gas stream (Asif *et al.*, 2018). The chemical absorption process has been commercialized to capture CO₂ from large-scale fossil-fuel power plant. Some completed projects still in operation include SaskPower Boundary Dam Carbon Capture and Petra Nova Carbon Capture (Akinola *et al.*, 2019). Commonly used chemical solvents include aqueous alkanolamines (MEA, DEA, MDEA, etc.), piperazine (GPSA, 2004). Among which aqueous MEA is the most widely used solvent. Figure 1-6 gives a schematic process flow diagram of a chemical absorption process. Flue gas from fossil fuel-fired power plants flows into absorber bottom and it encounters lean solvent counter-currently, where the solvent chemically absorbs CO₂. The rich solvent is regenerated in the

stripper using heat input from steam taken out from the power plant after going through a heat exchange (Lawal *et al.*, 2010; Wang *et al.*, 2011). It was recommended by Lucquiaud & Gibbins, (2011) that the steam extraction point should be between the Intermediate pressure (IP) and low pressure (LP) turbines to obtain maximum power output. Aqueous solution of the solvent from the bottom of stripper is recycled back into the absorber while CO₂ from the stripper top is compressed and transported via a pipeline for either underground storage or utilized for enhanced oil recovery (EOR), chemical and food manufacturing (Abu-Zahra *et al.*, 2007). The flue gas from coal-fired power plant goes through a Flue Gas Desulphurization (FGD) unit to remove SO_x and either a Selective Catalytic Reduction (SCR), Selective Non-catalytic Reduction (SNCR) or low NO_x burners to remove NO_x, before flowing into the absorber, based on environmental regulations (Wang *et al.*, 2011).

Chemical absorption is selected as the most suitable technology due to its technological maturity and capability to be retrofitted in an existing power plant (Lawal *et al.*, 2010). Despite its maturity, the issue of its large energy requirement for solvent regeneration has been a major concern. This is because a large amount of steam from the coal-fired power plant is extracted to meet this requirement, resulting in a lower net power generated by the power plant, thereby reducing its efficiency (Wall, 2007; Skorek-Osikowska *et al.*, 2012; Goto *et al.*, 2013). This study will focus on the chemical absorption process.

MEA has generally been considered as a benchmark for solvents adopted in PCC through on chemical absorption process (Oko *et al.*, 2017). However, the solvent regeneration requirement has been a major challenge. In addition, the corrosive and degradable nature of MEA solvent in the presence of the flue gas by-products such as SO_x and NO_x will increase electricity production cost (Bui *et al.*, 2014). Thus, the need

to develop strategies to enhance the energy efficiency of the capture plant through developing an environmentally friendly solvent that has high reaction rate with CO₂ and low energy requirement for regeneration. Many solvents have been developed or under development to tackle the drawbacks of the conventional MEA solvent (Cadena *et al.*, 2004; Mokhtarani *et al.*, 2009; Bandrés *et al.*, 2010; Supasitmongkol & Styring, 2010; Llovel *et al.*, 2012; Tomida *et al.*, 2013; Huang *et al.*, 2014, Zacchello *et al.*, 2017; Isa *et al.*, 2018; Oko *et al.*, 2018; Akinola *et al.*, 2019). More investigations are required to have a better understanding of the reaction mechanism of new solvents. For this PhD study, MEA is selected to capture CO₂ from flue gas in the PCC process based on chemical absorption.

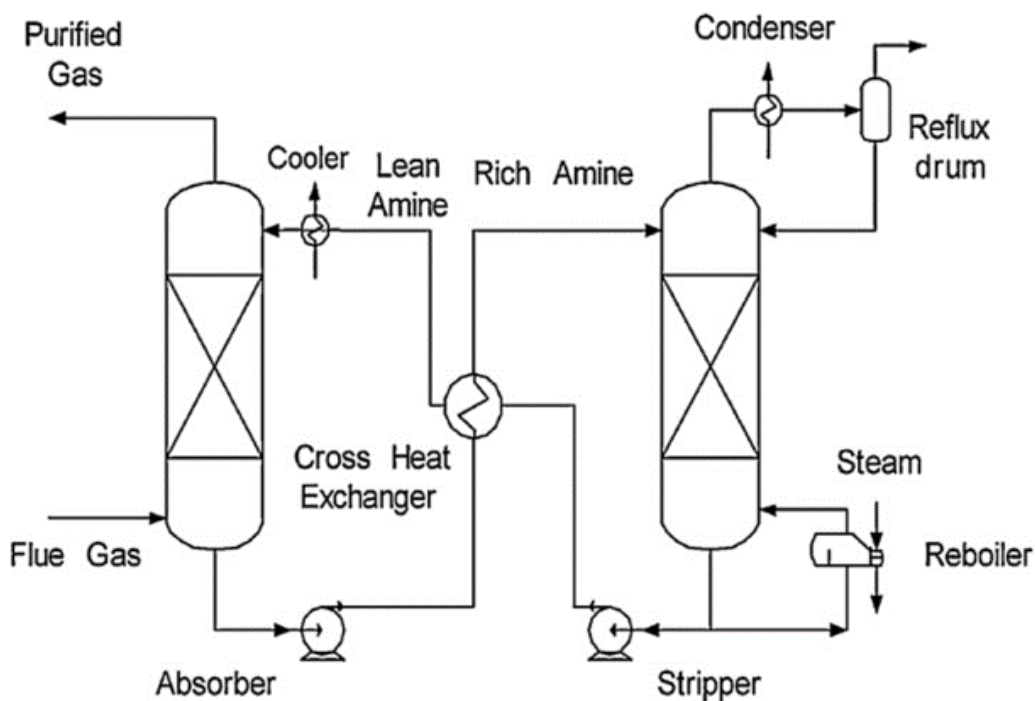


Figure 1-6 Process flow diagram of the chemical absorption plant (Lawal *et al.*, 2010)

1.2 Motivations for this study

Stringent environmental legislations around the world to reduce CO₂ emissions have prompted the need to deploy new energy sources such as nuclear and renewable energy. This will bring a significant shift in the dominant role of fossil fuel, especially coal, in the energy system and the need for flexible operation of coal-fired power plants (Mac Dowell & Staffell, 2015). The flexible operation of the coal-fired plant will lead to fluctuation in the flue gas flowrate and composition flowing to the absorption column, as well as steam to the reboiler. This introduces disturbances into the capture plant, thus affecting the dynamics of the solvent-based PCC plant. The flexible operation of the solvent-based PCC plant (i.e. variation of the capture rate in accordance with electricity demand) is important to cope with the power plant operation. Investigation of the solvent-based PCC plant response to disturbances during various flexible operation modes such as start-up, shutdown and load following attention (Chalmers *et al.*, 2009; Cohen *et al.*, 2011; Wiley *et al.*, 2011; Bui *et al.*, 2014; Mac Dowell and Shah, 2014). In addition, a suitable control strategy is required for the solvent-based PCC plant to handle these disturbances.

An accurate dynamic model is required to have a comprehensive study of the CO₂ capture process (especially interactions between the coal-fired power plant and capture plant), optimize the operational procedure for dynamic periods (such as start-up and shutdown operation) and develop a suitable process control strategy. Many studies on dynamic modelling of a solvent-based PCC were carried out on first principles models (Lawal *et al.*, 2009, 2010, 2012, Biliyok *et al.*, 2012a, 2012b; Mac Dowell *et al.*, 2013; Mac Dowell and Shah, 2014). Challenges with high computational time when developing a detailed solvent-based PCC capture model especially when integrated with coal-fired power plant and its high level of complexity makes it difficult

to implement relevant process control strategies. Thus, simplification of the first principles model is required to reduce the computational time for simulation (Peng *et al.*, 2003; Oko *et al.*, 2015). This has significantly motivated the use of data-driven modeling approach via system identification techniques, to represent the solvent-based PCC model. This involves constructing a suitable model that best describes the relationship between the process input and output variables.

1.3 Aim and Objectives of this study

This research is aimed at the development of a reliable dynamic model via system identification technique as well as a suitable process control strategy for the solvent-based post-combustion CO₂ capture plant. The research objectives include the following:

- To provide a comprehensive review of current research status in dynamic modelling, system identification and control of solvent-based PCC plant.
- To carry out data collection from the first principles solvent-based PCC model at pilot scale.
- To carry out a data-driven dynamic model development via nonlinear system identification of the solvent-based PCC process.
- To develop a conventional PI control scheme on the identified solvent-based PCC model.
- To develop a linear model predictive control (MPC) scheme on the identified solvent-based PCC model.
- To develop a nonlinear model predictive control (NMPC) scheme on the identified solvent-based PCC model.

1.4 Novel Contribution of the Thesis

Extensive studies have been carried out on model development via system identification and controllability analysis of the solvent-based PCC plant. Most of these studies have represented the CO₂ capture process as a linear model (Dunia *et al.*, 2011; Nittaya *et al.*, 2014a; Sahraei & Ricardez-Sandoval, 2014; Luu *et al.*, 2015; Mehleria *et al.*, 2015; He *et al.*, 2016). However, the capture process exhibits highly nonlinear behaviour (Manaf *et al.*, 2016). As a result, existing linear models fail to capture the process dynamics especially during large load variation scenarios encountered during flexible operation (He *et al.*, 2016). Only a few studies have represented the CO₂ capture process as nonlinear model (Sipöcz *et al.*, 2011; Li *et al.*, 2015, 2017; Abdul Manaf *et al.*, 2016). However, the techniques adopted for the nonlinear model development in these studies is developed on the basis of an assumed model order. Model developed based this assumption might contain irrelevant model terms that does not have significant effect on the process output.

In contrast, this thesis proposes a nonlinear transparent parsimonious NARX model that captures the relationship between the input variables and output variables in the CO₂ capture process. This is developed using forward regression orthogonal least square (FROLS) algorithm. This algorithm selects the important model terms one by one, in a stepwise manner, based on their significance, which is measured using a simple but useful index called the error reduction ratio (ERR). In addition, new linear (PI and MPC) and NMPC control schemes are developed, implemented and compared using the model developed through FROLS-ERR algorithm.

1.5 Scope of this study

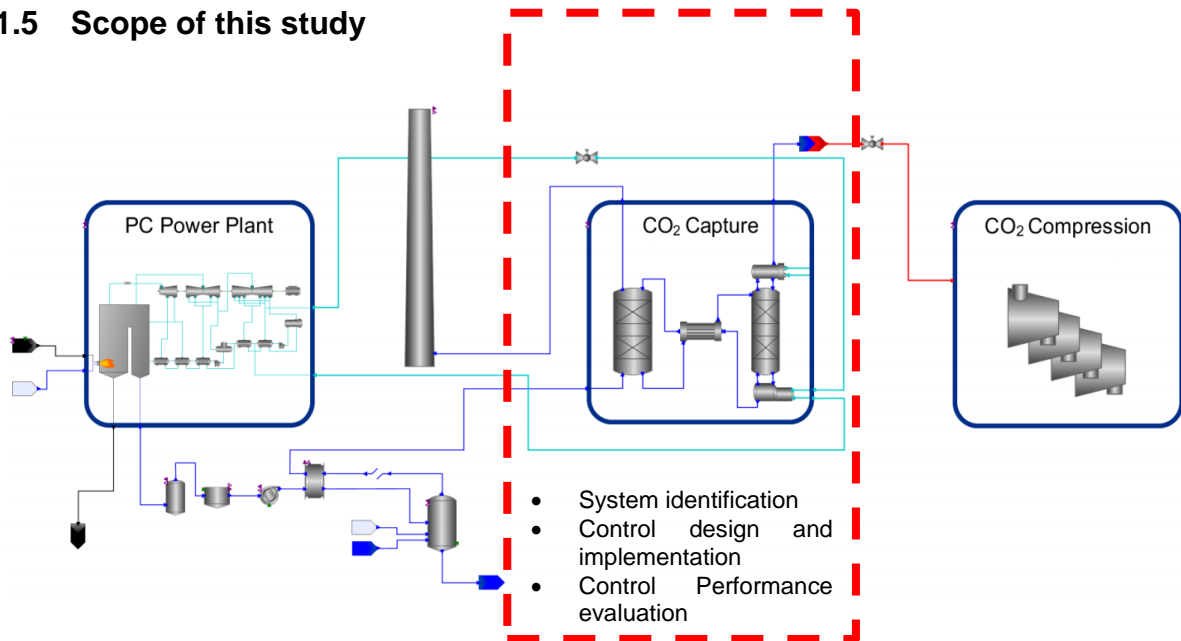


Figure 1-7 scope of the study

The study is mainly focused on the solvent-based PCC process (see Figure 1-7). The scope of the study is limited to data-driven modelling via system identification and control of the solvent-based PCC process. The study utilizes the first principles model developed at pilot scale by Lawal *et al.*, (2010). It should be noted that the following are outside the battery limit of the study:

- Power plant model development
- CO₂ compression and transport design
- Flue gas desulphurization (FGD) design

The interconnectivity of the power plant to the CO₂ capture plant includes the flue gas stream to the absorber and the steam draw-off at the IP/LP crossover configuration in the power plant to the reboiler located at the regeneration column. In this research, it was ensured that the variation in the process condition of these streams reflect the operational changes in the power plant.

1.6 Research methodology and tools used for the study

1.6.1 Research methodology

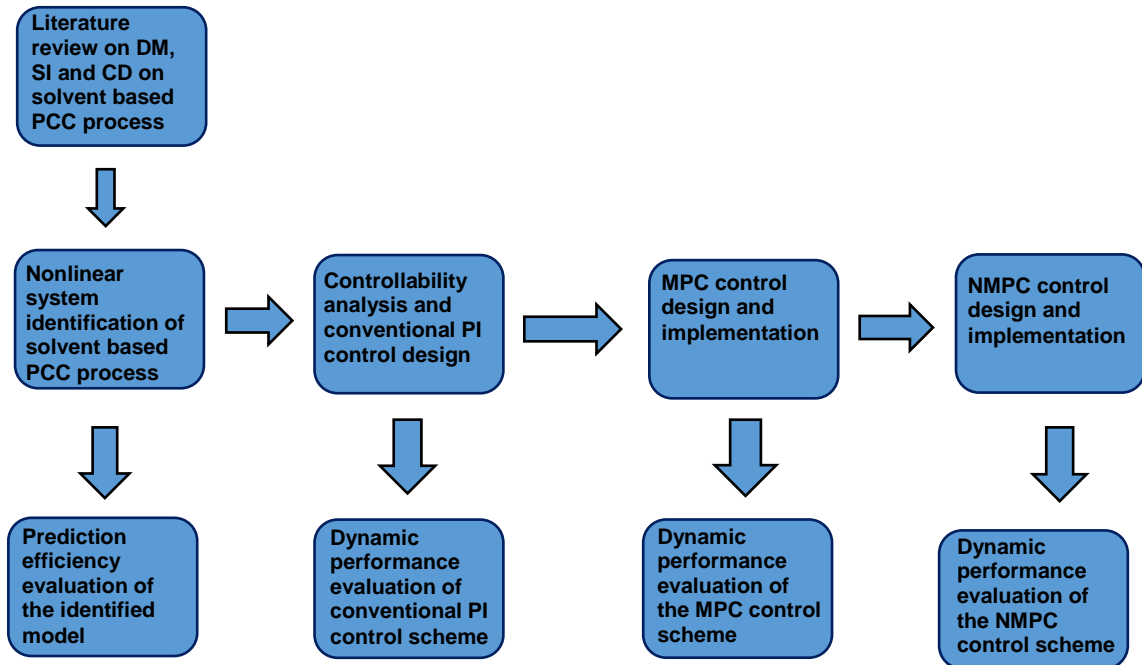


Figure 1-8 Overview of Research methodology (in the Figure, 'DM' refers to 'Dynamic Modelling'; 'SI' refers to 'system identification'; 'CD' refers to-control design)

The control scheme design and implementation on the solvent-based PCC process is essential to adequately handle process interactions with the system. Figure 1-8 gives an overview of the research methodology.

1.6.2 Software tools used for the study

1.6.2.1 gPROMS®

gPROMS® (general **PRO**cess **MO**delling **S**ystem) is an advanced process modelling platform for creating and managing custom (equation-based) models ranging from a single unit to entire process and optimization environment. In this study, the first principles gPROMS® model developed by Lawal *et al.*, (2010) at pilot scale was utilized

to obtain a dynamic operational data. It was referred to in chapter 3 in the nonlinear system identification of the solvent-based PCC model. The gPROMS model utilised have been validated both in steady-state and dynamic operation (Biliyok *et al.*, 2012a; Lawal *et al.*, 2010). Thus, the dynamic model is reliable to be adopted for this study.

1.6.2.2 Matlab® Toolbox/ Simulink®

Matlab® (**Matrix laboratory**) is a high-performance technical computing language. It allows for the integration of computation, visualization and programming in a user-friendly interface (Mathworks, 2019). This enables algorithm development, data analysis, modelling and simulation. Simulink® is an additional block diagram environment for model based design and simulation (MathWorks, 2015). The Matlab®/ Simulink® was adopted to carry out the following:

- Development of the forward regression least square (FROLS) algorithm as the nonlinear system identification technique using Matlab scripts.
- State representation of the solvent-based PCC process in Simulink® environment.
- Conventional PI control scheme design and implementation in Simulink® environment.
- MPC scheme design and implementation in Simulink® environment.
- NMPC scheme and implementation using Matlab® script.

1.7 Outline of the Thesis

Chapter 2 presents a comprehensive literature review on past and current research activities (both experimental and computational) on dynamic model development, system identification and process control design of the solvent-based PCC process.

Chapter 3 presents the nonlinear system identification of the solvent-based PCC process using the FROLS-ERR algorithm. This chapter focused on the process data acquisition and implementation of system identification technique on the data acquired. Identified models obtained were evaluated based on prediction efficiency (PE) evaluation, statistical analysis and process dynamic analysis to ensure that the identified models capture the essential dynamics of the solvent-based PCC process.

Chapter 4 presents the multivariable control design of the solvent-based PCC process using the conventional PI controller. In this chapter, state-space realisation of the identified CO₂ capture model and multivariable control structure analysis were discussed. In the end, the performance evaluation of the conventional PI control scheme was investigated.

Chapter 5 presents the design and implementation of a linear model predictive control (MPC) scheme on the solvent-based PCC process. The model linearization of the solvent-based PCC model was discussed as well as the MPC design. The performance evaluation of the MPC scheme on the solvent-based PCC process model under different scenarios was investigated.

Chapter 6 presents the design and implementation of nonlinear model predictive control (NMPC) on the solvent-based PCC process. NMPC utilizes the identified nonlinear CO₂ capture model. The chapter details the NMPC design. Control performance evaluation of the NMPC scheme was also investigated.

Chapter 7 draws the conclusion of the study and gives recommendation for future work.

2 Literature review

2.1 Introduction

The chapter is aimed at giving a summary of recent research activities on dynamic modelling (steady state and dynamic), system identification and process control of the solvent-based PCC process. Section 2.2 presented a review of existing pilot and commercially deployed PCC plant. Review of recent studies on the model development of solvent-based PCC process (first principles and data-driven modelling (SI) approach is presented in Section 2.3. Section 2.4 presented a review of current studies on process control system design of the solvent-based PCC process. The summary of the literature review is presented in section 2.5.

2.2 Review of Pilot plants and commercially deployed plants

2.2.1 Review of solvent-based post-combustion CO₂ capture pilot plants

This section summarizes recent R&D activities on post-combustion CO₂ pilot plant. Past R&D activities on pilot scale PCC plant was summarized by Wang *et al.*, (2011), Mumford *et al.*, (2015) and Oko *et al.*, (2017). A few successful operational pilot PCC plant integrated with power plant are shown chronologically in Table 2-1. The solvent-based PCC pilot plant test bridge the gap between lab-scale experiments and commercialised scale plants (Mumford *et al.*, 2015). Various Investigations are carried out during pilot plant studies, which include solvent evaluation (either single amine, amine-based blends or proprietary solvents), corrosion studies, solvent degradation, operation study and process energy efficiency (Chi & Rochelle, 2002; Cottrell & Feron, 2011; Faber *et al.*, 2011; Lepaumier *et al.*, 2011; Seibert *et al.*, 2011; Rabensteiner *et al.*, 2014; Stec *et al.*, 2016). CO₂ captured during the tests were either vented to the atmosphere (Radgen *et al.*, 2014; Thimsen *et al.*, 2014; Lee *et al.*, 2015), transported

for EOR (CCS, 2016; Wu *et al.* 2016), stored underground (Hirata *et al.*, 2014; Tanaka *et al.*, 2014) or sold commercially (Wang & Xu, 2014). The successes documented in the demonstration plant has led to the commercialisation of some of its technologies.

In the United Kingdom, a recent milestone attained in solvent-based PCC development is the capture of CO₂ from a biomass-fired power plant at Drax Power Station using a proprietary solvent developed by C-Capture Ltd (Drax, 2019). Analysis is being carried out based on data obtained from the pilot plant to understand the potential of the technology and how it can be scaled up (Drax, 2019).

Table 2-1 Summary of operational solvent-based PCC Pilot plant integrated into a power plant

| s/n | Project | location | Company | Capacity (Amt of CO ₂ captured) | Cost | Operational date | Reference |
|-----|---------------------------|--------------|--|--|----------|------------------|--------------------------------|
| 1 | Shengli | China | Sinopec | 0.04Mt/yr | N/A | 2007 | Wu <i>et al.</i> (2016) |
| 2 | Sigma Power Ariake Mikawa | Japan | Toshiba Corporation | 10 t/day | N/A | 2009 | Ohashi <i>et al.</i> (2011) |
| 3 | Shidongkou | China | Huaneng | 0.1 Mt/yr | US\$24M | 2009 | Wang & Xu, (2014) |
| 4 | jilin | China | PetroChina | 0.2Mt/yr | US\$ 11M | 2009 | CCS, (2016) |
| 5 | Plant Barry | Alabama, USA | Southern Energy | 0.1-0.15 Mt/yr | N/A | 2011 | Hirata <i>et al.</i> , (2014) |
| 6 | Wilhelmshaven | Germany | E.ON | 70t/day | N/A | 2012 | Radgen <i>et al.</i> , (2014) |
| 7 | Mongstad | Norway | Statoil | 0.1 Mt/yr | N/A | 2012 | Thimsen <i>et al.</i> , (2014) |
| 8 | Boryeong Station | South Korea | Korea Electric Power Corporation (KEPCO) | 2t/day (phase1) 200t/day (phase2) | US \$42M | 2013 | Lee <i>et al.</i> , (2015) |
| 9 | Tomakomai | Japan | JCCS | 45kt/yr | US \$70M | 2015 | Tanaka <i>et al.</i> , (2014) |

2.2.2 Commercial deployment of solvent-based PCC plant

Commercial large-scale solvent-based PCC plant has been widely deployed in various industries (mostly natural gas processing plant) across the world. Most recently, 2 large scale PCC facilities became operational (Quest and Abu Dhabi CCS) attached to steam methane reformer (SMR) for hydrogen production and iron& steel production respectively. Despite the deployment of large-scale PCC facilities in various industrial sectors, this section only focuses on the deployment of large-scale PCC plants to power plants. For deployment of large-scale PCC plants to an existing power generation plant, the boundary Dam CCS plant in Canada and Petra Nova CCS plant in USA are the only operational CCS projects based on the chemical absorption process. Table 2-2 shows the specification of both operational CCS facilities.

Table 2-2 Specifications of both Boundary Dam and Petra Nova CCS project (Mantripragada *et al.*, 2019)

| Parameter | Boundary Dam CCS plant | Petra Nova CCS plant |
|--------------------------------------|-------------------------------|--|
| Location | Saskatchewan, Canada | Texas, USA |
| New or Retrofit | Retrofit | Retrofit |
| Gross Capacity (MW) | 160 | 240 |
| Net capacity (MW) | 110 | 240 (+ excess power from cogeneration plant) |
| Coal type | Lignite | Sub-bituminous |
| Capture level | 90% | 90% |
| Capacity of CO ₂ captured | 1 million t/yr | 1.4 million t/yr |
| CO ₂ fate | EOR | EOR |
| Solvent | Cansolv | KS-1 |

| Parameter | Boundary Dam CCS plant | Petra Nova CCS plant |
|----------------------|----------------------------|---|
| Regeneration | Steam from the power plant | Natural gas co-generation (70MW using GE 7 EA turbine, half the power for CCS, rest sold to grid) |
| Project capital cost | US \$1.3B | US \$1B |

As shown in Table 2-2, the main difference between Boundary Dam and Petra Nova CCS plant is the configuration of the regeneration steam source and auxiliary electricity. This affects the overall performance and cost of CO₂ capture (Mantripragada *et al.*, 2019). The Boundary Dam plant uses steam from the primary steam cycle, which reduces the power rate of the coal-fired power plant, for solvent regeneration (Mantripragada *et al.*, 2019). Thus, increasing its cost of electricity generation. However, the Petra Nova plant utilizes a dedicated natural gas combined cycle (NGCC) power plant to supply regeneration energy (Mantripragada *et al.*, 2019). Although it does not cause a parasitic load on the coal-fired power -plant, the net power station output increases as the NGCC power electrical output exceeds the demand for the CO₂ capture system (Mantripragada *et al.*, 2019). This brings about additional capital investment, operating expenses and CO₂ emissions (Mantripragada *et al.*, 2019).

A few large-scale CCS projects at the early development stage include; Sinopec Shengli power plant CCS project (China) and Caledonia Clean Energy Project (United kingdom) (GCCS, 2019).

2.2.3 Summary

The solvent-based post-combustion CO₂ capture technology based on chemical absorption is the first and only commercial technology that is operational for large-scale coal-fired power plant. This technology has been widely tested in pilot-scale

plants. Some completed solvent-based PCC projects attached to power plants include SaskPower Boundary Dam carbon capture and Petra Nova carbon capture Projects (Mumford *et al.*, 2015; Mantripragada *et al.*, 2019). Despite the commercial deployment of this technology, the cost of each project was unacceptably high (Oko *et al.*, 2017). Thus, there has been a quest to reduce the CO₂ capture cost by either process reconfiguration, new solvent development or both to improve the overall plant performance (Joel *et al.*, 2014; Oko *et al.*, 2017). To assess the technical and economic performance of each approach, technical and economic analysis via modelling and simulation are required. This is due to the convenience and cost-effectiveness of adopting the modelling approach. This is further expounded upon in the next section.

2.3 Model Development of the solvent-based post-combustion CO₂ capture process

This section details the model development of the solvent-based post-combustion CO₂ capture based on different approaches namely, first principles and data-driven modelling approach. The first principles approach utilizes chemical engineering principles to develop a mathematical model while the data-driven modelling approach uses the operational data from the process to obtain a mathematical model that relates the input variables with the out variables.

2.3.1 First principles modelling approach

The solvent-based post-combustion CO₂ capture process involves gas-liquid mass transfer and chemical reactions occurring simultaneously. For model development via first principles approach, the gas-liquid mass transfer can be described based on either equilibrium based approach or rate-based approach. The equilibrium-based

approach assumes theoretical stages, where liquid and vapour attain equilibrium (Lawal *et al.*, 2009). The gas-liquid equilibrium is rarely attained. As such, the assumption is unrealistic. Thus, each stage performance can be adjusted by using a tray efficiency correction factor to reflect a real stage performance. The rate-based approach gives a more accurate representation of the gas-liquid mass transfer within each column. For the rate-based approach, gas-liquid mass transfer is described using either two-film theory (Kvamsdal *et al.*, 2009; Lawal *et al.*, 2009, 2010; Harun *et al.*, 2011; Biliyok *et al.*, 2012b) or penetration theory (Rahimpour & Kashkooli, 2004). Extensive details on these theories are readily available in literature Aroonwilas & Veawab, (2016).

The chemical reaction of CO₂ with chemical solvent is, however, described by either 3 major reaction mechanism, namely zwitterion, termolecular and base-catalyzed hydration. Extensive details of these reaction mechanisms are available in literature (Da Silva & Svendsen, 2005). For the first principles model approach, CO₂ reaction kinetics can be expressed as an approximation, assuming the reaction reaches equilibrium. This assumption is sufficient for fast reacting chemical solvent such as MEA (Lawal *et al.*, 2010). For slow reacting chemical solvents, such as DEA and MDEA, the assumption is not sufficient and thus an accurate reaction kinetics description is required (Zhang *et al.*, 2009). This is simplified by assuming pseudo first-order reaction and introducing enhancement factor that accounts for the kinetics (Kvamsdal *et al.*, 2009).

Based on the combined mass transfer and chemical kinetics description, model development of the solvent-based PCC can be classified into 5 different levels of complexities as shown in Figure 2-1 (Kenig *et al.*, 2001). Level 1 is considered to be the least accurate while level 5 is considered to be the most accurate. This is because

level 5 adopts a rate-based approach for mass transfer and the accurate reaction kinetics.

The model development of the solvent-based PCC process are also classified as either steady models or dynamic models. Reviews on this model classification are presented in the next 2 sections.

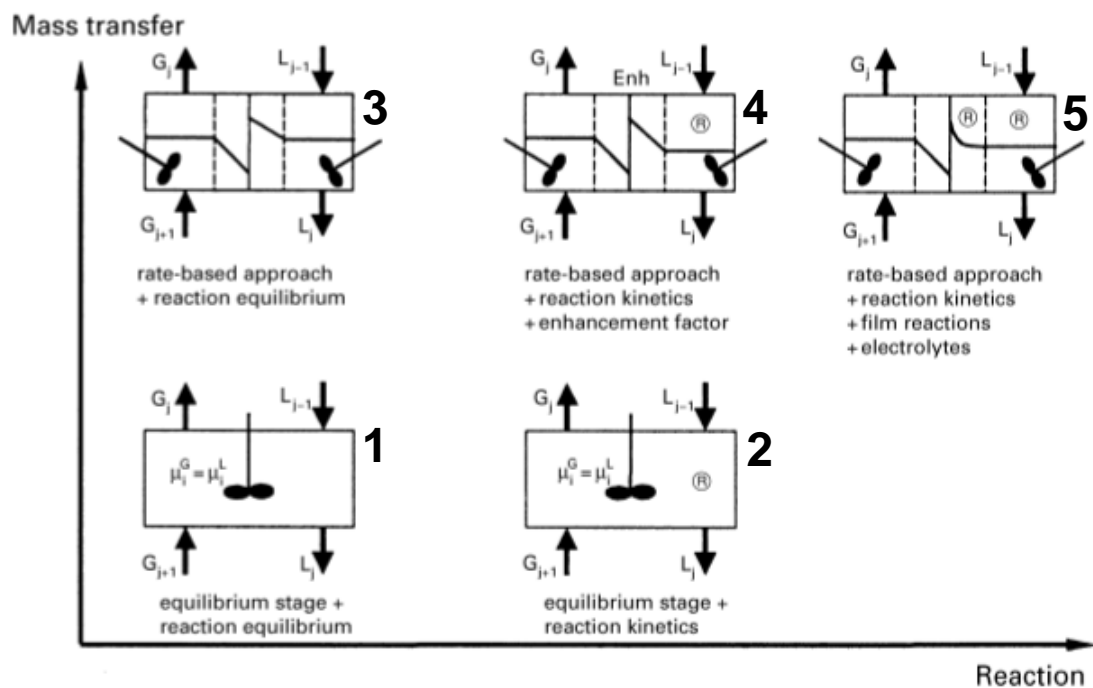


Figure 2-1 Representation of the level of complexity when modelling solvent-based PCC (Lawal et al., 2009)

2.3.1.1 Current status on steady-state modelling of post-combustion capture plant

Evaluation of a process plant performance through commercially available simulation software packages are proven to be a cost-efficient and timely approach (Bui *et al.*, 2014). The steady-state model development of solvent-based PCC plant is utilized for technical performance and economic impact on power plant. Several studies available

in literature utilizes the solvent-based PCC steady-state model to investigate the following to improve the CO₂ capture plant efficiency and cost:

- Solvent performance evaluation (Abu-Zahra *et al.*, 2007; 2007b)
- Process configuration modification of both packed columns (Karimi *et al.*, 2011; Ahn *et al.*, 2013; Joel *et al.*, 2014).
- Process integration with power plant (Aroonwilas & Veawab, 2007, 2009; Lucquiaud & Gibbins, 2011; Liu *et al.*, 2015; Luo *et al.*, 2015; Alcaráz-Calderon *et al.*, 2019)
- Scale-up studies (Canepa *et al.*, 2013; Agbonghae *et al.*, 2014; Luo & Wang, 2017).

Commercially available software used to carry out these studies include Aspen Plus[®], Aspen HYSYS[®] and Honeywell Unisim. Findings from these studies revealed that key parameters that affect the CO₂ capture efficiency, as well as cost, include the specific heat duty at the stripper and L/G ratio in the absorber. Ahn *et al.*, (2013) proposed an amine-based process modification design where the heat duty is reduced to as low as around 2.22 MJ/kg_{CO2} from that attained in the conventional configuration (3.52 MJ/kg_{CO2}). This leads to a significant reduction in the energy penalty, which in turn reduces the operating cost of the capture plant. However, the modifications in the plant might increase the capital cost based on the complication of design. Studies on solvent performance revealed the need to develop new chemical solvents that are environmentally friendly, highly reactive with CO₂ and requires low energy for regeneration (Zhou *et al.*, 2010).

Most investigations on the solvent-based PCC plant at steady state condition considered the plant at baseload. This highlights the limitation of the steady-state model development as the CO₂ capture plant is required to operate at flexible mode

to take advantage of the peak and off-peak electricity demand of the power plant. Thus, dynamic model development is required to investigate the dynamic operations such as start-up, shutdown and load following.

2.3.1.2 Current status of dynamic modelling of solvent-based post-combustion capture plant

Despite numerous studies on the evaluation of the technical and economic impact of solvent-based PCC process on power plant through modelling and simulation under steady-state conditions, development of a dynamic model is essential to capture the nonlinear behaviour of the PCC plant. This includes capturing process variables interactions within the capture plant and the influence of disturbances from the power plant on the capture plant (Manaf *et al.*, 2016).

Several studies on dynamic model development of solvent-based PCC have been carried. Research focus started with development of a single component of the PCC plant (either Absorber or stripper) (Kvamsdal *et al.*, 2009; Lawal *et al.*, 2009; Ziaii *et al.*, 2009; Greer *et al.*, 2010), then advanced into model development of a standalone PCC plant (Lawal *et al.*, 2010; Harun *et al.*, 2011; Gaspar & Cormos, 2012; Jayarathna *et al.*, 2013) and integration of the capture plant with coal-fired power plant (Lawal *et al.*, 2012; Bui *et al.*, 2013; Jayarathna *et al.*, 2013; Mac Dowell & Shah, 2013; Posch & Haider, 2013; Gardarsdóttir *et al.*, 2015).

Commercially available simulation software used to carry out these studies are gPROMS[®] (Kvamsdal *et al.*, 2009; Lawal *et al.*, 2010; Harun *et al.*, 2011; Mac Dowell *et al.*, 2013; Mac Dowell & Shah, 2014; Walters *et al.*, 2016), Aspen Plus[®] dynamics (Lin *et al.*, 2011; Fan *et al.*, 2015; Zhang *et al.*, 2016), Aspen HYSYS[®] (Sahraei & Ricardez-Sandoval, 2014), Modelica[®] (Prolss *et al.*, 2011; Åkesson *et al.*, 2012) and

Matlab[®] (Greer *et al.*, 2010; Gaspar & Cormos, 2012; Enaasen *et al.*, 2013; Jayarathna *et al.*, 2013).

Most researchers adopted E-NRTL physical property method to describe the vapour-liquid equilibrium, the chemical reaction and the physical properties of the system. In some of these studies, chemical reactions within the column were assumed to attain chemical equilibrium at the interface (Biliyok *et al.*, 2012b) while others described the chemical reaction kinetics using an enhancement factor (Harun *et al.*, 2011). Other physical property methods used by other researchers were Wilson-NRF (Gáspár & Cormoş, 2011) and SAFT-VR (Mac Dowell *et al.*, 2013). The SAFT-VR equation of state (EOS) model is said to eliminate the need to describe the chemical reactions within the column (Luu *et al.*, 2015; Mac Dowell & Shah, 2014).

Validation of these dynamic solvent-based PCC models developed is required to ensure the accuracy of the model. Although most dynamic solvent-based PCC models were validated under steady conditions using Dugas, (2006) data from the pilot plant in separation research program (SRP) at the University of Texas at Austin, it is essential that dynamic validation is carried out. This is to ensure that the model developed predicts accurate dynamic responses. Despite insufficient dynamic experimental data for dynamic validation of solvent-based PCC models developed, there have been a few validations of solvent-based PCC models against dynamic pilot plant data. Biliyok *et al.*, (2012a;2012b) validated dynamic solvent-based PCC model developed by Lawal *et al.*, (2010) using dynamic experimental data from the pilot plant at the University of Texas at Austin. Three cases were considered for comparison, using the absorber temperature profile, reboiler duty and CO₂ concentration in the treated gas as parameters to be compared. The model satisfactorily predicted the dynamic behaviour of the pilot plant (Biliyok *et al.*, 2012a, 2012b). Dynamic validation

carried out by Flø *et al.*, (2015) demonstrated satisfactory agreement with Gloschaugen pilot plant data. Other studies on dynamic validation of a solvent-based PCC model with pilot plant data are Gaspar *et al.*, (2016) and Bui *et al.*, (2016).

Dynamic analysis of solvent-based PCC model is necessary to investigate the feasibility of flexible operation of a capture plant integrated with power plant and understand the PCC dynamic behaviour under different scenarios such as start-up, shutdown and varying load. As it was earlier established, the flexible operation of power plant imposes disturbances on process parameters, which affect the PCC process dynamic performance. One of these parameters is power plant load change, which results in a change in the flue gas flowrate and a variation in the steam supplied for solvent regeneration to the reboiler. Change in the energy source also can lead to an alteration in flue gas CO₂ composition sent to the PCC plant. Other process parameters that affect the capture plant performance are solvent residence time within each column, CO₂ lean loading, liquid/gas (L/G) ratio and solvent concentration and flowrate. Analysis carried out by Lawal *et al.*, (2010) on the absorber alone indicated that the absorber performance is more sensitive to L/G and the stripper performance is influenced by the reboiler duty. The importance of maintaining the right water balance within the solvent-based PCC system to avoid operational issues such as corrosion was highlighted. Similar observations on the importance of water balance within the PCC system were reported by Biliyok *et al.*, (2012b) and Kvamsdal *et al.*, (2009). A study from Biliyok *et al.*, (2012b) also indicated that the absorber performance is influenced by the flue gas composition. An increase in the flue gas moisture content resulted in a reduction in the capture level and changes the shape of the temperature profile within the absorber.

Various studies on dynamic analysis using the solvent-based PCC model (Lawal *et al.*, 2010; Harun *et al.*, 2011; Lin *et al.*, 2011; Mac Dowell & Shah, 2013) showed that the flue gas flowrate affects the capture plant efficiency if the lean solvent flow rate is fixed, indicating that a flue gas flowrate increase will result in a reduction in the L/G ratio, which ultimately reduces the capture level. Lin *et al.*, (2011) and Mac Dowell & Shah, (2013) pointed out the influence of lean solvent temperature on the capture efficiency. Analysis by Mac Dowell & Shah, (2013) also showed that a decrease in lean solvent flowrate (when flue gas flowrate doesn't change) reduces the CO₂ capture efficiency as well as shifts the region of temperature bulge within the column.

Lawal *et al.*, (2012) integrated a power plant model with a scaled-up solvent-based PCC model and investigated the effects of MEA concentration, power plant output and CO₂ capture level on the overall plant performance. Results from this study showed that the capture plant has a slower response compared to the power plant.

Peng *et al.*, (2003) and Oko *et al.*, (2015) highlighted challenges with high computational period when simulating a detailed rate-based solvent-based PCC model especially when integrated with a coal-fired power plant. This makes it difficult to implement relevant process control strategies. Thus, simplification of the solvent-based PCC model is required to reduce the computational time for simulation. Oko *et al.*, (2015) simplified a detailed rate-based solvent-based PCC model by replacing non-linear algebraic correlations used to determine the wetted area and gas-phase mass transfer coefficient within the packed column with a constant, the liquid phase mass transfer coefficient with a linear correlation against pressure, temperature and superficial mass velocity. PCC model simplification carried out by Prolss *et al.*, (2011) for implementation of a NMPC involved replacement of the chemical equilibrium computation, and enthalpy expression with a semi-empirical algebraic correlation

while the mass transfer expressions, specific heat capacities and liquid density were assumed to be constant.

Recently, there has been an emergence of data-driven modelling approach to develop solvent-based PCC model. This involves estimating a model from process operational data. Further details are discussed in the next section.

2.3.2 Data-driven modelling approach- System identification (SI)

SI is a data-driven model development approach, which involves the use of experimental data to develop a mathematical model that represents accurately the system dynamics (solvent-based PCC plant) without the knowledge of the physical system behaviour (see Figure 2-2). The model (system) is determined, based on input-output data, within a set of class systems to which the model is identical (Zhu, 2001). Input-output data are collected during an identification test, which is designed to ensure that the data measured contains relevant information about the system that is useful to the user (Zhu, 2001). A suitable model structure is selected within the set of model term candidate (Ljung, 1987; Zhu, 2001). The model parameters are obtained based on an error criterion (loss function) specified (Zhu, 2001). Data-driven model developed are classified as either linear model or nonlinear model.

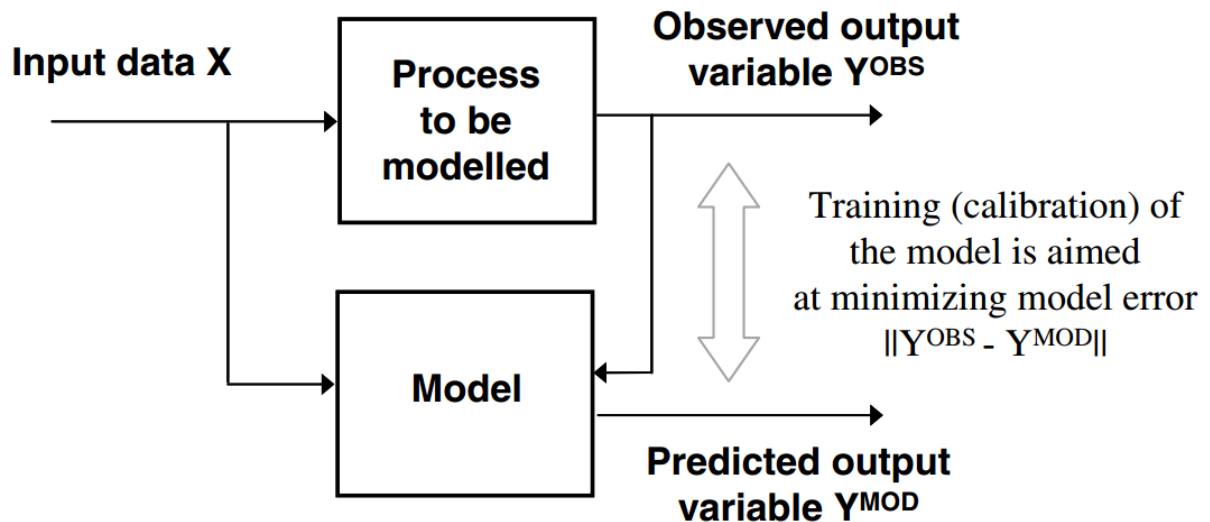


Figure 2-2 SI approach (Solomatine & Ostfeld, 2008)

2.3.2.1 Linear SI

Linear models are used to represent systems that are linear in nature (i.e. the systems that satisfy the superposition principle). Linear SI approach can be categorised into non-parametric identification and parametric identification. The non-parametric identification approach uses correlations and spectral analysis to obtain estimates of the impulse response or frequency response system (Ljung, 1987). This provides insight for parametric identification techniques to estimate the model.

The parametric identification techniques adopt the use of a model structure, parameter estimation and model validation (Ljung, 1987). The parametric techniques gained much attention due to the need for control system development (Billings, 2013). Common models in SI are black-box model, grey-box model and user-defined model (Zhu, 2001; Ljung, 1987). The black-box model assumes the system is completely unknown and the model parameters are adjusted without considering the background of the physical system. Parametric identification approach is usually adopted for a black-box model (Zhu, 2001; Ljung, 1987). The grey-box model uses some obtained

information about the process dynamics or some known physical parameters of the system to estimate the unknown parameters (Zhu, 2001; Ljung, 1987). User-defined model is adopted when it is assumed that the physical system cannot be accurately represented by either a black-box model or a grey-box model (Zhu, 2001; Ljung, 1987).

2.3.2.2 Nonlinear SI

Nonlinear systems are primarily defined as a system that does not satisfy the superposition principle (Billings, 2013; Ljung, 1987). The broad definition of nonlinear systems makes it nearly impossible to write down a description that accurately captures all classes that exist under the definition of nonlinear systems. Several authors, in the early years, have focused on specific classes of nonlinear systems. These specific classes are well defined but are limited. A few of these nonlinear systems classes include Volterra series, Wiener and Hammerstein models.

The Volterra series represents mildly nonlinear systems as a series of multi-summations, or integrals in the continuous-time, of the Volterra kernels and inputs (Billings, 2013). Though Volterra series is used as a method of analysing nonlinear systems, it is challenging for SI due to the following:

- 1) Assumption on the number of terms and special inputs, which might not accurately define or be realistic for some real processes and
- 2) Large amount of data required to accurately give a good estimate.

This shortcomings brought about various forms of block-structured nonlinear models, which include wiener and Hammerstein models. The wiener model consists of a linear dynamic element followed by a static nonlinear element, which is considered to describe a wide range of nonlinear behaviour (Norquay *et al.*, 1998; Billings, 2013).

The Hammerstein model is the reverse combination where the static nonlinear characteristics is before the linear dynamic element. A combination of the block-structured models include sandwich models, where the static nonlinear model is between two linear models, and a Hammerstein-wiener model, where a linear model is between two static nonlinear models (Zhu, 2001; Billings, 2013). Too many assumptions are required on these forms of model to be fitted and if little prior knowledge on the system dynamics is known, application of such models will be inadequate to capture the system dynamics (Billings, 2013). This led to a new representation of a wide class of nonlinear systems, called Nonlinear Auto-Regressive Moving Average with eXogenous input (NARMAX), introduced by Billings and Leontaritis (1981).

2.3.2.2.1 NARMAX

The NARMAX model is defined as (Billings, 2013; Leontaritis & Billings, 1985):

$$y(t) = f(y(t-1), y(t-2), \dots, y(t-n_y), u(t-d), u(t-d-1), \dots, u(t-d-n_u), e(t-1), e(t-2), \dots, e(t-n_e) + e(t) \quad 2-1$$

Where $y(t)$, $u(t)$ and $e(t)$ are the system output, input and noise sequences respectively. n_y , n_u and n_e are the maximum lags for the system output, input and noise. $f(\cdot)$ represents a nonlinear function, which is generally unknown but can be approximated using various types of nonlinear forms and d is the time delay. This model is basically an expansion of the past outputs, inputs and noise terms. A standout attribute is the inclusion of past output terms in its expansion unlike the Volterra series model that expands the current output in terms of the past inputs only. Also, less data are needed to adequately estimate the system. Many existing linear and nonlinear model including ARX, ARMAX, Volterra and block-structured model can conveniently

be represented as subclasses of the NARMAX model. Many results and algorithms have been derived based on the NARMAX description.

There are many function expansions available to approximate the nonlinear function, $f(\cdot)$. A few of these expansions include polynomial models, rational models, wavelet expansion, radial basis function (RBF) networks. The most popular expansion is the polynomial model. This is due to the ease of implementation and the transparency of the model, which makes it possible to relate it to the underlying system. It is used to describe a wide range of nonlinear systems. NARMAX model can be represented in the polynomial form as:

$$\begin{aligned}
 y(t) = & \theta_0 + \sum_{i_1=1}^n f_{i_1}(x_{i_1}(t)) \\
 & + \sum_{i_1=1}^n \sum_{i_2=i_1}^n f_{i_1 i_2}(x_{i_1}(t), x_{i_2}(t)) + \dots \\
 & + \sum_{i_1=1}^n \dots \sum_{i_l=i_{l-1}}^n f_{i_1 i_2 \dots i_l}(x_{i_1}(t), x_{i_2}(t), \dots, x_{i_l}(t)) + e(t)
 \end{aligned} \tag{2-2}$$

Where l is the degree of polynomial nonlinearity.

$$f_{i_1 i_2 \dots i_l}(x_{i_1}(t), x_{i_2}(t), \dots, x_{i_l}(t)) = \theta_{i_1 i_2 \dots i_l} \prod_{k=1}^m x_{i_k}(t), 1 \leq m \leq l \tag{2-3}$$

$$x_m(t) = \begin{cases} y(t-m) & 1 \leq m \leq n_y \\ u(k - (m - n_y)) & n_y + 1 \leq m \leq n_y + n_u \\ e(t - (m - n_y - n_u)) & n_y + n_u + 1 \leq m \leq n_y + n_u + n_e \end{cases} \tag{2-4}$$

$\theta_{i_1 i_2 \dots i_m}$ are model parameters. Equation 2-2 can be explicitly written as

$$\begin{aligned}
y(t) = & \theta_0 + \sum_{i_1=1}^n \theta_{i_1} x_{i_1}(t) + \sum_{i_1=1}^n \sum_{i_2=i_1}^n \theta_{i_1 i_2} x_{i_1}(t) x_{i_2}(t) + \dots \\
& + \sum_{i_1=1}^n \dots \sum_{i_l=i_{l-1}}^n \theta_{i_1 i_2 \dots i_l} x_{i_1}(t) x_{i_2}(t) \dots x_{i_l}(t) + e(t)
\end{aligned} \tag{2-5}$$

A special case of the NARMAX model is the NARX model, where the noise dependent model terms are excluded. Thus, equation 2-4 becomes

$$x_m(t) = \begin{cases} y(t-m) & 1 \leq m \leq n_y \\ u(k - (m - n_y)) & n_y + 1 \leq m \leq n_y + n_u \end{cases} \tag{2-6}$$

The total number of potential model terms in the polynomial NARX model is

$$M = \frac{(n+l)!}{(n!l!)} \tag{2-7}$$

where $n = n_y + n_u$. The total number of potential model terms can be large, especially when the degree of nonlinearity is large. This increases the complexity of the model developed. The structure detection step in the NARMAX approach identifies significant model terms among the full candidate model terms that should be included in the model. Further details on other nonlinear function expansions can be found in relevant publications (Billings & Zhu, 1991, 1994; Billings & Wei, 2005; Billings, 2013).

2.3.2.2.1.1 Multiple-input multiple-output (MIMO) system

The solvent-based PCC plant is seen as a multivariable system due to the interactions between the various variables. The capture plant also has more than one input and output variables. Thus, the solvent-based PCC plant is best represented as a MIMO system. Previous sections have been focused on single-input single-output (SISO) system. The SISO system is easily extended to a MIMO system as follows:

$$\begin{aligned}
u_i^{[t-1]} &= [u_i(t-1), u_i(t-2), \dots, u_i(t-n_u)] \\
& \qquad \qquad \qquad i = 1, 2, \dots, r; j = 1, 2, \dots, s \qquad \qquad \qquad 2-8 \\
y_j^{[t-1]} &= [y_j(t-1), y_j(t-2), \dots, y_j(t-n_y)]
\end{aligned}$$

Where r is the number of input variables and s is the number of output variables. The NARX representation of MIMO system is shown below (Billings, Chen, & Korenbergs, 1989; Billings, 2013):

$$\begin{aligned}
y_1(t) &= F_1 [y_1^{[t-1]}, \dots, y_s^{[t-1]}, \dots, u_1^{[t-1]}, \dots, u_r^{[t-1]}] + e_1(t) \\
y_2(t) &= F_2 [y_1^{[t-1]}, \dots, y_s^{[t-1]}, \dots, u_1^{[t-1]}, \dots, u_r^{[t-1]}] + e_2(t) \\
& \qquad \qquad \qquad \vdots \\
y_s(t) &= F_s [y_1^{[t-1]}, \dots, y_s^{[t-1]}, \dots, u_1^{[t-1]}, \dots, u_r^{[t-1]}] + e_s(t)
\end{aligned} \qquad \qquad \qquad 2-9$$

Where $F_1[\cdot]$, $F_2[\cdot]$, ..., F_s are nonlinear functions that can be specified and implemented as a polynomial expansion. The models are obtained by estimating each model as a multiple-input single-output model (MISO) system.

2.3.2.2.1.2 NARMAX SI Approach

NARMAX SI approach includes several steps: (1) Identification tests or experiments, (2) Structure detection, (3) Parameter estimation, (5) Performance evaluation, which involves model validation, prediction and analysis. The identification test involves exciting and collecting control relevant information about the process dynamics and its surroundings (Ljung, 1987; Zhu, 2001). The process input is perturbed by sending carefully designed test signals, either pseudo-random binary sequence (PRBS), generalized binary noise (GBN) or filtered white noise and sum of sinusoids (Zhu,

2001). Details of the design of these input test signals can be obtained from Zhu, (2001) and Ljung, (1987). Data collected are used to estimate the best model fit. It is necessary that after data has been collected from the identification test, the data undergo a pre-treatment like peak shaving, signal slicing, high-pass and low-pass filtering and scaling & offset correction (Ljung, 1987; Zhu, 2001).

Model structure detection is the core part of NARMAX SI approach. This involves selection of significant model terms sequentially that can accurately capture the system dynamics. It is numerically efficient and will lead to simple parsimonious model that adequately describes the underlying dynamics (Billings, 2013). This is achieved by using the orthogonal least squares (OLS) algorithm and its derivatives (Billings *et al.*, 1988; Chen *et al.*, 1989), which include the forward regression with orthogonal least square algorithm (FROLS) (Wei *et al.*, 2004; Li *et al.*, 2013).

The FROLS algorithm has been widely discussed and applied in various literature (Billings *et al.*, 1989; Wei *et al.*, 2004; Billings, 2013). The FROLS algorithm essentially selects and ranks candidate model terms based on their significance for a system expressed as a linear in parameter model (Billings *et al.*, 1989; Wei *et al.*, 2004; Billings, 2013). A measure of significance for the candidate model terms is the error reduction ratio (ERR) criterion. ERR is a measure of the explained desired output variance increment for each model term (Wei *et al.*, 2004; Billings, 2013). Consider the linear in parameter model

$$y_s(t) = \sum_{j=1}^{M_s} \varphi_{sj} x_{sj}(t) + e_s(t) \quad 2-10$$

where $y_s(t)$, $x_{sj}(t)$, φ_{sj} and M_s , with $(s = 1,2,3; j = 1,2, \dots, M_s)$, are the response signal (output), regressors, model parameter and number of model terms. Equation 2-10 can be written in a compact form as:

$$Y = P\Phi + \xi \quad 2-11$$

where $Y = [y(1), y(2), \dots, y(N)]^T$ is the measured output vector at N time instants, $P = [P_1, P_2, \dots, P_M]$ is a matrix whose j th column $P_j = [P(1), P(2), \dots, P(N)]^T$ is a vector formed by the j th candidate model term φ_j , with $j=1, 2, \dots, M$. $\Phi = [\theta_1, \theta_2, \dots, \theta_M]^T$ is the parameter vector and ξ is the modelling error vector. M is the number of candidate model terms (or the number of candidate basis vectors). The regression matrix P is assumed to be full rank in columns and can be orthogonally decomposed as

$$P = WA \quad 2-12$$

where A is an $M \times M$ unit upper triangular matrix and W is an $N \times M$ matrix with orthogonal columns w_1, w_2, \dots, w_M . It should be noted that the condition for the above assumption is that the data collected for identification contains sufficient information on the process dynamics. This is by ensuring the data is large enough and sampled correctly. Equation 2-12 can be expressed as:

$$Y = (PA^{-1})(A\Phi) + \xi = WG + \xi \quad 2-13$$

where $G = [g_1, g_2, \dots, g_M]^T$ is an auxiliary parameter vector, which is calculated from Y and W by means of orthogonality property as follows:

$$g_i = \frac{\langle Y, w_i \rangle}{\langle w_i, w_i \rangle} \quad 2-14$$

with $i=1, 2, \dots, M$, the parameter vector Φ is related by the equation $G = A\Phi$. The error reduction ratio (ERR), which provides an effective means for seeking in a subset of significant model term, is calculated as

$$ERR_i = \frac{\langle Y, w_i \rangle^2}{\langle Y, Y \rangle \langle w_i, w_i \rangle} \times 100\% \quad 2-15$$

The significant model terms are selected in a forward-regression pattern as shown in the algorithm steps (Wei *et al.*, 2004; Billings, 2013):

Step 1: $= [P_1, P_2, \dots, P_M], \sigma = y^T y$.

For $m = 1, 2, \dots, M$, calculate

$$P_m = w_m$$

$$g_m^{(1)} = \frac{y^T w_m}{w_m^T w_m}$$

$$ERR^{(1)}[m] = \frac{(y^T w_m)^2}{\sigma (w_m^T w_m)} \times 100\%$$

$$l^{(1)} = \arg \max_{1 \leq m \leq M} \{ERR^{(1)}[m]\}$$

End

$$a_{11} = 1$$

$$w_1 = w_{l_1}$$

$$g_1 = g_{l_1}^{(1)}$$

$$err[1] = ERR^{(1)}[l_1]$$

Step s ($s \geq 2$): let $m \neq l_1, m \neq l_2, \dots, m \neq l_{s-1}$,

For $m = 1, 2, \dots, M$, calculate

$$w_m^{(s)} = P_m - \sum_{i=1}^{s-1} \frac{P_m^T q_i}{q_i^T q_i} q_i, P_j \in D - D_{m-1}$$

$$g_m^{(s)} = \frac{y^T w_m^{(s)}}{(w_m^{(s)})^T w_m^{(s)}}$$

$$ERR^{(s)}[m] = \frac{(y^T w_m^{(s)})^2}{\sigma((w_m^{(s)})^T w_m^{(s)})} \times 100\%$$

$$l^{(s)} = \arg \max_{1 \leq m \leq M} \{ERR^{(s)}[m]\}$$

End

$$w_s = w_{l^s}^{(s)}$$

$$g_s = g_{l^s}^{(s)}$$

$$err[s] = ERR^{(s)}[l^s]$$

$$a_{i,s} = \frac{(w_i^T P_{l^s})}{(w_i^T w_i)}, i = 1, 2, \dots, s-1$$

$$a_{ss} = 1$$

Parameter vector, Φ , is calculated $A\Phi = G$, where $G = [g_1, g_2, \dots, g_{M_0}]^T$ and A is defined as:

$$A = \begin{bmatrix} 1 & \cdots & a_{1M_0} \\ \vdots & \ddots & \vdots \\ 0 & \cdots & 1 \end{bmatrix}$$

Determination of the number of model terms is important for dynamic modelling and various model selection criteria have been proposed in the literature. In this study, the

Bayesian information criterion (BIC) is used to determine the number of model terms (Wei & Billings, 2009).

$$BIC(n) = \left[1 + \frac{n \ln(N)}{N - n} \right] MSE(n) \quad 2-16$$

where N is the number of samples in the training data set, n is the effective number of model terms, $MSE(n)$ is the mean square error associated with the n -terms model.

BIC is commonly used to avoid over-fitting through the penalty factor $\left[\frac{n \ln(N)}{N - n} \right]$.

The performance of identified models is evaluated based on the prediction efficiency and statistical analysis. The model prediction performance can be categorised into the one-step-ahead (OSA) prediction and multi-step prediction output (MSP). The OSA prediction performance is primarily based on the mean squared error validation methods and might give a misleading performance, making it not sufficient to give a reliable assertion on the performance of the identified model. MSP performance, on the other hand, will help detect the quality of the identified model by exposing the built-up errors with the identified model (Akinola et al., 2019). Only the first few known measured data are used to initialise the model. Prediction efficiency of the identified models is calculated as:

$$VAF = \left[1 - \frac{\text{var}(y_{measure} - y_{predict})}{\text{var}(y_{measure})} \right] \times 100\% \quad 2-17$$

where $y_{measure}$ is the measured output of the test data and $y_{predict}$ is the one-step-ahead prediction/ multi-step prediction output.

Statistical analysis involves the evaluation of the identified model in terms of R , R^2 and adjusted R^2 of the identified models. R , which is the multiple correlation coefficient, is a measure of how much the combination of model terms in each identified model

correlates with the respective output variables. The multiple correlation coefficient, R , value is within the range 0 and 1. As the R -value is closer to 1, this indicates that the input and output variables are highly correlated. When the R -value is closer to 0, the input and output variables are not correlated. The R^2 represents the portion of variance in the response variable that is explained by the combination of model terms, while the adjusted R^2 is a measure of the accuracy of a model across different samples. R , R^2 and adjusted R^2 are calculated as follows:

$$R = \frac{N \sum y_{measure} y_{predict} - \sum y_{measure} \sum y_{predict}}{\sqrt{N \sum y_{measure}^2 - (\sum y_{measure})^2} \sqrt{N \sum y_{predict}^2 - (\sum y_{predict})^2}} \quad 2-18$$

$$R^2 = 1 - \frac{SSE}{SST} \quad 2-19$$

$$R_{adj}^2 = 1 - \left(\frac{N-1}{N-n} \right) \frac{SSE}{SST} \quad 2-20$$

Where $y_{measure}$ is the measured output; $y_{predict}$ is the multi-step prediction (MSP); SSE is the sum of squares error; SST is the total sum of squares; N is the number of observations and n is the number of model terms.

2.3.2.3 Current status on SI of PCC process plant

The application of SI approach for the modelling solvent-based PCC plant is beginning to gain much attention (Wu *et al.*, 2010; Dunia *et al.*, 2011; Zhou *et al.*, 2012; Arce *et al.*, 2012; Li *et al.*, 2015; Luu *et al.*, 2015; Manaf *et al.*, 2016). This is due to the ease of implementation compared to the first principles model, which requires a lot of computational time. The complexity of the first principles model also limits its use for process control strategy.

At early years, the SI technique was adopted to obtain a linear model that represents the solvent-based PCC plant using Matlab[®] for controllability study and process control implementation. Arce *et al.* (2012) focused on the application of advanced control strategies for flexible operation of the solvent regeneration system and developed linear transfer function models to represent the regeneration system. Data were collected from a first principles model. The identified model were shown to duplicate the dynamic behaviour of the solvent regenerative system. Luu *et al.*, (2015) also used a linear first order plus delay time (FOPDT) transfer function model to represent the PCC system as 4 (inputs) x 3 (outputs) MIMO model for controllability study. The MIMO model contains a series of sub-models, which are SISO models. Step input signals were sent to the input variables while the output variables were recorded (Luu *et al.*, 2015). Data collected were fitted into the FOPDT transfer function model structure (Luu *et al.*, 2015). It should be noted that for these studies and others, the input variable signals were carefully developed to not excite the nonlinearity within the capture process. The step input signal used in Luu *et al.*, (2015), for example, linearizes the nonlinearity within the system. However, a major concern is the inability of the identified linear model to adequately capture the nonlinear dynamics of the PCC plant, as it is known that the PCC plant exhibits nonlinear dynamics (Manaf *et al.*, 2016; Wu *et al.*, 2018) . Thus, the need for nonlinear SI is vital.

In the quest to obtain an accurate model to capture underlying dynamics of the PCC plant, Li *et al.*, (2015, 2017) used bootstrap aggregated neural networks, which is a form of non-parametric SI, to develop a PCC model. These studies indicated that the neural network model, developed using data collected from a first principles model, could accurately predict the CO₂ capture rate and CO₂ capture level. Li *et al.*, (2017) included an extreme learning machine feature to the bootstrap aggregated neural

network, which assigns weights between the input and hidden layers and obtains weights between the hidden and output layer. Although this gave a major improvement to the model developed, the computational burden is increase for optimisation studies and NMPC implementation due to complexity of the model as a result of the large number of hidden neurons.

Manaf *et al.*, (2016) developed a mathematical model of an amine-based PCC plant using nonlinear ARX SI approach. The amine-based PCC plant was characterized as a multivariable 4 x 3 black-box model under wavelet nonlinearity class to capture the nonlinearity within the model. In this study, the nonlinear SI was carried out for major equipment within the amine-based PCC plant such as the absorber, heat exchanger and stripper individually using the SI Matlab[®] toolbox. The models obtained were then linked using Simulink software package. This is to observe interactions between the input and output variables of each model. Data were obtained from PCC pilot plant. The study showed that the identified model gave a similar PCC dynamic behaviour compared to the pilot plant. It should be noted that the prediction performance of the identified model was evaluated based on one-step-ahead (OSA) prediction. OSA prediction is not sufficient to give a reliable assessment of the prediction performance of the identified model. In addition, the model order was assumed. This might result in obtaining models that are complex or omission of relevant model terms. However, the SI approach with the use of FROLS algorithm helps to determine the simplest model that capture adequately the underlying dynamics of the capture process.

2.3.3 Summary

Dynamic (first principles) models are necessary to carry out comprehensive dynamic studies on the capture plant and optimize operational procedure for dynamic periods within the capture plant. The rate-based modelling approach is considered to give a more accurate result compared to the equilibrium based modelling. Model validation with dynamic data from pilot plant is essential to ensure model accuracy and reliability.

Analysis from literature indicates that the solvent-based PCC plant is a much slower process compared to the power plant and an appropriate control strategy is essential to minimize constraints on the power plant. The implementation of process control strategies requires simplification of the first principles solvent-based PCC model to reduce the computational time for simulation, which has resulted in the emergence of data-driven modelling approach through SI. The SI approach, which involves estimating a model from the process operational data, enables the control implementation. Various researchers adopted the SI approach to estimate linear model, which is only valid around its operating points. This linear identified model does not capture the nonlinearity within the capture plant. Just a few papers have focused on the use of nonlinear SI approach to estimate the solvent-based PCC process. In these studies, the model order was assumed. This assumption might result in including or omitting model terms that are relevant to the process output accuracy. However, the nonlinear SI approach with the use of FROLS algorithm helps to determine the adequate model terms that best capture adequately the underlying dynamics of the capture process.

2.4 Process Control System Design for PCC Plant: Multivariable System

The control system design involves control structure selection, controller selection and controller design and tuning. This section reviews previous studies on the control system design of a solvent-based PCC process.

The complex nature of the chemical process plants like the solvent-based PCC plant has prompted the need to implement an appropriate control philosophy focused mainly on structural decisions in the control system design. Control structure selection mainly involves selection of both primary and secondary controlled variables, selection of manipulated variables, selection of measurements, selection of control configuration and selection of controller type (Skogestad, 2004). Control structure can be generally categorised into decentralised and centralised control structure (Skogestad & Postlethwaite, 2007).

Figure 2-3 shows a control hierarchy system in a chemical plant. The regulatory control layer, which mainly contains SISO feedback and feedforward control loops, control the process to reach its steady-state. The supervisory control layer assigns set points for the individual control loops within the regulatory control layer. The supervisory control layer's purpose is to keep the primary controlled output variables at optimal set points. The local and site-wide optimization assigns the optimal set-points for the supervisory control layer based on economic and environmental factors. This local and site-wide optimization are beyond the scope of this research.

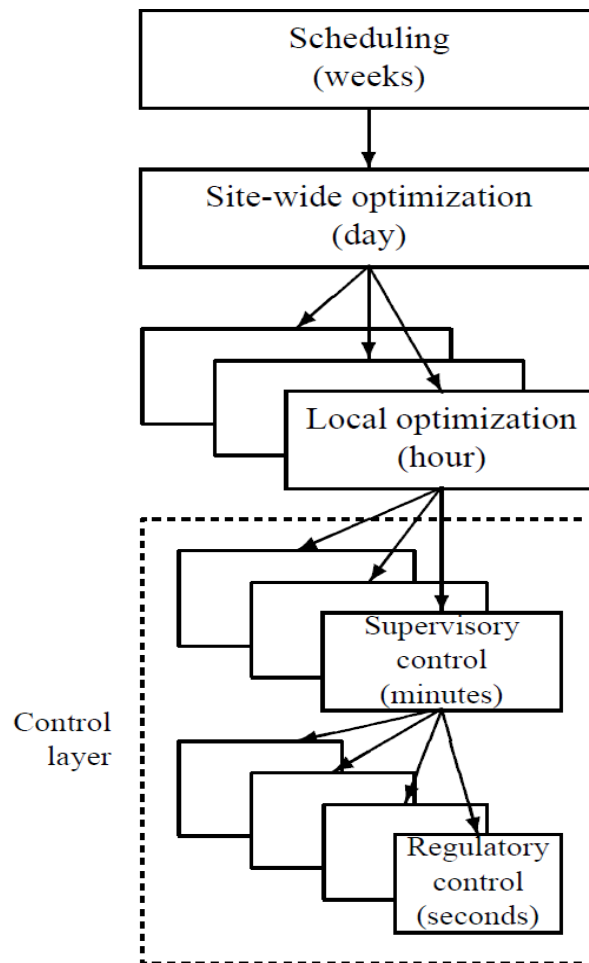


Figure 2-3 Control Hierarchy system in a chemical plant (Skogestad, 2004)

The selection of controlled variables entails selecting variables to be controlled at given set points, which are assigned at a higher layer in the control hierarchy system. Control configuration selection mainly involves selecting the appropriate pair of controlled and manipulated variables so that there are no limiting/conflicting interactions within the control system. The pairing of input-output variables is determined through either relative gain array (RGA) or insight from the process dynamics (process oriented).

2.4.1 Control structure configuration

There are two major approaches to implement the control structure configuration which are mathematically oriented approach and process-oriented approach (Larsson & Skogestad, 2000).

2.4.1.1 Mathematical oriented approach

The mathematically oriented approach is a two-stage method, which are Top-down and bottom-up analysis (Skogestad, 2004). Details of this approach can be obtained in Skogestad, (2004). For the mathematical oriented approach, the input-output pairing is determined using the RGA analysis. The RGA is a variable pairing tool proposed by Bristol, (1966). RGA is a measure of the SISO control loop interactions in a control structure. The RGA is a dimensionless matrix. This is defined as:

$$\lambda_{ij} = \frac{\left(\frac{\delta c_i}{\delta m_j}\right)_m}{\left(\frac{\delta c_i}{\delta m_j}\right)_c} = G_{p,ij}(s) \cdot (G_p^{-1})_{ij}^T(s) \quad \text{For } i, j = 1, 2, \dots, N \quad 2-21$$

RGA are unaffected by scaling and provide a quantitative comparison of how each manipulated variable affects each controlled variable.

2.4.1.1.1 Niederlinski Index (NI) and Morari Index of Integral controllability (MIC)

Niederlinski Index (NI) and Morari index of integral controllability (MIC) analyses the stability of the selected control loop pairings at steady state ($s=0$). NI is calculated as follows:

$$NI = \frac{\det(G_p(0))}{\prod_{i=1}^N G_{P,ii}(0)} \quad 2-22$$

For all the SISO controllers that have positive loop gains and contains integral action, a negative NI indicates that the control structure will be closed-loop unstable. Thus, any input-output pairing with negative NI should be eliminated.

MIC is calculated as

$$MIC = \lambda_{G_p^+(0)} \quad 2-23$$

Where $\lambda_{G_p^+(0)}$ is the vector of the eigenvalues of the process at steady state $G_p^+(0)$. This is obtained by adjusting the signs so that all the diagonal elements are positive. Just as NI, a negative $\lambda_{G_p^+(0)}$ will give an unstable control configuration, for all SISO controllers containing positive loop gains and integral action. Thus, a configuration with a negative MIC is to be eliminated.

2.4.1.2 Process Oriented approach

The process-oriented approach, which is mostly implemented in the process industry, designs the control structure based on insight gained from the process dynamics (Nittaya *et al.*, 2014b). Details on the approach can be seen in publications (Luyben *et al.*, 1997; Larsson & Skogestad, 2000; Nittaya *et al.*, 2014b). In this thesis, both approaches were explored to select the appropriate control configuration.

2.4.2 Type of Control

2.4.2.1 Traditional PID control

The traditional Proportional –Integral –Derivative controller is a feedback control loop mechanism widely adopted in industrial control system (Khare & Singh, 2010). The transfer function of the basic form of PID controller is (Stephanopoulos, 1984)

$$G_c(s) = K_c \left(1 + \frac{1}{\tau_I s} + \tau_D s \right) \quad 2-24$$

Where K_c is the proportional gain of the controller; τ_I is the integral time constant and τ_D is the derivative time constant (Stephanopoulos, 1984). Thus, the control input (u) the process plant from the controller is given as:

$$u(t) = K_c e(t) + \frac{K_c}{\tau_I} \int_0^t e(t) dt + K_c \tau_D \frac{de}{dt} \quad 2-25$$

Variation of the PID control include P controller, PI controller and PID controller. In most industrial feedback control applications, PI controller is mostly adopted, where the derivative time constant is zero. The different approaches for tuning the PID control parameters include open-loop tuning, closed-loop tuning and model-based tuning. Further details on PID tuning can be found in relevant literature (Luyben, 1986; Lee & Edgar, 2005; Vu & Lee, 2010). Major characteristics of the closed-loop step response that assess the control performance and robustness include (Poorani & Anand, 2013; Stephanopoulos, 1984):

- rise time (i.e. time required for the plant output to rise beyond 90% of the desired level for the first time),
- overshoot (i.e. how much the peak level is higher than the steady-state, normalized against the steady-state) and
- Settling time (time for the system to attain its new steady-state).

2.4.2.2 Model Predictive Control

Model predictive control (MPC) is majorly adopted for the centralised control scheme. The multivariable control approach requires an accurate process model to predict explicitly the output (Camacho & Alba, 2013). The control actions of the manipulated

variables are determined to minimize the objective function formulated (Camacho & Bordons, 2012; Camacho & Alba, 2013). The application of MPC controllers in the process industry has been successful despite the difficulty in implementing them compared to the PID controller. Extensive reviews on various MPC strategy development and implementation in the process industry are available in literature (Marco *et al.*, 1997; Roberts, 2000; Grancharova & Johansen, 2004; Bequette, 2007; Camacho & Bordons, 2007; Garriga & Soroush, 2010; Al-Gherwi *et al.*, 2011).

2.4.3 Current Status on Control system design on solvent-based PCC process

Extensive studies on control system design and implementation of a solvent-based PCC process have been carried out. This mainly includes decentralised and centralised control schemes (Lin *et al.*, 2011, 2012; Panahi & Skogestad, 2011, 2012; Nittaya *et al.*, 2014b).

For decentralised control scheme, Lin *et al.*, (2011) investigated a plant-wide control of a solvent-based PCC process using dynamic simulation on Aspen Plus[®] dynamics. The publication came up with a multi-loop control structure, CO₂ removal percentage – lean solvent flowrate, reboiler liquid level – make-up water flowrate and reboiler temperature – reboiler duty. The decision was informed by preliminary analysis carried out to understand the process dynamics. Results from dynamic simulation revealed that the set point target (CO₂ removal percentage) was attained under disturbances (flue gas flowrate, CO₂ concentration and H₂O concentration) while the optimum lean loading is kept fixed. Using reboiler duty as a manipulated variable to control reboiler temperature seems impractical in a real capture plant making the control scheme infeasible. Lin *et al.*, (2012) compared two control scheme, variation of lean solvent flow (VLSF) and variation of lean solvent loading (VLSL) using a scaled-up capture plant integrated with a power plant steam cycle. It was concluded that VLSL control

scheme was preferable because it is able to maintain stable hydraulics in both packed columns within the capture plant during flexible operation. The unavailability of competent and efficient CO₂ loading measuring instrument makes the VLSL control scheme difficult to be implemented on a real capture plant.

Panahi & Skogestad, (2011,2012) adopted the mathematical oriented approach proposed by Skogestad, (2004) to develop control schemes for a solvent-based PCC plant. Panahi & Skogestad, (2011) adopted a self-optimizing method to select the best-controlled variables (CVs) under three different operational regions (low, mid and high flue gas flowrate). Panahi & Skogestad, (2012) later proposed four control schemes based on a plant-wide approach. The publication concluded that the dynamic performance of best control scheme was comparable to MPC and was preferred due to its simplicity in implementation.

Nittaya *et al.*, (2014b) proposed three process control structures for the PCC dynamic model developed by Harun *et al.*, (2011). The first control structure was designed based on the RGA analysis while the other two control structures were designed based on process heuristics approach. Performance evaluation of the control structure reveals that although the control objectives were attained with each structure, the second control structure (pairing CO₂ removal percentage with solvent flowrate and reboiler temperature with reboiler duty) gave a better performance than other control structures. Nittaya *et al.*, (2014b) also highlighted that the control structure designed based on RGA analysis gave a poor performance because the analysis does not consider the process dynamics.

Performance evaluation by Sahraei & Ricardez-Sandoval, (2014) on two control structures (decentralized multi-loop control structure and centralised MPC control structure) based on set point tracking and disturbance rejection indicated that the

centralised MPC control structure recovered faster than the decentralised control structure. Control configuration (input-output variables pairing) within the decentralised control structure to minimize interactions between the loops were based on RGA analysis

Manaf *et al.*, (2016) proposed a decentralised control structure based on RGA and MIC analysis. Findings from the multivariable control analysis (RGA and MIC) suggested that CO₂ capture efficiency was controlled by lean solvent flowrate and energy performance was controlled by reboiler heat duty, which is similar to what was proposed by Nittaya *et al.*, (2014b)

Gaspar *et al.*, (2016) adopted a similar approach with Sahraei & Ricardez-Sandoval, (2014) to develop a decentralized control structure comparing the capture process with MEA with the capture process with PZ. They concluded that the PZ- based capture process could reject more disturbances with less room for change in the manipulated variables. For the decentralised control structure, PI controllers is implemented for each loop pairing (Panahi & Skogestad, 2011; Lin *et al.*, 2012; Ziaii, 2012; Nittaya *et al.*, 2014a,2014b; Sahraei & Ricardez-Sandoval, 2014; Luu *et al.*, 2015; Manaf *et al.*, 2016). The benefit of multivariable PI controller includes its simplified implementation & design, fault tolerance and flexible operability(Jones & Hengue, 2009). However, it should be noted that the implementation of PI control on a multivariable system could be extremely problematic depending on the level of process interactions within the system especially during large load changes or disturbances. Findings from Sahraei & Ricardez-Sandoval, (2014) exposes issues with the decentralised control scheme with PI controller in comparison with multivariable MPC control scheme. MPC control scheme recovered faster than the decentralised control scheme. The issue of process loop interactions can be

suppressed by adding de-couplers to the control system, which might complicate the PID tuning (Jones & Hengue, 2009). Another alternative is to implement a multivariable centralised controller such as MPC or NMPC to handle the interactions within the process adequately.

There are several studies on multivariable centralised control scheme design and implementation on the solvent-based PCC process. Most of these studies focused on the implementation of MPC scheme (Panahi & Skogestad, 2012; Sahraei & Ricardez-Sandoval, 2014; Mehleri *et al.*, 2015; Luu *et al.*, 2015; He *et al.*, 2016; Wu *et al.*, 2018, 2019). The MPC scheme utilizes a linear model to predict the system dynamics (Findeisen & Allgöwer, 2002). Performance evaluation comparison with decentralised multi-loop control scheme showed that the MPC scheme gave a better and faster performance (Sahraei & Ricardez-Sandoval, 2014; Luu *et al.*, 2015; Wu *et al.*, 2018). However, the solvent-based PCC process is inherently nonlinear (Manaf *et al.*, 2016). In addition, the CO₂ capture process might have to run at extremely tight specification due to stringent environmental restrictions as well as the large load variation during flexible operation because of demanding economic considerations. For this case, the CO₂ capture process might operate outside the boundary where the linear model is not able to adequately predict the process dynamics and the nonlinear model is needed (Findeisen & Allgöwer, 2002). This motivates the use of nonlinear model predictive control (NMPC).

Only a few studies on NMPC design and implementation for the solvent-based PCC process are available in literature (Åkesson *et al.*, 2012; Zhang *et al.*, 2018; Hauger *et al.*, 2019). Åkesson *et al.*, (2012) implemented NMPC scheme on a solvent-based PCC process using first principles model developed by Pröhl *et al.*, (2011) in

modelica[®]. The high computational time and complexity of the model limited its application online. This has led to the need for the simplification of the solvent-based PCC model for NMPC implementation. Zhang *et al.*, (2018) implemented NMPC scheme on a nonlinear additive autoregressive with exogenous input (NAARX model). In this publication, the nonlinear model was assumed to be first-order model with cross terms. Results revealed that the NAARX model could not accurately predict the output of the dynamic simulation for a wide operating range. The performance of the NMPC scheme is largely dependent on the accuracy of the nonlinear model used. The FROLS-EER algorithm could be implemented to select model terms that best described the capture process dynamics for the nonlinear model development, which improves the accuracy of the model. Thus, studies on the design, implementation and performance evaluation of NMPC scheme on a solvent-based PCC process in comparison with linear controller (PI and MPC) using model developed through FROLS-ERR algorithm should be explored.

2.5 Summary

This chapter reviewed various research aspects of the solvent-based post-combustion CO₂ capture process. This includes reviews on pilot plants, commercially deployed CO₂ capture plant, model development (first principles and data-driven approach) and process control system design of the CO₂ capture process. The concluding remarks are as follows:

- Extensive R&D on the solvent-based PCC pilot plants have been carried out. In addition, only two (2) commercial large-scale solvent-based PCC plants attached to a power generation plant are operational. However, the limitations on the process modification of the pilot-scale plant highlight the relevance of model development and simulation.

- Extensive studies have been carried out on the model development of the process via the first principles approach. The limitation of high computational time and high complexity has resulted in the need for a simplified model for process control design and implementation. This has brought about the need for model development via a data-driven approach.
- Most studies represented the solvent-based PCC as a linear model. However, the capture process exhibits highly nonlinear behaviour (Manaf *et al.*, 2016; Wu *et al.*, 2018) and the linear model tends to deviate when it exceeds the linear operating region boundary. This highlights the need for the development of a nonlinear model through SI to accurately capture the dynamics of the solvent-based PCC process.
- Few studies on the nonlinear SI of the solvent-based PCC were based on assuming the model order (mostly first order). This assumption might result to inclusion of model terms that do not have significant effect on the process output. Thus, making the model complex and affecting the accuracy of the model.
- The FROLS algorithm can determine the important model regressors (model terms), in a stepwise manner, based on their significance. To our knowledge, the advantages and potentials of nonlinear SI techniques, especially dynamic NARMAX models identification with the FROLS-ERR algorithm, have not been explored for solvent-based PCC process.
- Increased power generation from renewable energy source and stringent environmental regulations (such as attaining the CO₂ emission reduction targets) has resulted in the need for extensive study of the NMPC scheme on the solvent-based PCC process to handle process interactions within the

capture process, in response to large power plant load variation, during flexible operation.

- Comparison between linear controllers (e.g. PI and MPC) using the model developed through FROLS-ERR algorithm and nonlinear controller has not been performed.

3 Non-linear SI of solvent-based post-combustion CO₂ capture process¹

3.1 Introduction

This chapter describes a nonlinear SI approach for the solvent-based PCC process using the forward regression orthogonal least-squares - error reduction ratio (FROLS-ERR) algorithm. The solvent-based PCC process is represented using a nonlinear autoregressive with exogenous input (NARX) model. The FROLS algorithm was adopted to develop a transparent NARX model that captures the relationship between the input variables and output variables in the PCC process. The algorithm was used to identify and rank key model terms that contribute to the response variable based on the ERR and eliminate model terms with the least contribution to the system output. The FROLS-ERR algorithm has been extensively used in the literature (Macedo *et al.*, 2015 ;Dantas *et al.*, 2016) as an effective SI technique for different systems. The required process operation data for performing SI were obtained through simulation using a detailed and validated first principles model of a solvent-based PCC process implemented in gPROMS Model Builder[®]. Section 3.2 provides a summary of the first principles dynamic model of the solvent-based PCC process developed in gPROMS Model Builder[®]. Sections 3.3 and 3.4 focused on the process data acquisition from the gPROMS[®] model and the SI implementation using the data acquired. Performance evaluation as well as process dynamic analysis was carried out using the identified model developed in sections 3.5 and 3.6.

¹ Most of this Chapter has been published in Akinola, T. E., Oko, E., Gu, Y., Wei, H.-L., & Wang, M. (2019). Non-linear system identification of solvent-based post-combustion CO₂ capture process. *Fuel*, 239, 1213–1223

3.2 The first principles dynamic model for solvent-based PCC process

The first principles model of the solvent-based PCC process was developed by Lawal *et al.*, (2010) and validated dynamically in Biliyok *et al.*, (2012). The process has an absorber and a regenerator as the major unit operations (see Figure 1-6).

For the absorber and regenerator model, the mass transfer are described using two-film theory (rate-based approach). Thus, the vapour-liquid interaction is categorised into five regions, which are bulk liquid, liquid film, bulk vapour, vapour film and vapour-liquid interface region (Oko, 2015).

The vapour and liquid bulk region was described using one-dimensional distributed energy and mass conservation equations. In the bulk vapour model, energy and mass hold-ups were neglected due to the relatively small vapour phase residence time in the absorber compared with the liquid phase residence time. In addition, it is assumed that the chemical reactions of CO₂ with MEA takes place only via liquid phase reactions within liquid film. Thus, the heat of absorption is only accounted for in the liquid film. Lawal *et al.*, (2010) used the Maxwell–Stefan formulation to determine the mass fluxes of components in both the vapour and the liquid film. The mass transfer coefficients in the liquid and vapour films were determined by correlations given by Onda *et al.*, (1968).

Mass and energy hold-up in the liquid and vapour film region was not accounted for (Oko, 2015). The interface model is based on the equilibrium between liquid and vapour phases (Oko, 2015). The equilibrium molar compositions of the components in the vapour and liquid phases are estimated based on the vapour and liquid fugacity coefficients. The CO₂-MEA-H₂O reactions are assumed to reach equilibrium at the interface. This assumption is reasonable for a

fast-reacting solvent such as MEA. Additional assumptions made include plug flow regime, linear pressure drop along the column, and negligible solvent degradation (Oko, 2015). Heat loss to the regenerator surroundings is taken into consideration while the heat loss around the absorber is neglected. This is because of the regenerator higher operating temperature (up to 120°C) compared with the absorber (40°C-70°C) (Oko, 2015).

Lawal *et al.* (2010) carried out the physical property estimation using Multiflash physical property package for estimation of viscosities, enthalpies and densities, while the fugacity coefficient calculations in the reboiler and condenser were estimated using the Electrolyte Non-random-two-liquid (NRTL) model. The absorber was linked to the regenerator by including the following auxiliary unit operation models: Lean MEA storage Tank; Rich MEA pump; Lean/Rich MEA heat Exchanger; Lean MEA cooler. Modelling details of each auxiliary unit operation can be seen in Biliyok *et al.*, (2012b) and Lawal *et al.*, (2010, 2012).

3.3 Process data acquisition

3.3.1 Selection of Input and Output Variables

The input and output variables were selected based on the control objectives of the solvent-based PCC process. The input variables are manipulated variables and measured disturbance(s) while output variables are controlled variables. The key control objective in the capture process is to minimize energy consumption while maintaining environmental regulations (maintaining corresponding CO₂ capture level) at varying operating conditions through a flexible control strategy, especially when a disturbance is introduced to the system.

The output variables were selected based on control requirements of the solvent-based PCC process highlighted above. Key variables sensitive to the control objectives are CO₂ capture level and solvent regeneration energy. The CO₂ capture level (CCL) is expressed mathematically as follows:

$$\text{CO}_2 - \text{CL}(\%) = \left(1 - \frac{n_{\text{CO}_2}^{\text{ABSout}} \times F_{\text{FG}}^{\text{ABSout}}}{n_{\text{CO}_2}^{\text{ABSin}} \times F_{\text{FG}}^{\text{ABSin}}} \right) \times 100\% \quad 3-1$$

where, $n_{\text{CO}_2}^{\text{ABSout}}$, $F_{\text{CO}_2}^{\text{ABSout}}$, $n_{\text{CO}_2}^{\text{ABSin}}$, $F_{\text{CO}_2}^{\text{ABSin}}$ are CO₂ mass fraction at the absorber gas outlet, flue gas flowrate at the absorber gas outlet, CO₂ mass fraction at the absorber gas inlet and flue gas flowrate at the absorber gas inlet respectively. For this study, the capture level is selected as a key output variable (CO₂ -CL).

The solvent regeneration energy, which accounts for the bulk of the energy consumption, is a measure of energy utilised in the regenerator, where most of the energy consumption takes place, thus dictates the operational cost of the capture process. The solvent regeneration energy is mathematically expressed as:

$$\text{RE} \left(\frac{\text{MJ}}{\text{kg}_{\text{CO}_2}} \right) = \frac{Q_r}{F_{\text{CO}_2_regen_vap_outlet}} \quad 3-2$$

Where Q_r and $F_{\text{CO}_2_regen_vap_outlet}$ are reboiler duty and CO₂ mass flowrate at the regenerator outlet. A good measure of the regeneration energy is the reboiler temperature. For this study, the reboiler temperature (Y_2) was selected as an output variable. This is due to ease of measurement in real-time. In addition, controlling the reboiler temperature is relevant to limiting solvent degradation in the reboiler (Davis & Rochelle, 2009). Hence, a safe and reliable operation of the capture process is guaranteed.

The selection of input variables was based on the principle that key input variables should have a significant effect on the output variables via step analysis of the first principles model available in literature (Lawal *et al.*, 2010). Key input variables selected for this study includes flue gas flowrate, lean solvent flowrate and steam flowrate. Thus, the solvent-based PCC process was represented as a 3-input and 2-output system.

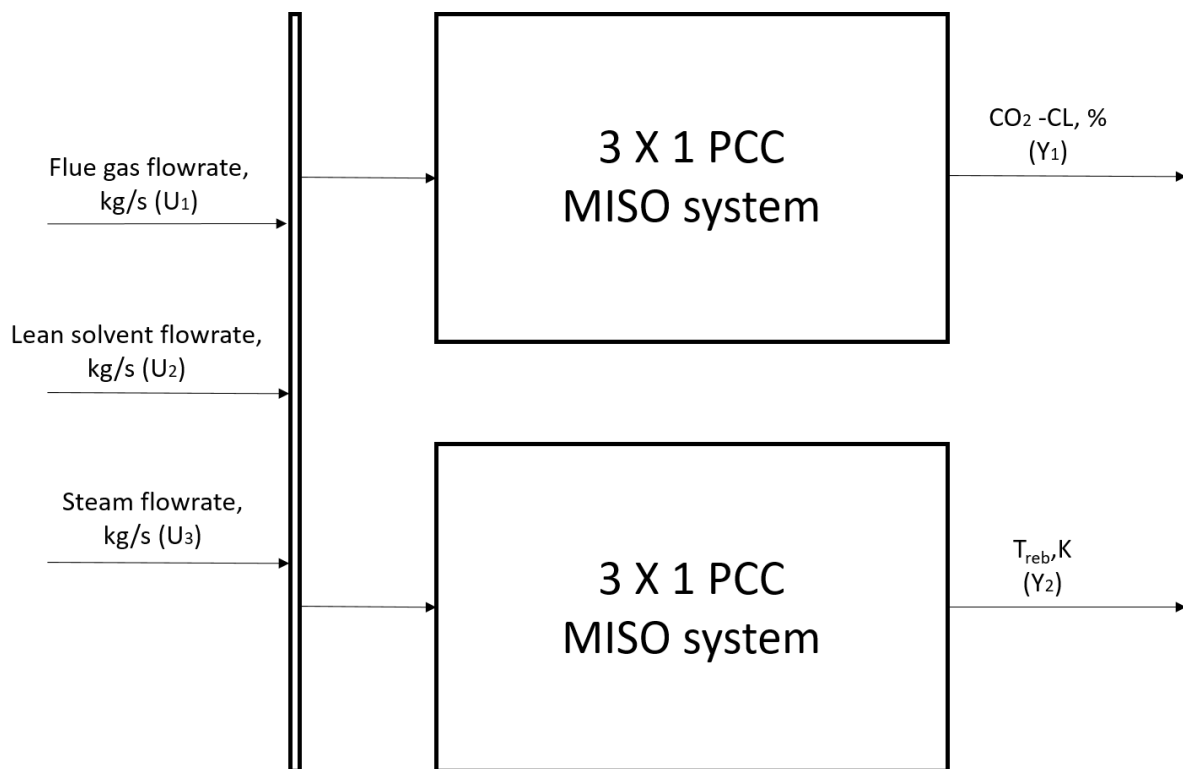


Figure 3-1 Multiple Input Single Output MEA based PCC Model

3.3.2 Input signal design and Data Collection

The input signals for each input variable were designed to cover a wide amplitude range and frequency bandwidth capturing the PCC process nonlinear dynamics. For a multivariable system like the solvent-based PCC process, it is essential that the input signal is designed so that the system is excited in all gain directions (more importantly

the weak gain direction) to limit the relative uncertainties associated with gain directions (Hägglom & Böling, 1998). Uniformly distributed random noise signals were developed for each input variable. The range for each input variable as well as signal characterization based on the crest factor (CF) and performance index for perturbation signals (PIPS) are shown in Table 3-1. These parameters give measurement of the goodness of the energy distribution along the span of the signal.

Table 3-1 CF and PIPS for each input variable

| Input variable | range | Crest Factor (CF) | PIPS (%) |
|------------------------------|-----------------------|--------------------------|-----------------|
| Flue gas flowrate, u_1 | 0.12kg/s – 0.2kg/s | 2.137 | 51.562 |
| Lean solvent flowrate, u_2 | 0.66kg/s – 0.86kg/s | 1.579 | 64.117 |
| Steam flowrate, u_3 | 0.024kg/s – 0.063kg/s | 1.877 | 56.842 |

Each signal was sent to each input variable simultaneously at a sample time of 60s. The gPROMS[®] model was run for a simulation period of 86400s (24hr) to get 1440 data set. Data obtained were carefully observed and outliers were removed. Outliers includes data that reflects initialization of the gPROMs model at start time and within run time. Data obtained were standardised and centralised to equalise the energy content on each input signal. Figure 3-2 shows the data obtained from solvent-based PCC model developed in gPROMS. Figure 3-3 displays the power spectrum distribution of each input variable across a wide frequency range (0 – 3.5 rad/s). This is to show that the energy content of each input signal is uniform. The power spectrum is mainly focused around the lower frequency region.

The whole data were split into estimation data (75%) and validation (test) data (25%). The estimation (training) data were used for model construction, whereas the test data

were used to test the model performance in predicting capture level, ($\text{CO}_2\text{-CL}$), (y_1) and reboiler temperature (T_{reb}), (y_2). The input variables used for this model development are flue gas flowrate (u_1), lean solvent flowrate (u_2) and steam flowrate (u_3).

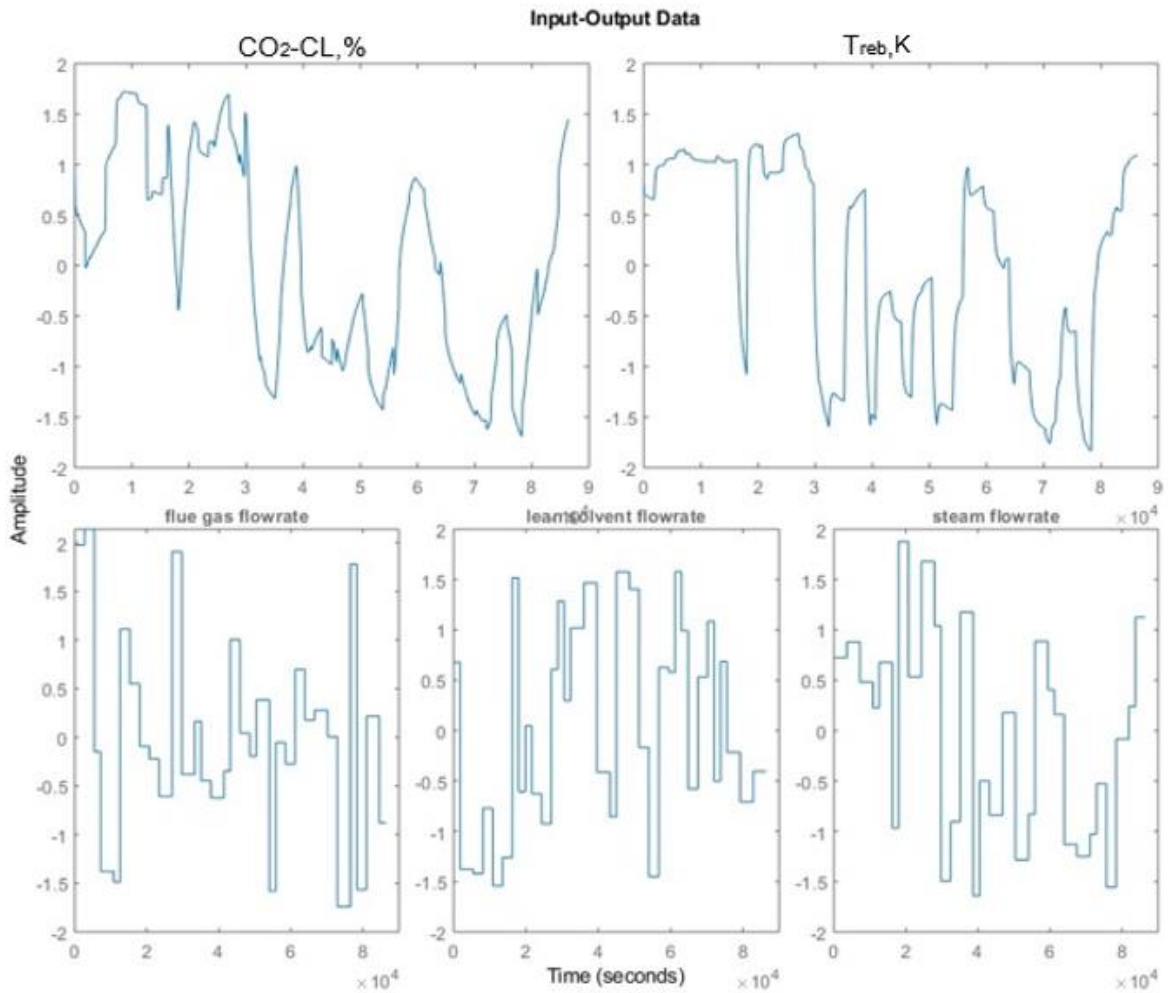


Figure 3-2 Input-output data obtained from an MEA-based PCC model developed in gPROMS; $\text{CO}_2\text{-CL}$: CO_2 Capture level; T_{reb} : reboiler temperature

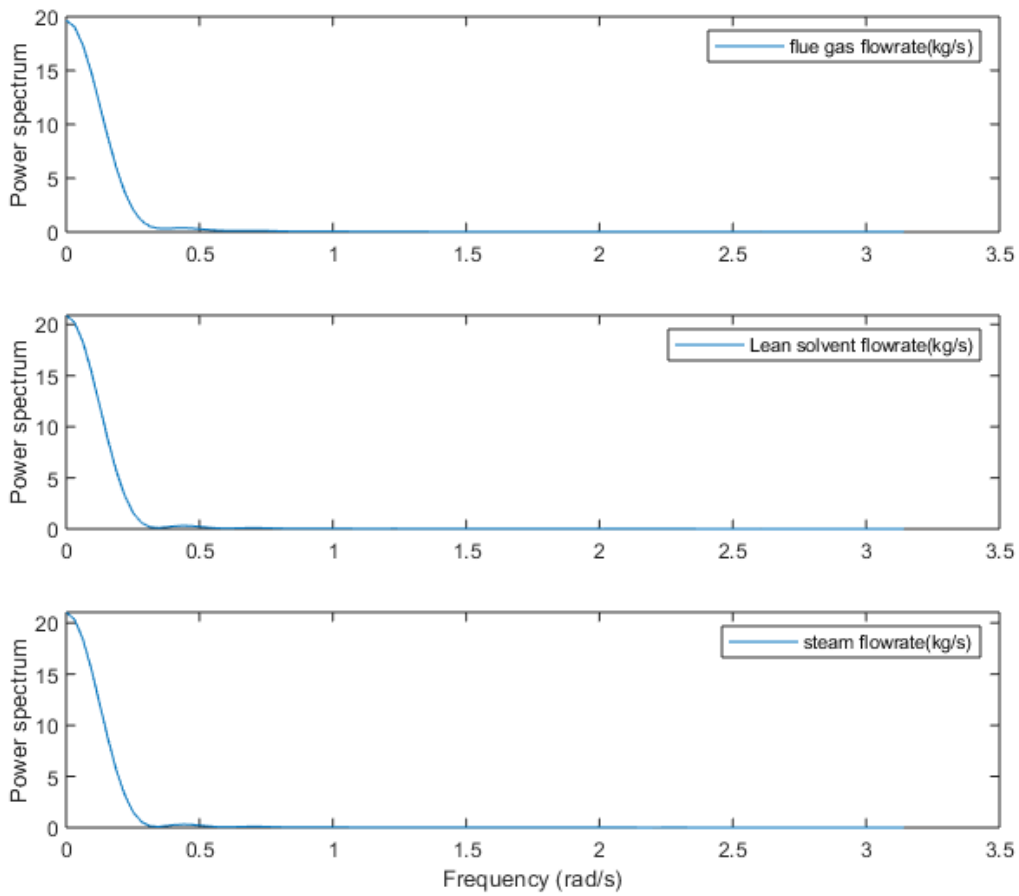


Figure 3-3 Power spectrum distribution across frequency range on each input variable

3.4 SI

3.4.1 NARX SI using FROLS

The multivariable NARX input model, which is a special form of NARMAX, is adopted to represent the solvent-based PCC process. The MISO-NARX model is described as:

$$y(t) = f(y(t-1), \dots, y(t-n_y), u_1(t), u_1(t-1), \dots, u_1(t-n_u), \dots, u_r(t), u_r(t-1), \dots, u_r(t-n_u)) + e(t) \quad 3-3$$

where r is the number of external input signals; $y(t), u_j(t)$, and $e(t)$, with $j = 1, 2, \dots, r$ and $t = 1, 2, \dots, N$ are measured system output, input and unmeasurable noise sequences, respectively; n_y and n_u are the maximum lags in the output and input; $f(\cdot)$ represents a nonlinear function, which is generally unknown but can be approximated using various types of nonlinear forms. Polynomial expansion of $f(\cdot)$ is most commonly used due to its good properties including transparency and easy interpretation of the model (Billings, 2013).

The solvent-based PCC process considered in the present study is a typical MIMO system, involving three inputs (flue gas flowrate, lean solvent flowrate and steam flowrate) and two outputs ($\text{CO}_2\text{-CL}$ and T_{reb}). For this study, the identification of the MIMO system was achieved by estimating one model for each output variable. This is to avoid an excessively complex model and ill-conditioned identification problem. The MIMO system can be represented as two MISO sub-systems, each of which can be represented using the NARX model as:

$$y_1(t) = f(y_1(t-1), \dots, y_1(t-n_y), u_1(t), u_1(t-1), \dots, u_1(t-n_u), \dots, u_r(t), u_r(t-1), \dots, u_r(t-n_u)) + e_1(t) \quad 3-4$$

$$y_2(t) = f(y_2(t-1), \dots, y_2(t-n_y), u_1(t), u_1(t-1), \dots, u_1(t-n_u), \dots, u_r(t), u_r(t-1), \dots, u_r(t-n_u)) + e_2(t) \quad 3-5$$

where $r = 3$, u_1 = flue gas flowrate (kg/s), u_2 = Lean MEA flowrate (kg/s), u_3 = steam flowrate (kg/s), and e_1 and e_2 are unmeasurable noise sequences. Each MISO model can be re-arranged into a linear-in-the-parameters form as (Billings *et al.*, 1988):

$$y_r(t) = \sum_{j=1}^{M_r} \varphi_{rj} x_{rj}(t) + e_r(t) \quad 3-6$$

where $y_r(t)$, $x_{rj}(t)$, φ_{rj} and M_r , with $(r = 1,2,3; j = 1,2, \dots, M_r)$, are the response signal (output), regressors, model parameter and number of model terms. It should be noted that each φ_{rj} was built using lagged input and lagged output variables, such as $y_2(t-1)$, $y_1(t-1)^2$, $u_2(t-1)u_3(t-1)$.

FROLS was adopted to select significant model terms for each MISO sub-system based on ERR. Details on FROLS algorithm procedure for model structure selection is discussed in section 2.3.2.2.1.2.

3.4.2 Model term candidate development

This section discusses the term candidate development for the NARX model. For both subsystem 1 and subsystem 2, the maximum time lags for the input and output variables were chosen to be $n_y = n_u = 2$ and degree of nonlinearity be 2. The values of n_y and n_u and nonlinearity degree for both sub-systems are large enough to cover the PCC process dynamics. A model term candidate dictionary D is a set consisting of a great number of model building blocks (i.e., candidate model terms) (Wei & Billings, 2008).

The dictionaries of candidate model terms were defined as follows:

$$D_0^u = D_{0,2,0,2}, D_0^1 = D_{2,2,0,2}$$

$$D_1^u = D_{0,2,1,2}, D_1^1 = D_{2,2,1,2}$$

$$D_{n_y, n_u, n_k, l} = \{x_1^{i_1}(t) \dots x_l^{i_l}(t) : x_j^{i_j} \in V_{n_y, n_u, n_k}, \quad 1 \leq j \leq l, \quad 0 \leq i_j \leq l\}$$

$$V_{n_y, n_u, n_k} = \{y(t-1), \dots, y(t-n_y), u(t-n_k), \dots, u(t-n_k-n_u+1)\}$$

Here, the two dictionaries D_0^u and D_1^u only contain candidate model terms formed by all input variables alone (i.e., $u_1(t), u_2(t), u_3(t)$ and their lagged versions such as $u_1(t-1), u_2(t-2)$) but do not include autoregressive terms such as $y(t-1), \dots, y(t-n_k)$ with $n_k = 0$ and 1 respectively. The other two dictionaries, D_0^1 and D_1^1 , however, contain candidate model terms formed by all the lagged input and output variables. The main purpose that we separately treated these two groups of model candidates (with and without autoregressive variables) is to test whether feedback signals from the system outputs play an obviously important role in explaining the system's inherent dynamics.

Using the above 4 dictionaries, a total of 4 models, different model structures, were identified for each sub-system. The model terms were ranked in accordance with their level of significance (measured by ERR index) to the response variable in each sub-model. The BIC is used to determine the number of model terms (Wei & Billings, 2009). The minimum BIC (n) is adopted as the basis for selecting the model length. Thus, the FROLS algorithm stops its iteration at minimum BIC. Each model identified from the different model term dictionaries were compared based on OSA prediction and MSP. The models that best predict the system outputs were selected based on the MSP performance criterion.

3.5 Performance Evaluation

3.5.1 Sub-model 1

Sub-model 1 represents a MISO system to predict CO₂ capture level (CO₂-CL). Tables 3-2 – 3-5 give details of various model structures selected for each model term dictionary ($D_1^u, D_1^1, D_0^u, D_0^1$) using FROLS algorithm along with the parameter estimates and BIC. It can be deduced from the sum of error reduction ratio (SERR),

that the list of model terms selected from dictionaries D_1^1 gave the best explanation (99.98%) of the response variable variation compared to the identified model developed from other dictionaries (see Table 3-3).

Furthermore, comparisons of the identified models obtained from the different model dictionaries were carried out to assess the predictive ability of the models. Each model was applied to the test data for CO₂ Capture level (CO₂-CL). The associated OSA predictions and MSP are calculated and shown in Figures 3-4 – 3-7, where the solid line represents the original measurements and the dashed red and blue lines are for the OSA and MSP respectively.

As shown in Figure 3-4 and 3-6, models M_1^u (see Table 3-2) and model M_0^u (see Table 3-4) gave similar MSP and OSA performance. This is because these models only use exogenous inputs ($u_1(t-1), \dots, u_r(t-1), \dots, u_r(t-n)$) and do not use any autoregressive terms ($y(t-1), \dots, y(t-n)$). For models that only use exogenous inputs (without using autoregressive terms), their MSP and OSA predictions are always the same. Models M_1^1 and M_0^1 (see Table 3-3 and Table 3-5 respectively), however, involve both auto-regressive variables and exogenous input variables. Comparing Figures 3-4 – 3-7, it can be seen that model M_1^1 gave the best prediction performance (Figure 3-5), indicating that M_1^1 contains the appropriate model terms that capture the system dynamics. For M_0^1 , there was disparity between the MSP and OSA prediction performances. This is because M_0^1 does not contain the most appropriate model terms that can well capture the system dynamics. For such a deficient model, its MSP performance will usually deteriorate because the accumulative error can be significantly augmented through an iterative computation procedure when updating the system output variable. The OSA performance of such a deficient model, however,

normally does not suffer from any error accumulation and propagation. The discrepancy between MSP and OSA shown in Figure 3-7 is mainly caused by the error propagation and augmentation due to the deficiency of the model. MSP is often used to test the validity and stability of a dynamic model that cannot be easily revealed by OSA.

The variance accounted for (VAF), also called the prediction efficiency (PE), of the identified sub-models are shown in Table 3-6. VAF (PE) is calculated as:

$$VAF = \left[1 - \frac{\text{var}(y_{measure} - y_{predict})}{\text{var}(y_{measure})} \right] \times 100\% \quad 3-7$$

where $y_{measure}$ is the measured output of the test data and $y_{predict}$ is the OSA prediction/ MSP output. Among the 4 models, $M_1^u, M_1^1, M_0^u, M_0^1$ (obtained based upon the 4 dictionaries, $D_1^u, D_1^1, D_0^u, D_0^1$), It can be seen from Table 3-6 that model M_1^1 gave the best performance compared to the other 3 models with a prediction efficiency of 99.9% and 98.3% in terms of OSA and MPO respectively (see Figure 3-5). This indicates that the underlying dynamics between the inputs and the output (CO₂ capture level) is captured by model M_1^1 . Thus, model M_1^1 was selected to represent sub-system 1. From Table 3-3, the system model can be written as:

$$y_1 = 1.50 y_1(t - 1) + 0.0336 u_3(t - 2) - 0.469 y_1(t - 2) + \dots - 3.15 y_1(t - 2)u_1(t - 1) \quad 3-8$$

Table 3-2 Identified model (M_1^u) structures from D_1^u for sub-model 1 using FROLS algorithm

| s/n | Model Terms | Parameter Estimates | ERR (%) | BIC |
|-----|---------------------|---------------------|----------|----------|
| 1 | $u_3(t-2)$ | 2.43E+03 | 3.78E+01 | 6.30E-01 |
| 2 | $u_2(t-1)*u_3(t-1)$ | -5.13E+03 | 7.22E+00 | 5.61E-01 |
| 3 | $u_1(t-1)*u_2(t-1)$ | 2.09E+03 | 7.58E+00 | 4.87E-01 |
| 4 | $u_1(t-2)$ | -1.47E+02 | 1.12E+00 | 4.79E-01 |
| 5 | $u_1(t-1)*u_1(t-1)$ | 1.12E+04 | 3.16E+00 | 4.49E-01 |
| 6 | $u_2(t-1)*u_2(t-1)$ | -8.90E+01 | 2.09E+00 | 4.30E-01 |

| s/n | Model Terms | Parameter Estimates | ERR (%) | BIC |
|-----|---------------------|---------------------|----------|----------|
| 7 | $u_2(t-2)$ | 2.78E+01 | 4.67E-01 | 4.28E-01 |
| 8 | $u_3(t-1)*u_3(t-1)$ | 3.15E+04 | 6.11E-01 | 4.25E-01 |
| 9 | $u_1(t-1)$ | -5.25E+03 | 2.18E-01 | 4.25E-01 |

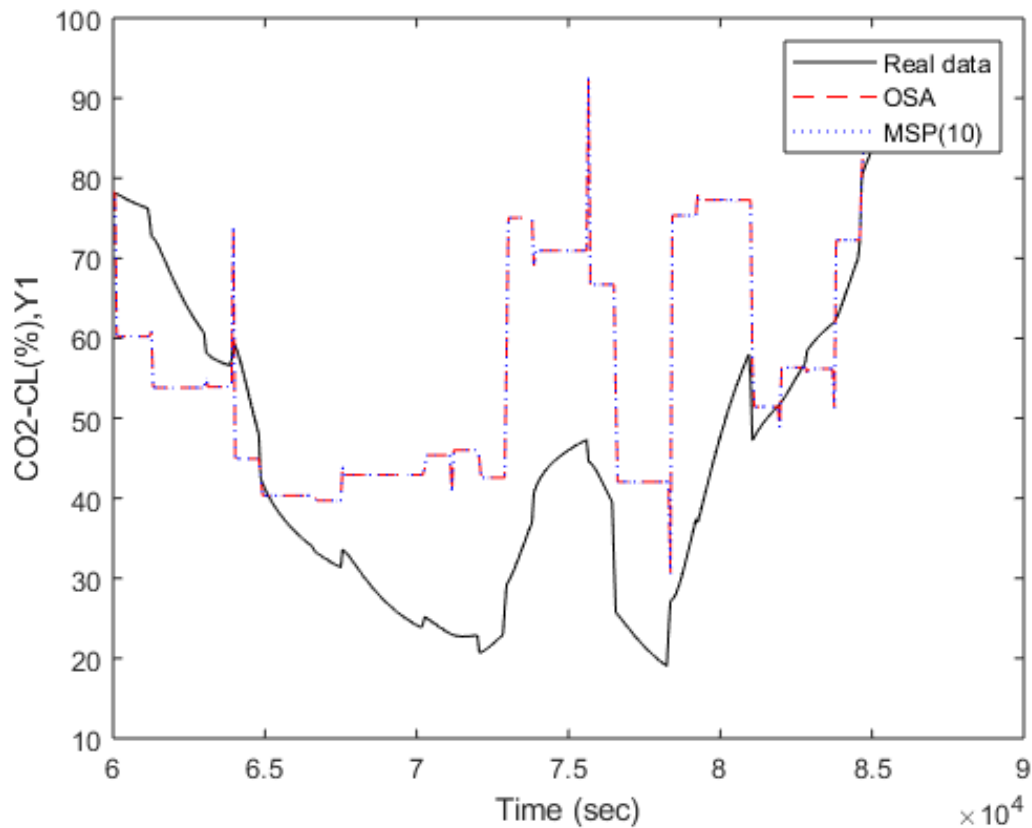


Figure 3-4 Comparison of the model predictions (OSA and MSP(10)) and measurements over the test data for sub-model 1 using M_1^u . Note: MSP(10) indicates 10-step ahead prediction.

Table 3-3 Identified model (M_1^1) structures from D_1^1 for sub-model 1 using FROLS algorithm

| s/n | Model Terms | Parameter Estimates | ERR (%) | BIC |
|-----|---------------------|---------------------|----------|----------|
| 1 | $y_1(t-1)$ | 1.50E+00 | 9.97E+01 | 2.85E-03 |
| 2 | $u_3(t-2)$ | 3.36E+02 | 5.57E-02 | 2.30E-03 |
| 3 | $y_1(t-2)$ | -4.69E-01 | 2.48E-02 | 2.06E-03 |
| 4 | $u_3(t-1)$ | -3.68E+02 | 1.78E-02 | 1.89E-03 |
| 5 | $y_1(t-1)*u_1(t-1)$ | -7.22E+00 | 6.23E-03 | 1.84E-03 |
| 6 | $y_1(t-2)*u_1(t-2)$ | -1.47E+00 | 2.93E-02 | 1.55E-03 |
| 7 | $u_2(t-2)$ | -4.42E+01 | 3.08E-03 | 1.53E-03 |
| 8 | $u_2(t-1)$ | 3.88E+01 | 5.79E-02 | 9.20E-04 |
| 9 | $u_1(t-1)$ | 2.49E+01 | 2.45E-03 | 9.00E-04 |
| 10 | $u_1(t-2)$ | -6.90E+00 | 5.51E-02 | 3.13E-04 |
| 11 | $u_2(t-1)*u_3(t-2)$ | 2.12E+02 | 8.12E-04 | 3.06E-04 |

| s/n | Model Terms | Parameter Estimates | ERR (%) | BIC |
|-----|---------------------|---------------------|----------|----------|
| 12 | $u_2(t-2)*u_3(t-2)$ | -5.57E+02 | 2.56E-03 | 2.80E-04 |
| 13 | $u_1(t-2)*u_2(t-1)$ | -1.34E+03 | 2.11E-04 | 2.80E-04 |
| 14 | $u_1(t-1)*u_2(t-1)$ | 1.29E+03 | 1.37E-03 | 2.67E-04 |
| 15 | $u_1(t-2)*u_2(t-2)$ | 1.24E+03 | 2.46E-04 | 2.66E-04 |
| 16 | $u_1(t-1)*u_2(t-2)$ | -1.20E+03 | 1.95E-03 | 2.45E-04 |
| 17 | $y_1(t-1)*u_1(t-2)$ | 5.31E+00 | 3.01E-04 | 2.44E-04 |
| 18 | $u_2(t-1)*u_3(t-1)$ | 4.70E+02 | 2.95E-04 | 2.42E-04 |
| 19 | $y_1(t-1)*u_3(t-1)$ | -1.95E-01 | 1.61E-04 | 2.42E-04 |
| 20 | $y_1(t-2)*u_1(t-1)$ | 3.15E+00 | 9.11E-05 | 2.42E-04 |

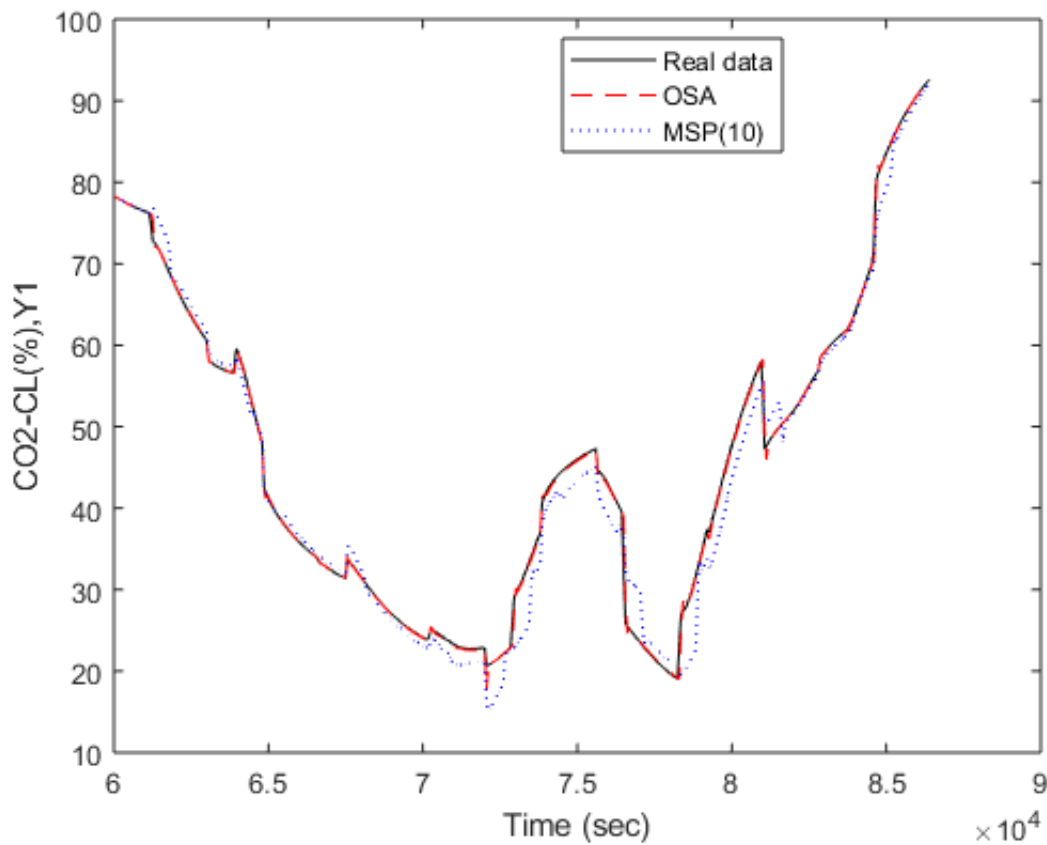


Figure 3-5 Comparison of the model predictions (OSA and MSP) and measurements over the test data for sub-model 1 using M_1^1 . Note: MSP(10) indicates 10-step ahead prediction.

Table 3-4 Identified model (M_0^u) structures from D_0^u for sub-model 1 using FROLS algorithm

| s/n | Model Terms | Parameter Estimates | ERR (%) | BIC |
|-----|---------------------|---------------------|----------|----------|
| 1 | $u_3(t-1)$ | 1.36E+04 | 3.56E+01 | 6.53E-01 |
| 2 | $u_2(t-1)*u_3(t-1)$ | -1.36E+04 | 7.55E+00 | 5.80E-01 |

| s/n | Model Terms | Parameter Estimates | ERR (%) | BIC |
|-----|---------------------|---------------------|----------|----------|
| 3 | $u_1(t-1)*u_2(t)$ | 6.05E+02 | 7.65E+00 | 5.06E-01 |
| 4 | $u_1(t)*u_1(t)$ | 1.55E+03 | 1.09E+00 | 4.98E-01 |
| 5 | $u_1(t-1)$ | -1.19E+03 | 3.26E+00 | 4.67E-01 |
| 6 | $u_2(t-1)*u_2(t-1)$ | -6.98E+02 | 2.04E+00 | 4.49E-01 |
| 7 | $u_2(t-1)$ | 1.58E+03 | 5.46E-01 | 4.46E-01 |
| 8 | $u_3(t)*u_3(t-1)$ | -1.95E+04 | 7.14E-01 | 4.42E-01 |
| 9 | $u_2(t)*u_3(t)$ | -6.79E-02 | 3.30E-01 | 4.41E-01 |
| 10 | constant | 1.36E+04 | 1.63E-01 | 4.42E-01 |

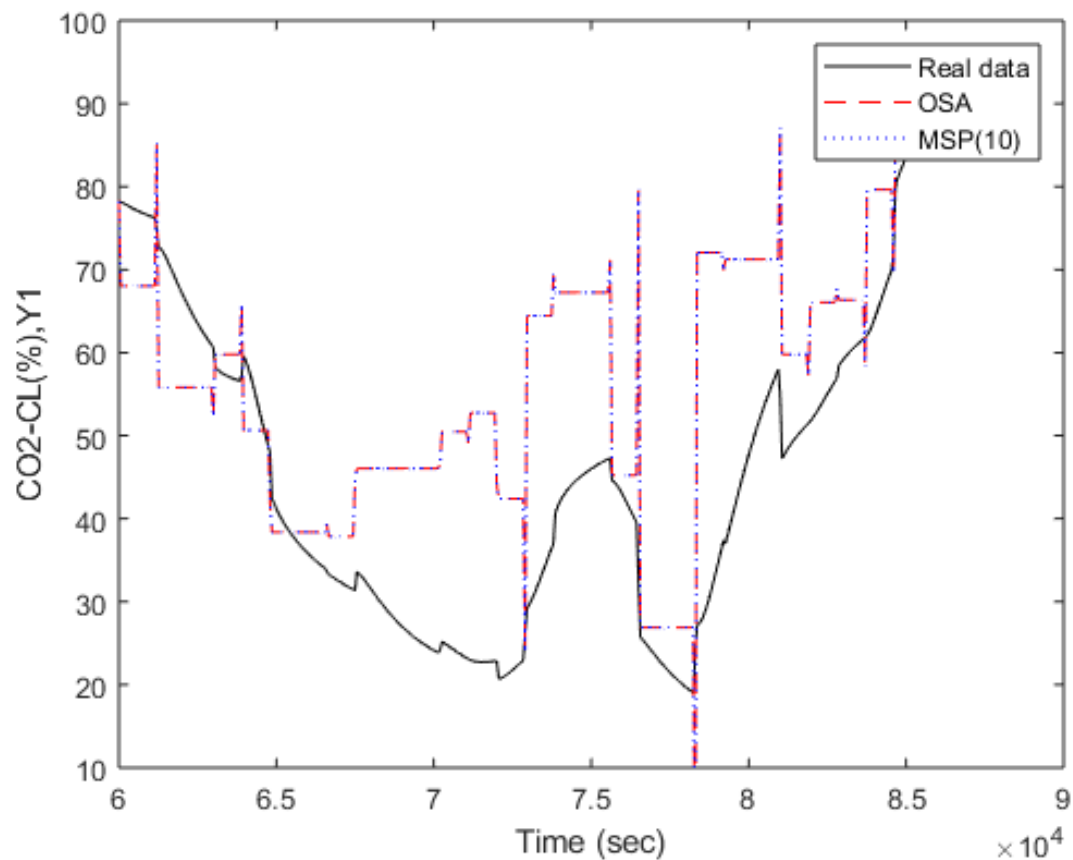


Figure 3-6 Comparison of the model predictions (OSA and MSP) and measurements over the test data for sub-model 1 using M_0^u . Note: MSP(10) indicates 10-step ahead prediction.

Table 3-5 Identified model (M_0^1) structures from D_0^1 for sub-model 1 using FROLS algorithm

| s/n | Model Terms | Parameter Estimates | ERR (%) | BIC |
|-----|---------------------|---------------------|----------|----------|
| 1 | $y_1(t-1)$ | -1.11256 | 9.97E+01 | 2.85E-03 |
| 2 | $y_1(t-2)$ | 45.87308 | 5.12E-02 | 2.35E-03 |
| 3 | $u_3(t-1)$ | -125.003 | 1.72E-02 | 2.19E-03 |
| 4 | $u_1(t)$ | 136.2412 | 6.03E-03 | 2.14E-03 |
| 5 | $u_1(t-1)$ | -1.27043 | 5.70E-03 | 2.10E-03 |
| 6 | $y_1(t-1)*u_1(t-1)$ | 4.932979 | 1.87E-03 | 2.09E-03 |
| 7 | $y_1(t-2)*u_1(t)$ | 0.006381 | 2.43E-03 | 2.08E-03 |
| 8 | $y_1(t-1)*u_2(t-1)$ | -3.94866 | 1.31E-03 | 2.08E-03 |
| 9 | $y_1(t-1)*u_1(t)$ | -1.11256 | 1.08E-03 | 2.08E-03 |

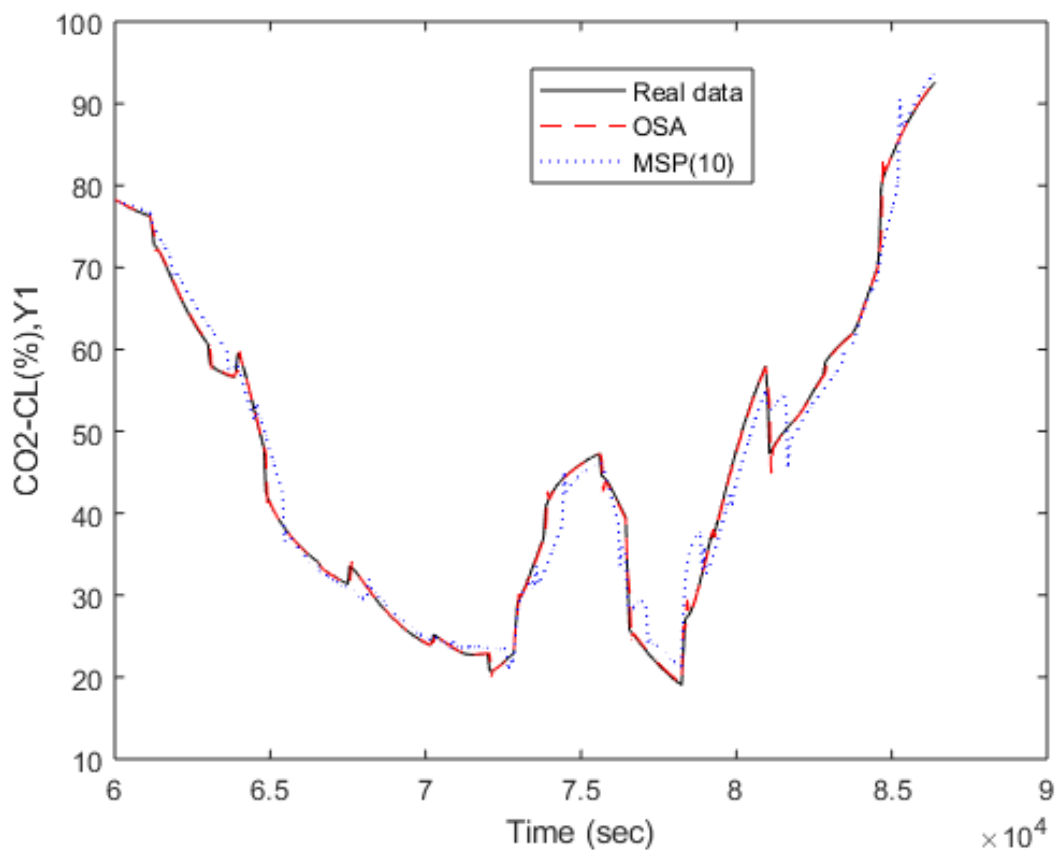


Figure 3-7 Comparison of the model predictions (OSA and MSP) and measurements over the test data for sub-model 1 using M_0^1 . Note: MSP(10) indicates 10-step ahead prediction.

Table 3-6 VAF (and PE) for the Identified sub-model 1 (OSA and MSP)

| Identified Models | OSA (%VAF) | MSP (%VAF) |
|-------------------|------------|------------|
| M_1^u | 31.0003 | 31.0003 |
| M_1^1 | 99.9090 | 98.2652 |
| M_0^u | 49.5279 | 49.5279 |
| M_0^1 | 99.8699 | 97.8917 |

3.5.2 Sub-model 2

The details of the models for sub-system 2, obtained from each model term dictionary based on FROLS algorithm, are summarized in Tables 3-7 – 3-10. OSA predictions and multi-step prediction (MSP) generated by these models, together with the true values (i.e. the system output measurements as test data), are shown in Figure 3-8 – 3-11, respectively. Also, the prediction efficiency for each identified model is tabulated in Table 3-11.

It was observed from Table 3.11 that M_1^1 (obtained from D_1^1) out-performed the other 3 models with a prediction efficiency of 99.994% and 99.587% based on OSA prediction and MSP (see Figure 3-9) and was selected as a suitable model to predict the reboiler temperature. Thus, from Table 3-8, the model should be written as:

$$y_2 = 1.67 y_2(t - 1) - 0.687 y_2(t - 2) + 0.0219 u_3(t - 1) + \dots - 0.428 u_1(t - 2) \quad 3-9$$

Table 3-7 Identified model (M_1^u) structures from D_1^u for sub-model 2 using FROLS algorithm

| s/n | Model Terms | Parameter Estimates | ERR (%) | BIC |
|-----|---------------------|---------------------|----------|----------|
| 1 | $u_3(t-2)$ | 3.57E+03 | 8.12E+01 | 1.83E-01 |
| 2 | $u_2(t-2)$ | 7.28E+01 | 6.14E+00 | 1.24E-01 |
| 3 | $u_1(t-2)*u_1(t-2)$ | 2.38E+03 | 9.60E-01 | 1.16E-01 |
| 4 | $u_3(t-2)*u_3(t-2)$ | -1.58E+04 | 9.84E-01 | 1.07E-01 |
| 5 | $u_2(t-2)*u_3(t-2)$ | -1.82E+03 | 7.30E-01 | 1.00E-01 |
| 6 | $u_1(t-2)$ | -7.89E+02 | 9.88E-01 | 9.07E-02 |

| s/n | Model Terms | Parameter Estimates | ERR (%) | BIC |
|-----|---------------------|---------------------|----------|----------|
| 7 | constant | 3.26E+02 | 1.98E-01 | 8.93E-02 |
| 8 | $u_2(t-1)*u_2(t-2)$ | -1.06E+01 | 9.18E-02 | 8.89E-02 |
| 9 | $u_3(t-1)$ | 6.69E+01 | 2.32E-02 | 8.93E-02 |

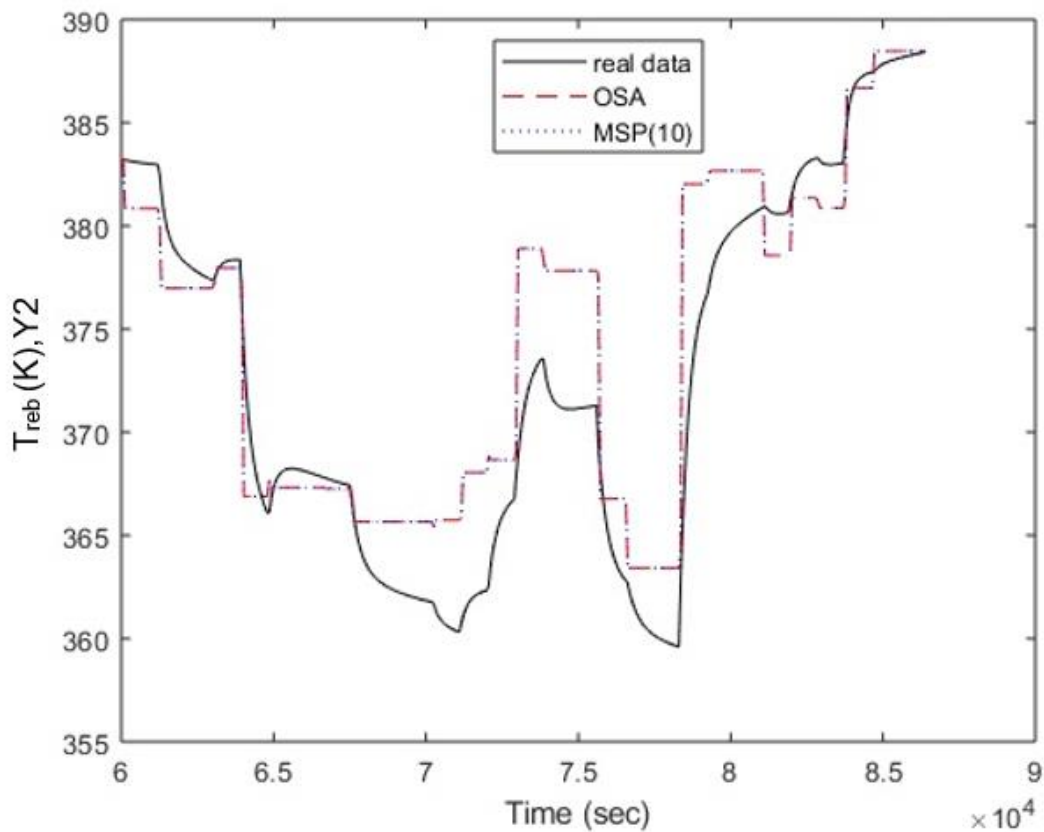


Figure 3-8 Comparison of the model predictions (OSA and MSP) and measurements over the test data for sub-model 2 using M_1^u . Note: MSP(10) indicates 10-step ahead prediction.

Table 3-8 Identified model (M_1^1) structures from D_1^1 for sub-model 2 using FROLS algorithm

| s/n | Model Terms | Parameter Estimates | ERR (%) | BIC |
|-----|---------------------|---------------------|----------|----------|
| 1 | $y_2(t-1)$ | 1.67E+00 | 9.96E+01 | 3.68E-03 |
| 2 | $y_2(t-2)$ | -6.87E-01 | 2.40E-01 | 1.35E-03 |
| 3 | $u_3(t-1)$ | 2.19E+02 | 2.65E-02 | 1.09E-03 |
| 4 | $u_3(t-2)$ | -1.86E+02 | 8.42E-02 | 2.61E-04 |
| 5 | $u_2(t-1)$ | -5.24E+00 | 9.02E-04 | 2.54E-04 |
| 6 | $u_3(t-1)*u_3(t-2)$ | -4.88E+03 | 8.89E-04 | 2.47E-04 |
| 7 | $u_3(t-2)*u_3(t-2)$ | 5.51E+03 | 1.00E-02 | 1.47E-04 |
| 8 | $u_3(t-1)*u_3(t-1)$ | -1.05E+03 | 4.47E-04 | 1.43E-04 |

| s/n | Model Terms | Parameter Estimates | ERR (%) | BIC |
|-----|---------------------|---------------------|----------|----------|
| 9 | constant | 7.48E+00 | 4.93E-04 | 1.39E-04 |
| 10 | $u_2(t-2)*u_3(t-1)$ | 3.18E+02 | 3.83E-04 | 1.36E-04 |
| 11 | $u_2(t-2)*u_3(t-2)$ | -3.66E+02 | 1.33E-03 | 1.23E-04 |
| 12 | $u_2(t-1)*u_3(t-2)$ | 7.66E+01 | 1.02E-04 | 1.22E-04 |
| 13 | $u_2(t-2)$ | 2.95E+00 | 8.13E-05 | 1.22E-04 |
| 14 | $u_1(t-2)$ | -4.28E-01 | 7.13E-05 | 1.22E-04 |

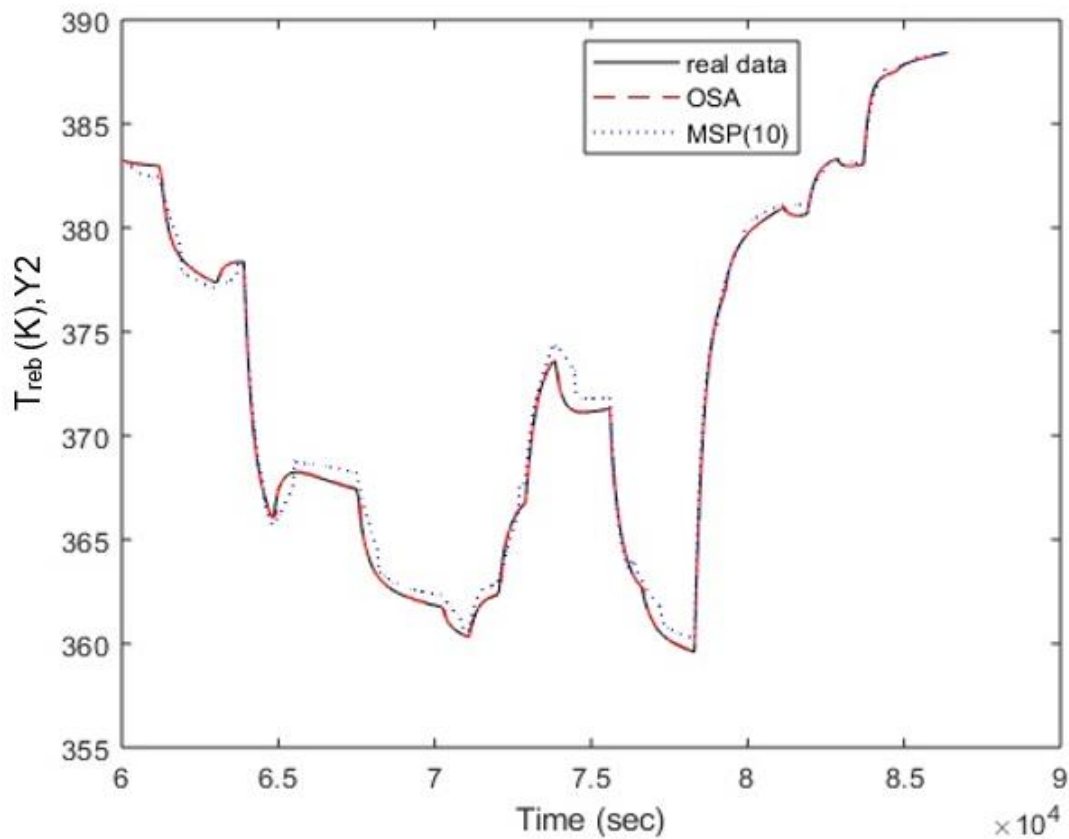


Figure 3-9 Comparison of the model predictions (OSA and MSP) and measurements over the test data for sub-model 2 using M_1^1 . Note: MSP(10) indicates 10-step ahead prediction.

Table 3-9 Identified model (M_0^u) structures from D_0^u for sub-model 2 using FROLS algorithm

| s/n | Model Terms | Parameter Estimates | ERR (%) | BIC |
|-----|---------------------|---------------------|----------|----------|
| 1 | $u_3(t-1)$ | 3.80E+03 | 7.91E+01 | 2.03E-01 |
| 2 | $u_2(t-1)$ | 6.72E+01 | 5.67E+00 | 1.49E-01 |
| 3 | $u_1(t-1)*u_1(t-1)$ | 2.53E+03 | 1.07E+00 | 1.40E-01 |
| 4 | $u_3(t-1)*u_3(t-1)$ | -1.55E+04 | 9.42E-01 | 1.31E-01 |
| 5 | $u_2(t)*u_3(t)$ | -1.13E+02 | 9.80E-01 | 1.22E-01 |
| 6 | $u_1(t-1)$ | -8.36E+02 | 9.53E-01 | 1.13E-01 |

| s/n | Model Terms | Parameter Estimates | ERR (%) | BIC |
|-----|---------------------|---------------------|----------|----------|
| 7 | Constant | 3.27E+02 | 1.57E-01 | 1.13E-01 |
| 8 | $u_2(t)*u_2(t)$ | 2.15E+00 | 9.01E-02 | 1.12E-01 |
| 9 | $u_2(t-1)*u_3(t-1)$ | -1.97E+03 | 3.13E-02 | 1.13E-01 |

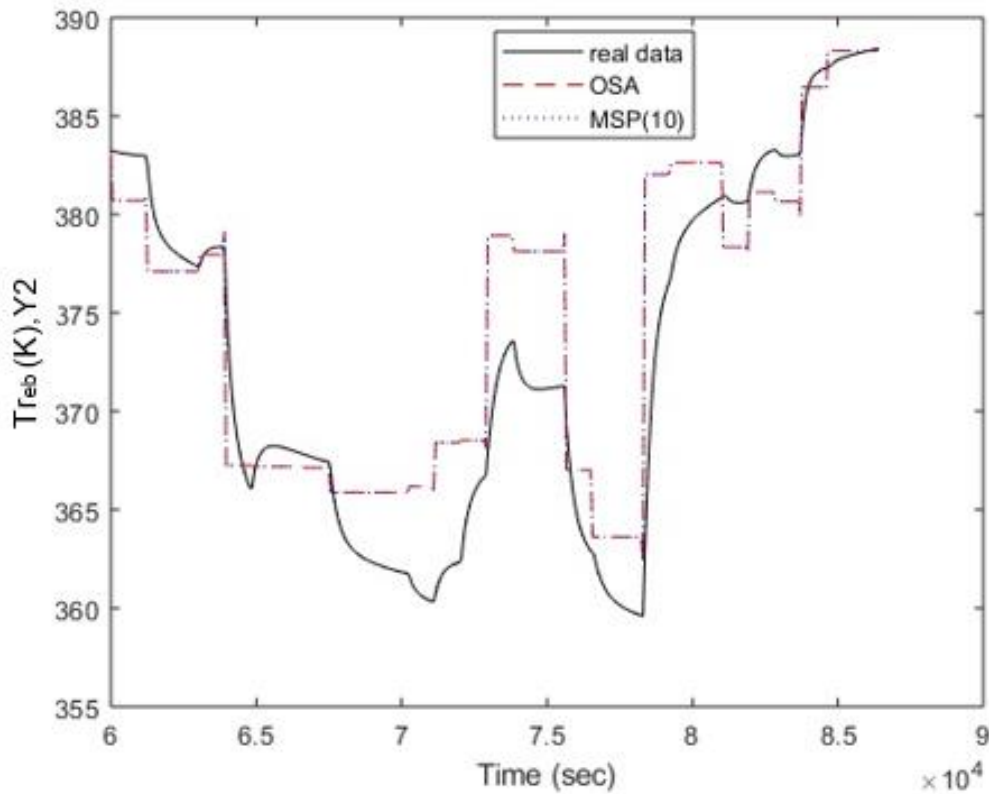


Figure 3-10 Comparison of the model predictions (OSA and MSP) and measurements over the test data for sub-model 2 using M_0^u . Note: MSP(10) indicates 10-step ahead prediction.

Table 3-10 Identified model (M_0^1) structures from D_0^1 for sub-model 2 using FROLS algorithm

| s/n | Model Terms | Parameter Estimates | ERR (%) | BIC |
|-----|---------------------|---------------------|----------|----------|
| 1 | $y_2(t-1)$ | -9.30E+00 | 9.96E+01 | 3.68E-03 |
| 2 | $y_2(t-2)$ | 7.96E+00 | 2.40E-01 | 1.35E-03 |
| 3 | $u_3(t-1)$ | 1.92E+03 | 2.65E-02 | 1.09E-03 |
| 4 | $u_2(t-1)$ | -3.30E+00 | 2.57E-02 | 8.44E-04 |
| 5 | $y_2(t-2)*u_3(t-1)$ | -4.84E+00 | 6.19E-03 | 7.88E-04 |
| 6 | constant | 4.41E+02 | 1.96E-02 | 5.95E-04 |
| 7 | $y_2(t-1)*y_2(t-1)$ | 2.42E-02 | 4.74E-03 | 5.51E-04 |
| 8 | $u_2(t)*u_3(t-1)$ | 8.89E+01 | 2.24E-03 | 5.32E-04 |
| 9 | $y_2(t-1)*y_2(t-2)$ | -2.11E-02 | 2.97E-03 | 5.05E-04 |
| 10 | $u_1(t-1)*u_2(t)$ | 4.04E+01 | 1.39E-03 | 4.94E-04 |
| 11 | $u_2(t)*u_2(t)$ | -7.54E+00 | 1.04E-03 | 4.86E-04 |
| 12 | $y_2(t-1)*u_1(t-1)$ | 6.28E-01 | 1.22E-03 | 4.76E-04 |

| | | | | |
|----|---------------------|-----------|----------|----------|
| 13 | $u_1(t-1)$ | -2.74E+02 | 1.48E-03 | 4.64E-04 |
| 14 | $u_1(t-1)*u_1(t-1)$ | 5.18E+01 | 5.59E-04 | 4.61E-04 |
| 15 | $u_3(t-1)*u_3(t-1)$ | -2.09E+02 | 3.79E-04 | 4.60E-04 |
| 16 | $u_1(t-1)*u_3(t-1)$ | -2.99E+02 | 1.92E-04 | 4.61E-04 |

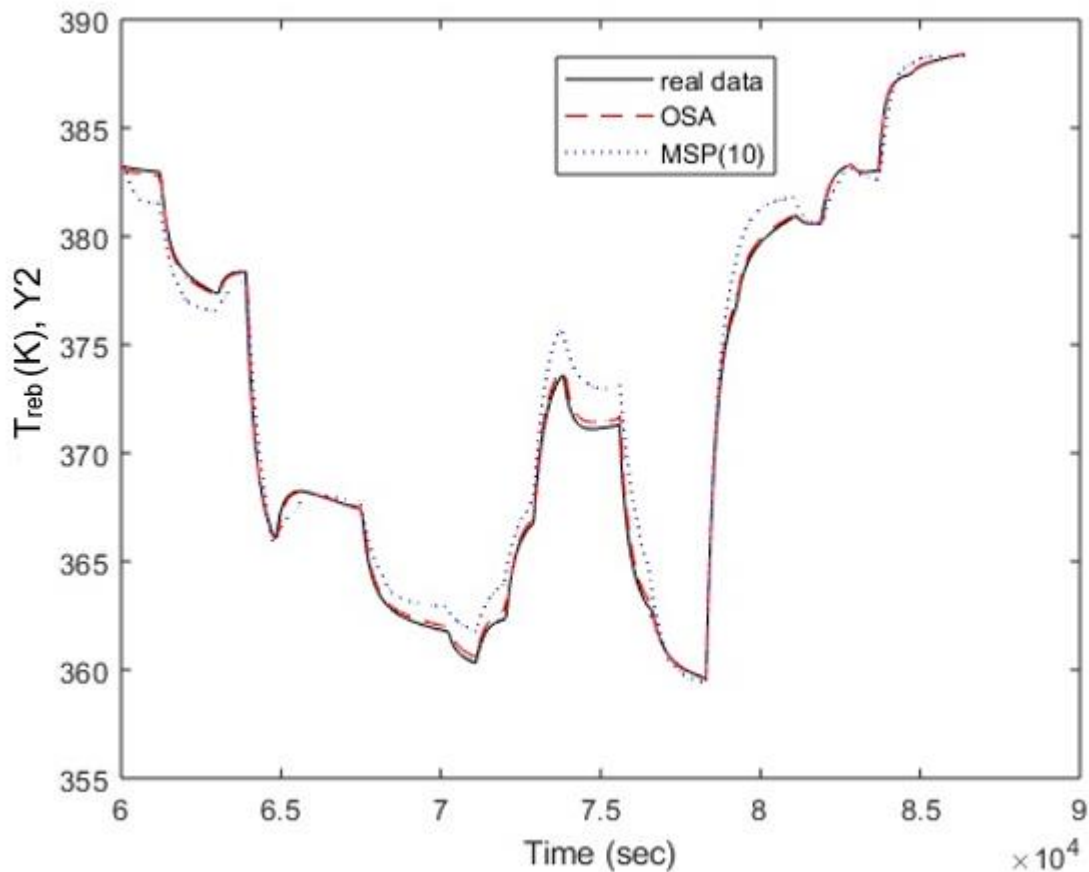


Figure 3-11 Comparison of the model predictions (OSA and MSP) and measurements over the test data for sub-model 2 using M_0^1 . Note: MSP(10) indicates 10-step ahead prediction.

Table 3-11 VAF (and PE) for the Identified sub-model 1 (OSA and MSP)

| Identified Models | OSA (%VAF) | MSP (%VAF) |
|-------------------|------------|------------|
| M_1^u | 86.5313 | 86.5313 |
| M_1^1 | 99.9937 | 99.5870 |
| M_0^u | 84.1887 | 84.1887 |
| M_0^1 | 99.9529 | 98.5890 |

3.5.3 Statistical Analysis

Statistical analysis was carryout on the suitable NARX models obtained using FROLS algorithm to represent the underlying dynamics between key variables in the solvent-based CO₂ capture plant. Table 3-12 shows the values of R, R² and adjusted R² of the identified models. R, which is the multiple correlation coefficient, is a measure of how much the combination of model terms in each identified model correlates with the respective output variables. The R² represents the portion of variance in the response variable that is explained by the combination of model terms, while the adjusted R² is a measure of the accuracy of a model across different samples (Zhou et al., 2008). R, R² and adjusted R² are calculated as follows

$$R = \frac{N \sum y_{measure} y_{predict} - \sum y_{measure} \sum y_{predict}}{\sqrt{N \sum y_{measure}^2 - (\sum y_{measure})^2} \sqrt{N \sum y_{predict}^2 - (\sum y_{predict})^2}} \quad 3-10$$

$$R^2 = 1 - \frac{SSE}{SST} \quad 3-11$$

$$R_{adj}^2 = 1 - \left(\frac{N-1}{N-n} \right) \frac{SSE}{SST} \quad 3-12$$

Where $y_{measure}$ is the measured output; $y_{predict}$ is the multi-step prediction; SSE is the sum of squares error; SST is the total sum of squares; N is the number of observations and n is the number of terms. The R-value for sub-model1 (1.0000) and sub-model 2 (1.0000) indicates that the combination of model terms in each identified model are highly correlated with the response variables. The R² value signifies that model 1 can explain 99.98% of the variation in CO₂ capture level (CO₂-CL) and model 2 can explain 99.99% of the variation in reboiler temperature (T_{reb}). The values of

adjusted R^2 indicates that the identified NARX models has high accuracy of prediction even across different samples.

Table 3-12 Statistical performance of the Identified NARX model

| Identified Model | R | R^2 | R^2_{adj} |
|------------------|--------|--------|-------------|
| Sub-model 1 | 1.0000 | 0.9998 | 0.9998 |
| Sub-model 2 | 1.0000 | 0.9999 | 0.9999 |

3.6 Process dynamics analysis

This section discusses the dynamic analysis carried out on the identified MEA based PCC model. Output responses plot for both the first principles model and the identified model were compared. This is to ensure that the identified model captures the basic dynamics of the CO₂ capture system. The following dynamic operational analysis were carried out:

- A step increase in flue gas flowrate to the absorber
- A step increase in lean solvent mass flowrate to the absorber
- A step increase in steam flowrate to the reboiler in regenerator

3.6.1 Increase in flue gas flowrate to the absorption column

The effect of the flue gas flowrate increase to the absorber on the CO₂ capture identified model outputs (CO₂-CL, T_{reb}) was investigated. The change in flue gas flowrate reflects the variation in the power plant output attached to the capture process and thus considered as a disturbance to the capture process. The flue gas flowrate was increased with 10% step change at simulation time of 30000s (8.33hr) and remained constant for the rest of the simulation period. Other input variables (lean solvent (MEA) flowrate and steam flowrate) were kept constant throughout the simulation time.

From Figure 3-12, the CO₂ capture level decreases significantly in a very short period, as flue gas flowrate increases. At the same period, reboiler temperature is slightly reduced. This indicates that flue gas flowrate has an immediate and significant effect on the CO₂ capture level but a slight effect on the reboiler temperature. The dynamic trends of the identified model aligns with the first principles (gPROMS) model responses.

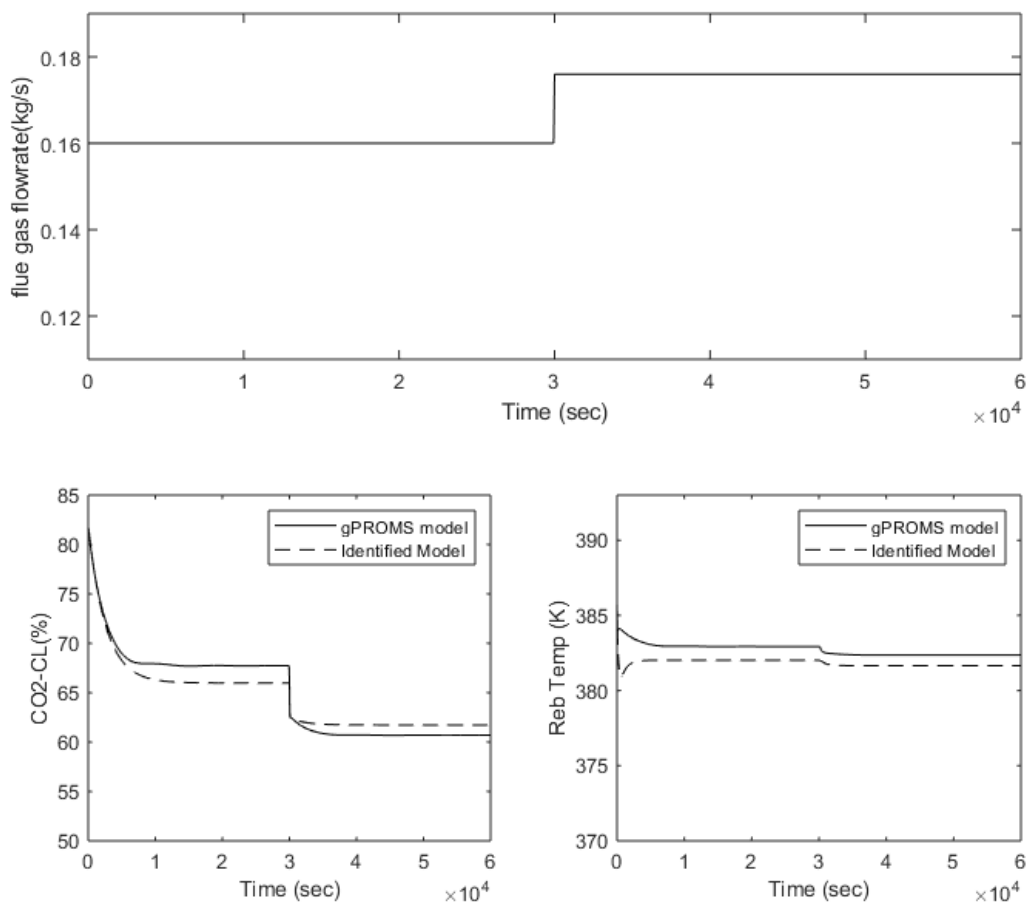


Figure 3-12 Output response to flue gas flowrate (kg/s) increase to the absorber: gPROMS model

3.6.2 Increase in lean solvent (MEA) flow rate

Similar investigation on the effect of lean solvent flowrate on the CO₂ capture (identified and first principles) model outputs. A 10% step increase in lean solvent

flowrate was effected at a simulation time of 30000s (8.33hr) while other input variables were left constant.

A sharp increase in CO₂ capture level was observed (see Figure 3-13) immediately after the step change was introduced. This is accompanied by a slow reduction in the CO₂ capture level until a new steady-state point is attained. A slow but significant decrease in the reboiler temperature was observed as lean solvent (MEA) flowrate increases (see Figure 3-13). Similar dynamic behaviour was observed for the first principles model as shown in Figure 3-13.

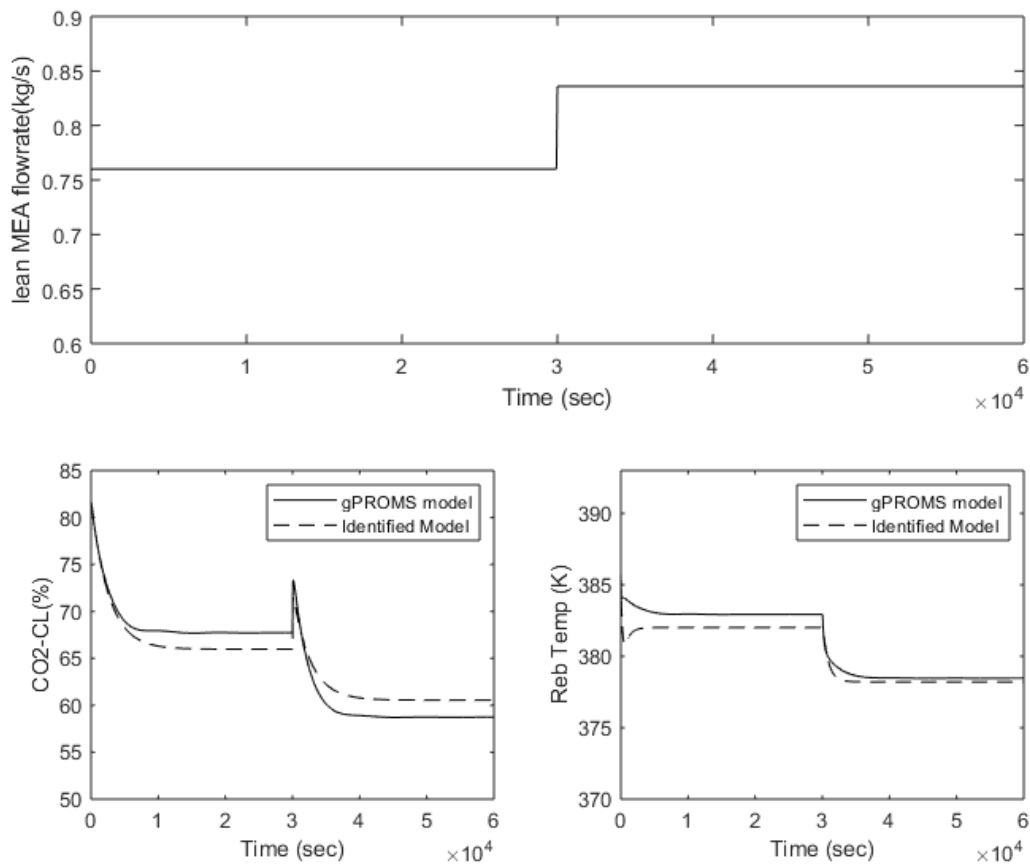


Figure 3-13 Output responses to a 10% step increase of lean solvent (MEA) flowrate (kg/s) to the absorber

3.6.3 Increase in steam flowrate to the reboiler

This section details the effect of the steam flowrate to the reboiler on the PCC model. Steam supplied to the reboiler is extracted from the power plant. An increase of 10% in steam flowrate was introduced at a simulation time of 30000s (8.33hr) and was maintained to the end of the simulation time.

It was observed that the steam flowrate had a significant but slow effect on both CO₂ capture level and reboiler temperature (see Figure 3-14). Both the CO₂ capture level and reboiler temperature increases for a long period as the step increment is introduced to the steam flowrate. Similar dynamic behavioural trend is also observed in the first principles model.

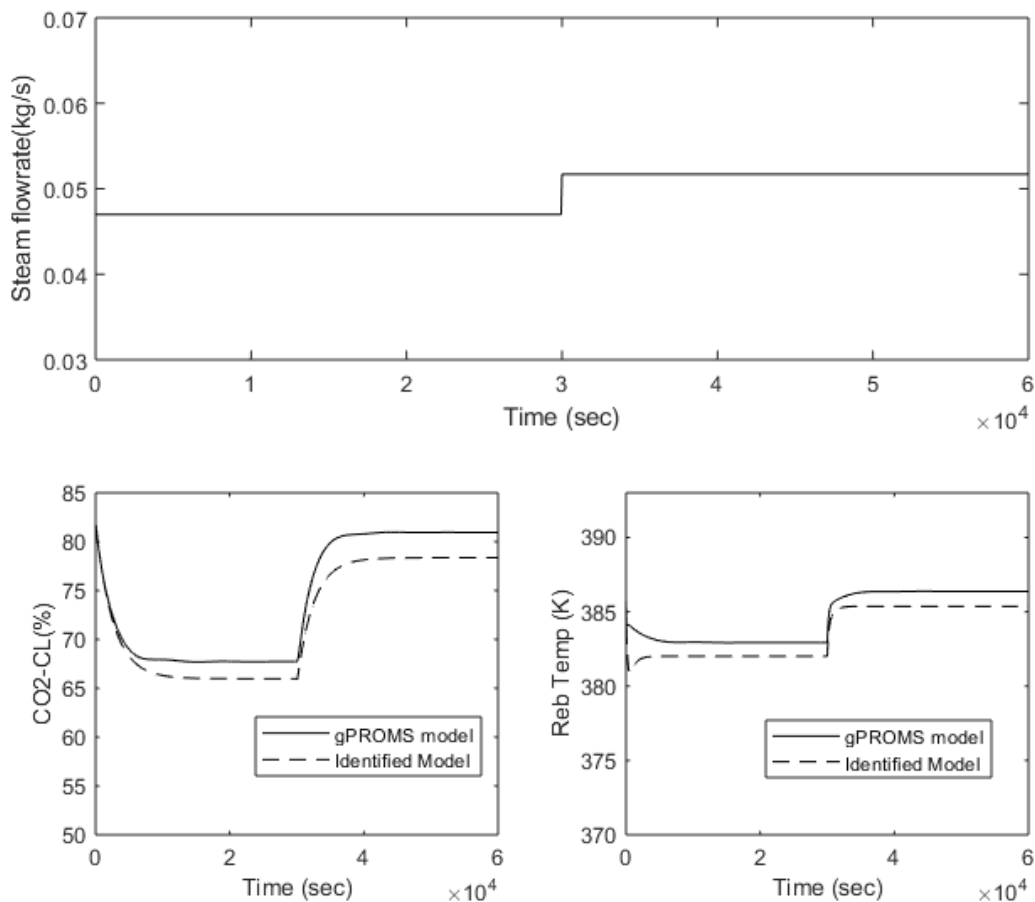


Figure 3-14 Output responses to a 10% step increase in steam flowrate (kg/s)

3.7 Summary

In this chapter, a parsimonious polynomial NARX model was developed to predict the dynamic responses of an MEA-based PCC plant (3-input and 2-output) using the FROLS-ERR algorithm. Process operational data was obtained from gPROMS model developed by Lawal *et al.*,(2010) for the SI implementation. The amine-based PCC plant was represented as two MISO sub-systems (3-input and 2-output). The key findings for this chapter are summarised as follows:

- The FROLS-ERR algorithm proved to be a powerful tool in selecting the most significant model terms for representing and predicting the response variables ($\text{CO}_2\text{-CL}$ and T_{reb}). These model terms were ranked based on ERR. This gives a simple and transparent mathematical representation of the systems where we can clearly know how the system outputs depend on the variables and their interactions.
- Identified models obtained from the different model term dictionaries were compared, in which the best model was selected based on the performance of MSP and OSA prediction. M_1^1 gave the best performances based on the prediction efficiency of both OSA and MPO for both subsystem-1 and subsystem-2. Statistical analysis of the identified model for each subsystem was carried out successfully.
- Process dynamic analysis of identified NARX models developed in comparison with the first principles (gPROMS®) model was carried out successfully. It was concluded that the identified model captures the underlying dynamics of the sub-systems.

4 Multivariable PI control Design on the solvent-based post-combustion CO₂ capture process

4.1 Introduction

This chapter describes the multivariable control design of the solvent-based PCC process model using the conventional PI controller. This includes development, implementation and performance evaluation of the decentralised control scheme on the CO₂ capture process. Multivariable controllability analysis was carried out on the identified model (developed in chapter 3) to develop potential suitable control structure configurations. This involved using 2 approaches (RGA analysis and process oriented approach). PI control was developed, implemented and evaluated based on set point tracking and disturbance rejection performance.

The state-space realisation of the identified CO₂ capture model and multivariable control structure analysis were presented in section 4.2 and 4.3 respectively. In section 4.4 and 4.5, the conventional PI control design and performance evaluation for the control structure were presented.

4.2 State-space realisation of the solvent-based PCC model

This section describes the state-space realisation of the solvent-based PCC model, which is represented as a multi-input multi-output polynomial NARX model. The NARX model is expressed as shown.

$$\begin{aligned}
y_1(t) = & a1y_1(t-1) + b1u_3(t-2) + a2y_1(t-2) + b2u_3(t-1) \\
& + c1 y_1(t-1)u_1(t-1) + c2 y_1(t-2)u_1(t-2) \\
& + b3u_2(t-2) + b4u_2(t-1) + b5u_1(t-1) + b6u_1(t-2) \\
& + c3u_2(t-1)u_3(t-2) + c4u_2(t-2)u_3(t-2) \\
& + c5u_1(t-2)u_2(t-1) + c6u_1(t-1)u_2(t-1) \\
& + c7u_1(t-2)u_2(t-2) + c8u_1(t-1)u_2(t-2) \\
& + c9y_1(t-1)u_1(t-2) + c10u_2(t-1)u_3(t-1) \\
& + c11y_1(t-1)u_3(t-1) + c12 y_1(t-2)u_1(t-1) + d
\end{aligned} \tag{4-1}$$

$$\begin{aligned}
y_2(t) = & a11 y_2(t-1) + a21y_2(t-2) + b11 u_3(t-1) + b21 u_3(t-2) \\
& + b31 u_2(t-1) + c11 u_3(t-1)u_3(t-2) \\
& + c21u_3(t-2)u_3(t-2) + c31 u_3(t-1)u_3(t-1) + d1 \\
& + c41 u_2(t-2)u_3(t-1) + c51 u_2(t-2)u_3(t-2) \\
& + c61 u_2(t-1)u_3(t-2) + b41 u_2(t-2) + b51 u_1(t-2)
\end{aligned} \tag{4-2}$$

The simple and transparent attribute of the polynomial NARX model has made the SI approach suitable. Despite the desirable attributes of the polynomial NARX, it is not suitable for many dynamic analysis and control applications (Sadegh, 2001). However, state models are often adopted for feedback control designs and stability analysis (Sadegh & Maqueira, 1994; Levin & Narendra, 1993). Hence the need for the state-space realisation of the nonlinear model. The state-space realisation of the nonlinear model includes the following (Kotta & Sadegh, 2002; Sadegh, 2001):

- Model reduction (i.e. observation representation of the model).
- State-space realisation of the observable representation of the model.

4.2.1 Model Reduction

This section details the determination of an observable representation of the identified model. This section adopted the procedural algorithm developed by Sadegh, (2001) to determine if the necessary condition to attain models that possess an observable state realisation. The algorithm is detailed as follows (Sadegh, 2001):

Step 1: Express model as an input/ output (i/o) map given as:

$$f(y_1, \dots, y_n, u_1, \dots, u_n)$$

Step 2: compute the scalar values for $\alpha_{i,j}$ and $\beta_{i,j}$, where are obtained as follows:

$$\alpha_{i,j}(y, u, v) := \gamma_j(y_i, \dots, y_n, f_1(y, u, v), \dots, f_{i-1}(y, u, v), u_i, \dots, u_n, v_1, \dots, v_{i-1}) \quad 4-3$$

$$\beta_{i,j}(y, u, v) := \gamma_{n+j}(y_i, \dots, y_n, f_1(y, u, v), \dots, f_{i-1}(y, u, v), u_i, \dots, u_n, v_1, \dots, v_{i-1}) \quad 4-4$$

Where $\gamma_j(y_i, \dots, y_n, u_i, \dots, u_n)$ and $\gamma_{n+j}(y_i, \dots, y_n, u_i, \dots, u_n)$ are the partial derivative of $f(y_1, \dots, y_n, u_1, \dots, u_n)$ with respect to y and u respectively. Move to the next step if $\alpha_{i,1}(y, u, v) \neq 0$ for $i = 1, \dots, n$. If not, the i/o map does not possess an observable state.

Step 3: for $i = 1, \dots, n$ and $j = 2, \dots, n - i + 1$ compute

$$\bar{\alpha}_{i,j} := \frac{\alpha_{i,j}}{\alpha_{i,1}}; \quad \bar{\beta}_{i,j} := \frac{\beta_{i,j}}{\alpha_{i,1}} \quad 4-5$$

Step 4: for $k = 0, \dots, n - 1$ and $i = 1, \dots, n - k$ compute

$$M_{i,i+k} = \bar{\beta}_{i,k+1} - \sum_{j=1}^k \bar{\alpha}_{i,j+1} M_{i+j,i+k} \quad 4-6$$

Step 5: the i/o maps has an observable state if $D_{v_l} M_{i,j}(y, u, v) = 0$, $l = 1, \dots, i - 1$, $v = (v_1, \dots, v_n)$. Where D_{v_l} is the partial derivative of $M_{i,j}(y, u, v)$ with respect to v .

Thus, the i/o map has an observable state-space representation of order n , if;

1. $\alpha_{i,1}(y, u, v)$ is nonzero for $i = 1, \dots, n$;
2. $M_{i,j}(y, u, v)$ for $i = 2, \dots, n, j = i, \dots, n$ are independent of v_1, \dots, v_{i-1}

The algorithms were implemented as follows:

The polynomial model in equations 4-1 and 4-2 can be expressed as:

$$y_i(t) = f(y_i(t-2), y_i(t-1), u_j(t-2), u_j(t-1)) \quad 4-7$$

Where i and j represent the number of output and input variables respectively. As the CO₂ capture process was identified as two (2) MISO system in chapter 3, equation 4-7 can be rewritten as:

$$y_1(t) = f(y_1(t-2), y_1(t-1), u_j(t-2), u_j(t-1)) \quad 4-8$$

$$y_2(t) = f(y_2(t-2), y_2(t-1), u_j(t-2), u_j(t-1)) \quad 4-9$$

Where

$$\begin{aligned} & f(y_1(t-2), y_1(t-1), u_j(t-2), u_j(t-1)) \\ &= a_1 y_1^2 + b_1 u_3^1 + a_2 y_1^1 + b_2 u_3^2 + c_1 y_1^2 u_1^2 + c_2 y_1^1 u_1^1 \\ &+ b_3 u_2^1 + b_4 u_2^2 + b_5 u_1^2 + b_6 u_1^1 + c_3 u_2^2 u_3^1 + c_4 u_2^1 u_3^1 \quad 4-10 \\ &+ c_5 u_1^1 u_2^2 + c_6 u_1^2 u_2^2 + c_7 u_1^1 u_2^1 + c_8 u_1^2 u_2^1 + c_9 y_1^2 u_1^1 \\ &+ c_{10} u_2^2 u_3^2 + c_{11} y_1^2 u_3^2 + c_{12} y_1^1 u_1^2 + d \end{aligned}$$

$$\begin{aligned}
& f(y_2(t-2), y_2(t-1), u_j(t-2), u_j(t-1)) \\
& = a_{11} y_2^2 + a_{21} y_2^1 + b_{11} u_3^2 + b_{21} u_3^1 + c_{11} u_3^2 u_3^1 + c_{21} u_3^1 u_3^1 \\
& + c_{31} u_3^2 u_3^2 + d_1 + c_{41} u_2^1 u_3^2 + c_{51} u_2^1 u_3^1 + c_{61} u_2^2 u_3^1 \\
& + b_{41} u_2^1 + b_{51} u_1^1
\end{aligned} \tag{4-11}$$

Following step 2, $\alpha_{i,j}$ and $\beta_{i,j}$ are computed as follows:

For equation 4-10,

$$\begin{aligned}
\alpha_{1,1} &= a_2 + c_2 u_1^1 + c_{12} u_1^2 \\
\alpha_{1,2} &= a_1 + c_1 u_1^2 + c_9 u_1^1 + c_{11} u_3^2 \\
\alpha_{2,1} &= a_2 + c_2 u_1^2 + c_{12} v_1 \\
\alpha_{2,2} &= a_1 + c_1 v_1 + c_9 u_1^2 + c_{11} v_3 \\
\beta_{1,1}^1 &= b_6 + c_2 y_1^1 + c_5 u_2^2 + c_7 u_2^1 + c_9 y_1^2 \\
\beta_{1,2}^1 &= b_5 + c_1 y_1^2 + c_5 u_1^1 + c_6 u_2^2 + c_8 u_2^1 + c_{12} y_1^1 \\
\beta_{2,1}^1 &= b_6 + c_2 y_1^2 + c_5 v_2 + c_7 u_2^2 + c_9 f(y_1^1, y_1^2, u_1^1, u_1^2, u_2^1, u_2^2, u_3^1, u_3^2) \\
\beta_{2,2}^1 &= b_5 + c_1 f(y_1^1, y_1^2, u_1^1, u_1^2, u_2^1, u_2^2, u_3^1, u_3^2) + c_5 u_1^2 + c_6 v_2 + c_8 u_2^2 + c_{12} y_1^2 \\
\beta_{1,1}^2 &= b_3 + c_4 u_3^1 + c_7 u_1^1 + c_8 u_1^2 \\
\beta_{1,2}^2 &= b_4 + c_{10} u_3^2 + c_5 u_1^1 + c_6 u_1^2 \\
\beta_{2,1}^2 &= b_3 + c_4 u_3^2 + c_7 u_1^2 + c_8 v_1 \\
\beta_{2,2}^2 &= b_4 + c_{10} v_3 + c_5 u_1^2 + c_6 v_1 \\
\beta_{1,1}^3 &= b_1 + c_3 u_2^2 + c_4 u_2^1 \\
\beta_{1,2}^3 &= b_2 + c_{10} u_2^2 + c_{11} y_1^2 \\
\beta_{2,1}^3 &= b_1 + c_3 v_2 + c_4 u_2^2 \\
\beta_{2,2}^3 &= b_2 + c_{10} v_2 + c_{11} f(y_1^1, y_1^2, u_1^1, u_1^2, u_2^1, u_2^2, u_3^1, u_3^2)
\end{aligned} \tag{4-12}$$

For equation 4-11,

$$\alpha_{1,1} = a_{21}$$

$$\alpha_{1,2} = a_{11}$$

$$\alpha_{2,1} = a_{21}$$

$$\alpha_{2,2} = a_{11}$$

$$\beta_{1,1}^1 = b_{51}$$

$$\beta_{1,2}^1 = 0$$

$$\beta_{2,1}^1 = b_{51}$$

$$\beta_{2,2}^1 = 0$$

$$\beta_{1,1}^2 = b_{41} + c_{41} u_3^2 + c_{51} u_3^1$$

$$\beta_{1,2}^2 = b_{31} + c_{61} u_3^1$$

$$\beta_{2,1}^2 = b_{41} + c_{41} v_3 + c_{51} u_3^2$$

$$\beta_{2,2}^2 = b_{31} + c_{61} u_3^2$$

$$\beta_{1,1}^3 = b_{21} + c_{11} u_3^2 + c_{21} u_3^1 + c_{51} u_2^1 + c_{61} u_2^2$$

$$\beta_{1,2}^3 = b_{11} + c_{11} u_3^1 + c_{31} u_3^2 + c_{41} u_2^1$$

$$\beta_{2,1}^3 = b_{21} + c_{11} v_3 + c_{21} u_3^2 + c_{51} u_2^2 + c_{61} v_2$$

$$\beta_{2,2}^3 = b_{11} + c_{11} u_3^2 + c_{31} v_3 + c_{41} u_2^2$$

4-13

Using steps 3 and 4, the elements that need to be checked for v independence is:

$$\bar{\beta}_{2,1}^m = \frac{\beta_{2,1}^m}{\alpha_{2,1}^n}$$

4-14

Where m and n are the number of input and output variables respectively. This is then rewritten as follows:

$$\bar{\beta}_{2,1}^1 = \frac{\beta_{2,1}^1}{\alpha_{2,1}^1} = \frac{b_6 + c_2 y_1^2 + c_5 v_2 + c_7 u_2^2 + c_9 f(y_1^1, y_1^2, u_1^1, u_1^2, u_2^1, u_2^2, u_3^1, u_3^2)}{a_2 + c_2 u_1^2 + c_{12} v_1}$$

4-15

$$\bar{\beta}_{2,1}^2 = \frac{\beta_{2,1}^2}{\alpha_{2,1}^1} = \frac{b3 + c4 u_3^2 + c7u_1^2 + c8v_1}{a2 + c2 u_1^2 + c12 v_1}$$

$$\bar{\beta}_{2,1}^3 = \frac{\beta_{2,1}^3}{\alpha_{2,1}^1} = \frac{b1 + c3v_2 + c4 u_2^2}{a2 + c2 u_1^2 + c12 v_1}$$

And

$$\bar{\beta}_{2,1}^1 = \frac{\beta_{2,1}^1}{\alpha_{2,1}^2} = \frac{b51}{a21}$$

$$\bar{\beta}_{2,1}^2 = \frac{\beta_{2,1}^2}{\alpha_{2,1}^2} = \frac{b41 + c41 v_3 + c51 u_3^2}{a21}$$

4-16

$$\bar{\beta}_{2,1}^3 = \frac{\beta_{2,1}^3}{\alpha_{2,1}^2} = \frac{b21 + c11 v_3 + c21 u_3^2 + c51 u_2^2 + c61v_2}{a21}$$

For equations 4-15 and 4-16, the conditions for the independence of v_1, v_2 and v_3 are satisfied if $c3 = c5 = c8 = c12 = 0$ and $c41 = c11 = c61 = 0$ for both models respectively. Thus, the models are reduced to the following:

$$\begin{aligned} y_1(t) = & a1y_1(t-1) + b1u_3(t-2) + a2y_1(t-2) + b2u_3(t-1) \\ & + c1 y_1(t-1)u_1(t-1) + c2 y_1(t-2)u_1(t-2) \\ & + b3u_2(t-2) + b4u_2(t-1) + b5u_1(t-1) + b6u_1(t-2) \\ & + c4u_2(t-2)u_3(t-2) + c6u_1(t-1)u_2(t-1) \\ & + c7u_1(t-2)u_2(t-2) + c9y_1(t-1)u_1(t-2) \\ & + c10u_2(t-1)u_3(t-1) + c11y_1(t-1)u_3(t-1) + d \end{aligned}$$

4-17

$$\begin{aligned}
y_2(t) = & a_{11} y_2(t-1) + a_{21} y_2(t-2) + b_{11} u_3(t-1) + b_{21} u_3(t-2) \\
& + b_{31} u_2(t-1) + c_{21} u_3(t-2) u_3(t-2) \\
& + c_{31} u_3(t-1) u_3(t-1) + c_{51} u_2(t-2) u_3(t-2) \\
& + b_{41} u_2(t-2) + b_{51} u_1(t-2) + d_1
\end{aligned}
\tag{4-18}$$

The parameters of each model term was re-estimated (see Table 4-1). The state realization of the observable i/o map representation was carried out in the next section.

Table 4-1 re-evaluated parameters for the observable i/o map representation of CO₂ capture model

| Sub-system 1 | | Sub-system 2 | |
|--------------|------------|--------------|-------------|
| <i>a</i> 1 | 1.33071 | <i>a</i> 11 | 1.66322 |
| <i>a</i> 2 | -0.30590 | <i>a</i> 21 | -0.68343 |
| <i>b</i> 1 | 350.72538 | <i>b</i> 11 | 282.04840 |
| <i>b</i> 2 | 373.71848 | <i>b</i> 21 | -251.35450 |
| <i>b</i> 3 | -14.21754 | <i>b</i> 31 | -2.36230 |
| <i>b</i> 4 | 7.57860 | <i>b</i> 41 | 0.12312 |
| <i>b</i> 5 | -169.52542 | <i>b</i> 51 | -0.35492 |
| <i>b</i> 6 | 178.52496 | <i>c</i> 21 | 1002.96807 |
| <i>c</i> 1 | -2.38873 | <i>c</i> 31 | -1379.39709 |
| <i>c</i> 2 | 0.68108 | <i>c</i> 51 | 28.13632 |
| <i>c</i> 4 | -365.18678 | <i>d</i> 1 | 7.86578 |
| <i>c</i> 6 | 191.65801 | | |
| <i>c</i> 7 | -193.17331 | | |
| <i>c</i> 9 | 1.50097 | | |
| <i>c</i> 10 | 482.89666 | | |
| <i>c</i> 11 | -0.21862 | | |
| <i>d</i> | 1.90568 | | |

4.2.2 Classical state-space realisation

This section focuses on the state-space realisation of observable i/o map representation of the nonlinear model (see equations 4-17 and 4-18). The classical state-space realization was carried out following Kotta & Sadegh, (2002). The state components are shown:

Output 1: CO₂ capture level (CO₂-CL)

$$x_1(t) = y_1(t)$$

$$x_2(t) = y_1(t+1) - a_1y_1(t) - b_2u_3(t) - c_1y_1(t)u_1(t) - b_4u_2(t) - b_5u_1(t) \\ - c_6u_1(t)u_2(t) - c_{10}u_2(t)u_3(t) - c_{11}x_1(t)u_3(t) - d$$

Output 2: Reboiler Temperature (T_{reb})

$$x_3(t) = y_2(t)$$

$$x_4(t) = y_2(t+1) - a_{11}y_2(t) - b_{11}u_3(t) - b_{31}u_2(t) - c_{31}u_3(t)u_3(t) - d_1$$

Shifting the equations above one-step forward the following was obtained:

$$x_1(t+1) = x_2(t) + a_1x_1(t) + b_2u_3(t) + c_1x_1(t)u_1(t) + b_4u_2(t) + b_5u_1(t) \\ + c_6u_1(t)u_2(t) + c_{10}u_2(t)u_3(t) + c_{11}x_1(t)u_3(t) + d$$

$$x_2(t+1) = a_2x_1(t) + b_1u_3(t) + b_3u_2(t) + b_6u_1(t) + c_2x_1(t)u_1(t) \\ + c_4u_2(t)u_3(t) + c_7u_1(t)u_2(t) + c_6x_1(t+1)u_1(t)$$

$$x_3(t+1) = x_4(t) + a_{11}x_3(t) + b_{11}u_3(t) + b_{31}u_2(t) + c_{31}u_3(t)u_3(t) + d_1$$

$$x_4(t+1) = a_{21}x_3(t) + b_{21}u_3(t) + b_{41}u_2(t) + c_{21}u_3(t)u_3(t) + c_{51}u_2(t)u_3(t) \\ + b_{51}u_1(t)$$

$$y_1(t) = x_1(t)$$

$$y_2(t) = x_3(t)$$

Step change analysis was carried out on the nonlinear state-space model was carried out to ensure that it captures the dynamics of the solvent-based PCC process. Figure 4-1 shows output responses to the step-change implemented on each input variable.

From Figure 4-1, it was observed that the nonlinear state-space realisation captures the inherent dynamics of the capture model as the step analysis of the state space model aligns with the step dynamics of the first principles model discussed in section 3.6 and reported in literature (Wu et al., 2018). The nonlinear state-space model was adopted for the control structure analysis.

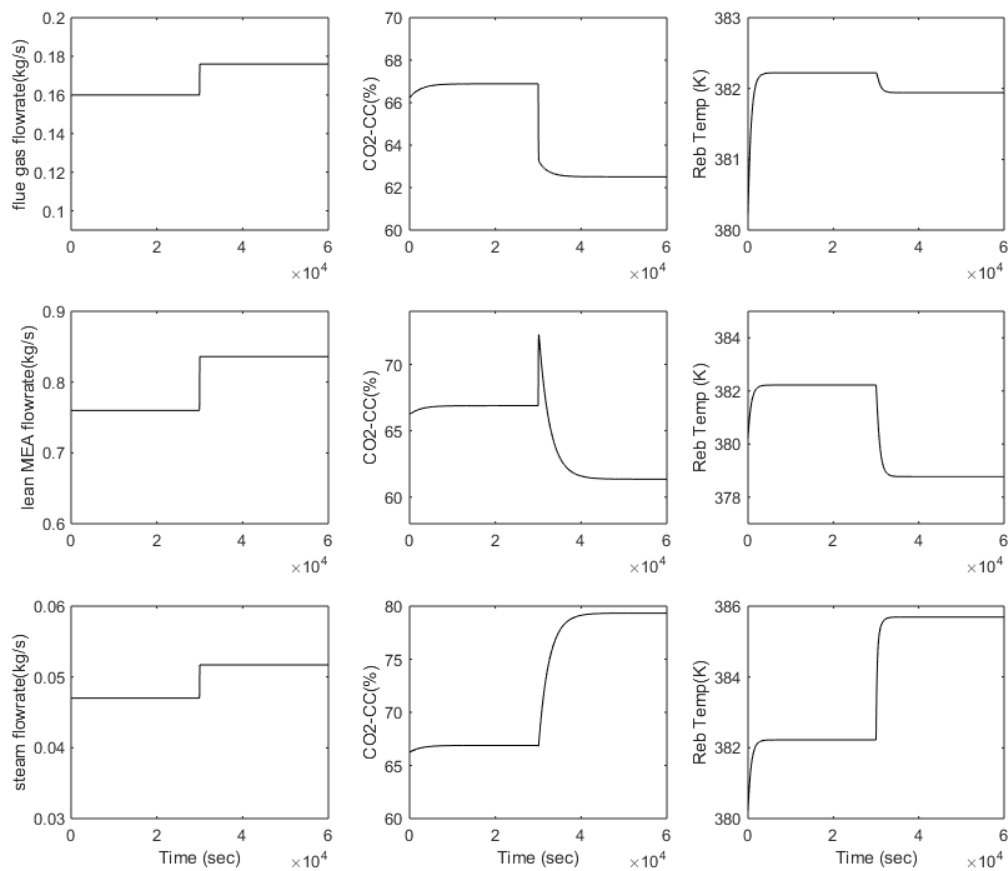


Figure 4-1 Output responses to step-change implemented on each input variable: for each input variables a step change of +10% was introduced one at a time.

4.3 Multivariable Control structure design and analysis

The solvent-based PCC model, which is a multivariable system, is very difficult to control due to the interactions between inputs and outputs, which affects the process

performance. Hence, the control structure analysis of the multivariable system is necessary to appropriately select the right loop pairings that minimize the interactions within the system. This section details the methodology involved in selecting the appropriate loop-pairing configuration within the CO₂ capture process. For the solvent-based PCC model, the controlled (output) variables include:

- CO₂ capture level (CO₂ –CL) and
- Reboiler temperature (T_{reb})

The manipulated variables includes:

- lean solvent flow rate and
- steam flowrate,

The disturbance variables is identified as:

- Flue gas flowrate

Thus, the capture model is identified as a (3 X 2) multivariable nonlinear system. Figure 4-2 shows the capture process model represented as a multivariable block system in Simulink. Two approaches adopted for the loop pairing selection includes:

- Relative gain array (RGA) analysis
- Process oriented approach

4.3.1 RGA analysis

RGA analysis was adopted to investigate the interactions within the solvent-based CO₂ capture model. RGA analysis was carried out at different steady-state conditions. Following RGA formulation in section 2.4.1.1 (equation 2-24), the RGA at each steady-state condition (SSC) is shown in Table 4-2. The steady-state gain for each SS

condition is determined by introducing a 10% step to the manipulated variables (lean solvent flowrate and steam flowrate).

Table 4-2 RGA at different steady-state condition; FGF: flue gas flowrate; LSF: lean solvent flowrate; SF: steam flowrate

| Steady-state condition | Input variable values | | | Output variable values | | RGA |
|------------------------|-----------------------|------------|-----------|-------------------------|----------------------|--|
| | FGF (kg/s) | LSF (kg/s) | SF (kg/s) | CO ₂ -CL (%) | T _{reb} (K) | |
| SSC 1 | 0.14 | 0.76 | 0.047 | 75.19 | 382.6 | $\begin{bmatrix} -0.8508 & 1.8508 \\ 1.8508 & -0.8508 \end{bmatrix}$ |
| SSC 2 | 0.16 | 0.76 | 0.047 | 66.89 | 382.2 | $\begin{bmatrix} -0.8086 & 1.8086 \\ 1.8086 & -0.8086 \end{bmatrix}$ |
| SSC 3 | 0.18 | 0.76 | 0.047 | 61.62 | 381.9 | $\begin{bmatrix} -0.7950 & 1.7950 \\ 1.7950 & -0.7950 \end{bmatrix}$ |

As shown in Table 4-2, The RGA analysis suggests that the off-diagonal pairing should be selected as the appropriate control configuration. This indicates that CO₂ –CL should be controlled using steam flowrate while reboiler temperature (T_{reb}) should be controlled using lean solvent flowrate. This finding was similar to what was obtained by Nittaya *et al.*, (2014a). This off-diagonal pairing is maintained for the different steady-state conditions, as the RGA element values are positive. Loop interactions within this pairing are expected as the off-diagonal elements are greater than 1.

Niederlinsky Index (NI) and Morari Index of Integral Controllability (MIC) are determined to certify the suitability of the pairing. The steady-state gain (G (0)) is re-ordered such that the paired variables were diagonal. The NI values shown in Table 4-3 are positive, indicating that the system is stable in close-loop. The negative MIC values for T_{reb} controlled variable eliminates the control configuration suggested by RGA analysis. The negative MIC indicates that the proposed loop pairings cannot

maintain the robustness and stability of the closed-loop system when tuned. Hence, an alternative approach is adopted to select a suitable control configuration.

Table 4-3 NI and MIC values for the RGA pairings; SSC-steady state condition

| SSC | NI | MIC |
|-----|--------|---|
| 1 | 0.5403 | $\begin{bmatrix} 3.2222E^3 \\ -24.6717 \end{bmatrix}$ |
| 2 | 0.5529 | $\begin{bmatrix} 2.6303E^3 \\ -25.2778 \end{bmatrix}$ |
| 3 | 0.5571 | $\begin{bmatrix} 2.2168E^3 \\ -25.5025 \end{bmatrix}$ |

4.3.2 Process-oriented approach

Insight from the process (step) dynamics of the solvent-based CO₂ capture model. Process dynamic analysis of the CO₂ capture model revealed that both the lean solvent flowrate and steam flowrate has a significant effect on the controlled variables (CO₂-CL and T_{reb}) (Lawal *et al.*, 2010). It was observed that the lean solvent flowrate has a quick effect on the CO₂ capture level, while the steam flowrate has a slow effect on the CO₂ capture level (Lawal *et al.*, 2010). The reverse effect of the respective manipulated variables on reboiler temperature was observed. This indicates that the CO₂-CL set point will be recovered faster when controlled using lean solvent flowrate (Nittaya *et al.*, 2014a). Thus, this approach suggests that CO₂-CL is controlled using lean solvent flowrate, while the reboiler temperature (T_{reb}) is controlled using steam flowrate. Similar loop pairing has been suggested by other researchers (Wu *et al.*, 2018; Mechleri *et al.*, 2017). This control configuration is shown below:

CO₂-CL - LSF

T_{reb} - SF

The controller design of each loop pairing is carried out in the next section.

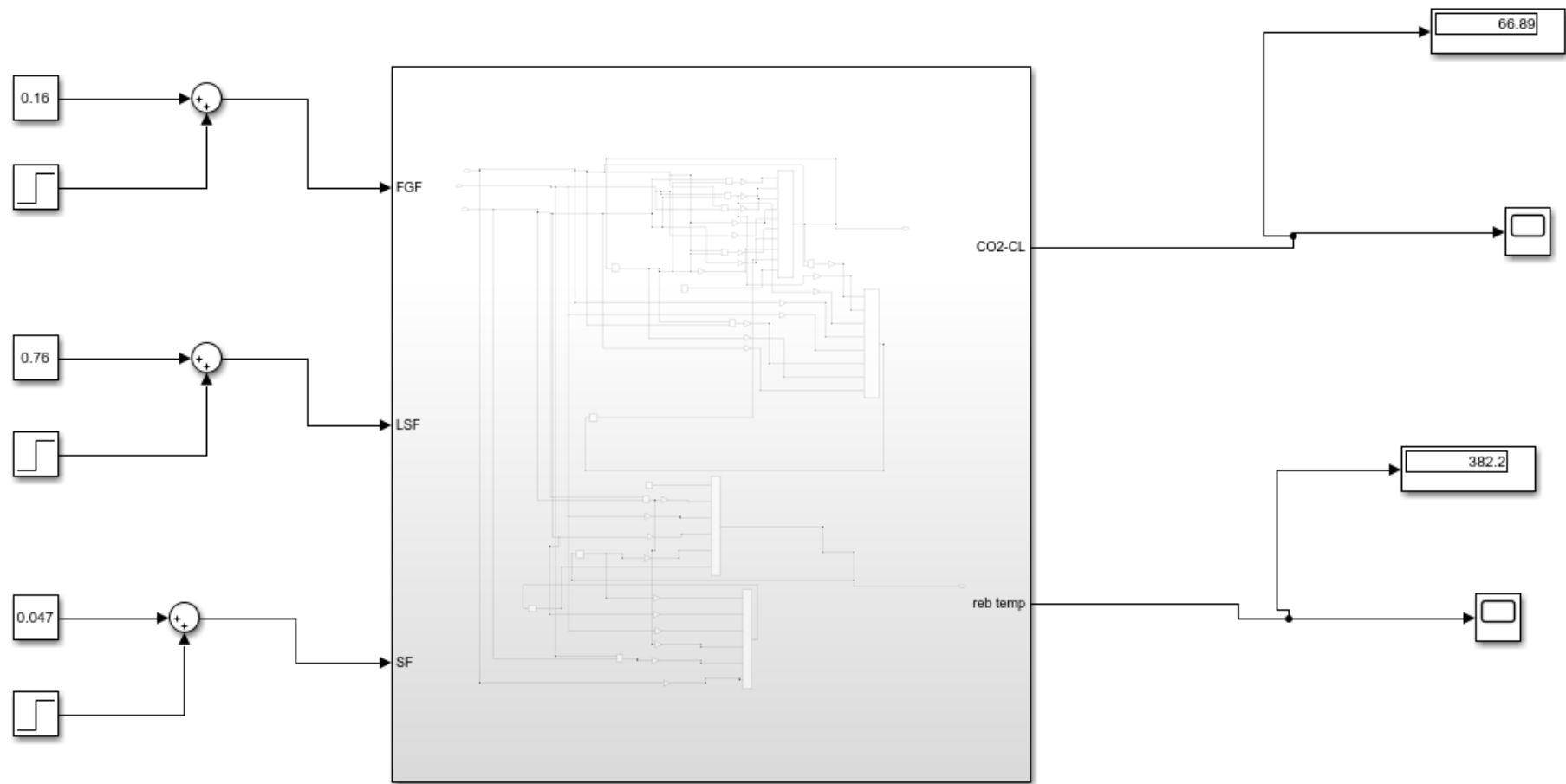


Figure 4-2 Solvent-based PCC model on Simulink® environment

4.4 Controller design

In this section, a Conventional PI controller is designed for each looping pairing. Figure 4-3 shows the schematic implementation of the Conventional PI controllers on the capture process model. The measurement sensor and actuator for each loop pairing were assumed to be unity gain (1). Conventional PI control parameters were tuned using MATLAB PID tuner app. The conventional PI control parameters are shown in Table 4-4.

Table 4-4 Conventional PI Control Parameters for each loop pairing

| | | |
|---------------------------|---|---------------|
| CO ₂ -CL - LSF | P | 0.0099743 |
| | I | 3.4604950e-06 |
| T _{reb} - SF | P | 0.0014937 |
| | I | 7.5053490-06 |

The PI control parameters for each loop pairing were updated into the Simulink model. Performance evaluation of the control configuration based on disturbance rejection and set point tracking was carried out in the next section.

4.5 Decentralised Control Performance Evaluation

The section details the performance evaluation of the conventional PI-control configuration proposed. The control configuration was evaluated under various scenarios for disturbance rejection and set-point tracking. These include:

Disturbance rejection:

- Scenario 1: 10% step increase in the flue gas flowrate.

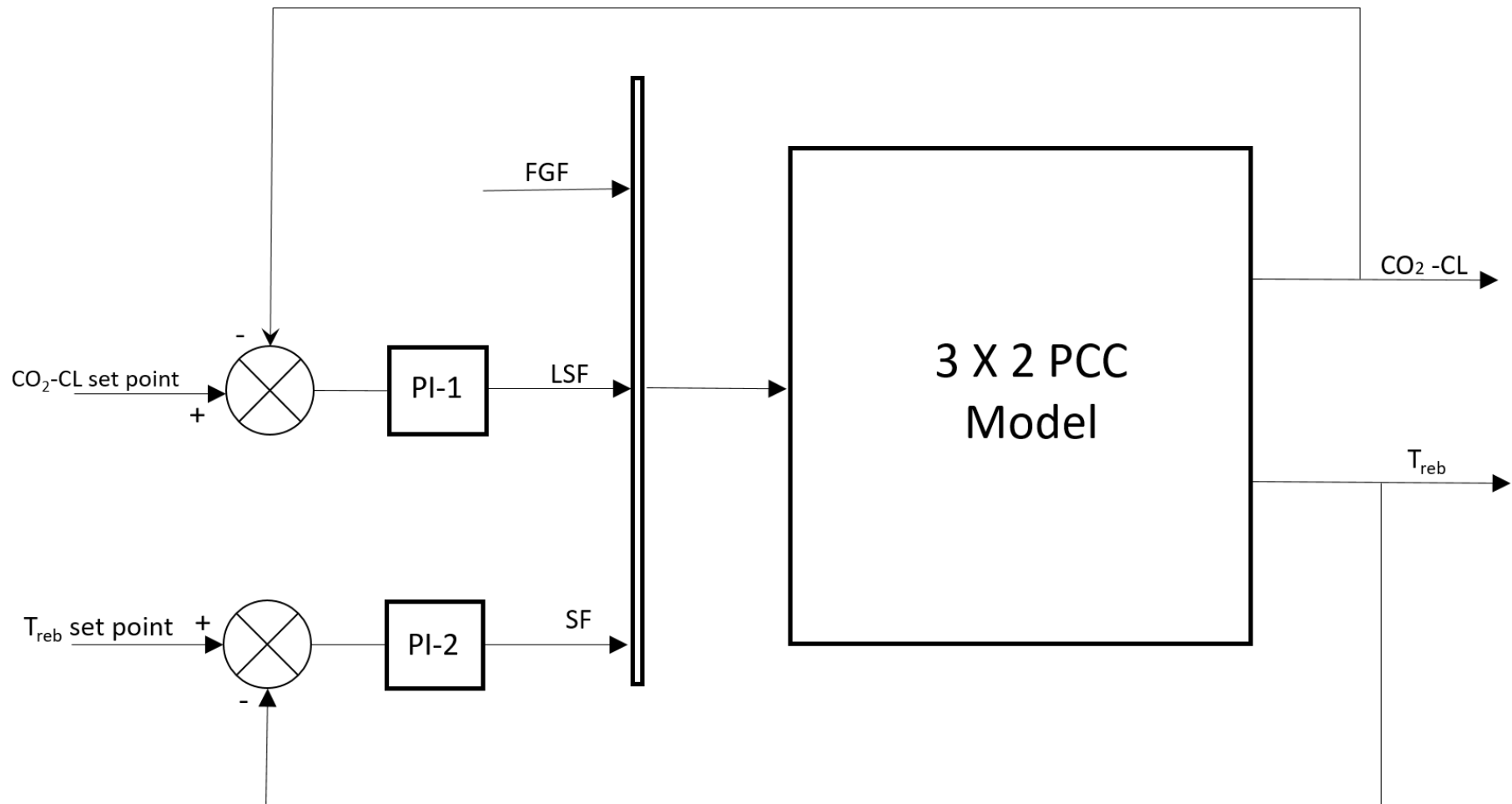


Figure 4-3 Design and implementation of PI controller on the PCC model; FGF-flue gas flowrate ; LSF- lean solvent flowrate; SF- steam flowrate; CO₂-CL – CO₂ capture level ; T_{reb} – Reboiler temperature.

Set-point tracking

- Scenario 2: CO₂ capture level (CO₂ –CL) step increase
- Scenario 3: Reboiler temperature (T_{reb}) step increase

For all scenarios, the desired closed-loop control performance target is to attain less overshoot, fast response and quick settling time (within minutes). For each scenario, the performance was evaluated based on integral squared error (ISE) of the controlled variables against its respective set-points (Nittaya et al., 2014a) and settling time. This is calculated as:

$$ISE(CV) = \int_{t=0}^{t_{final}} (CV_{SP} - CV(t))^2 dt \quad 4-19$$

4.5.1 Disturbance rejection (scenario 1)

This section evaluates the performance of the CO₂ capture plant-control system in a scenario where there is a change in the flue gas flowrate, which is recognised as a disturbance variable. This reflects a change in the power plant load. In this section, a 10% step increase in flue gas flowrate was introduced at simulation time 18000s (5hr) to the CO₂ capture model. The controlled variable (CO₂-CL and T_{reb}) set points are maintained at the nominal operating conditions (66.89% CO₂-CL and 382.2K T_{reb}). The controlled variables were monitored to observe the disturbance rejection performance of the decentralised control strategy.

Figure 4.4 showed the disturbance rejection performance of the conventional PI control configuration to a 10% step increase of the flue gas flowrate. It was observed that the PI control scheme rejects the effect of the flue gas flowrate on the controlled variables. A point of concern is the settling time (9hrs) for the controlled variables (especially CO₂-CL) to attain steady-state. Settling time around similar region was

recorded by Nittaya et al., (2014b) . As can be seen in Table 4.4, the conventional PI has a sluggish performance on the CO₂-CL controlled variable. This is a major limitation of the conventional PI controller, as a fast controller performance is required to quickly deal with the flexibility of the CO₂ capture plant.

A slight reduction in the reboiler temperature (T_{reb}) was observed, which was immediately counteracted by the steam flowrate. The minimal effect of flue gas flowrate on reboiler temperature (T_{reb}) enabled the performance of the PI control scheme on the loop.

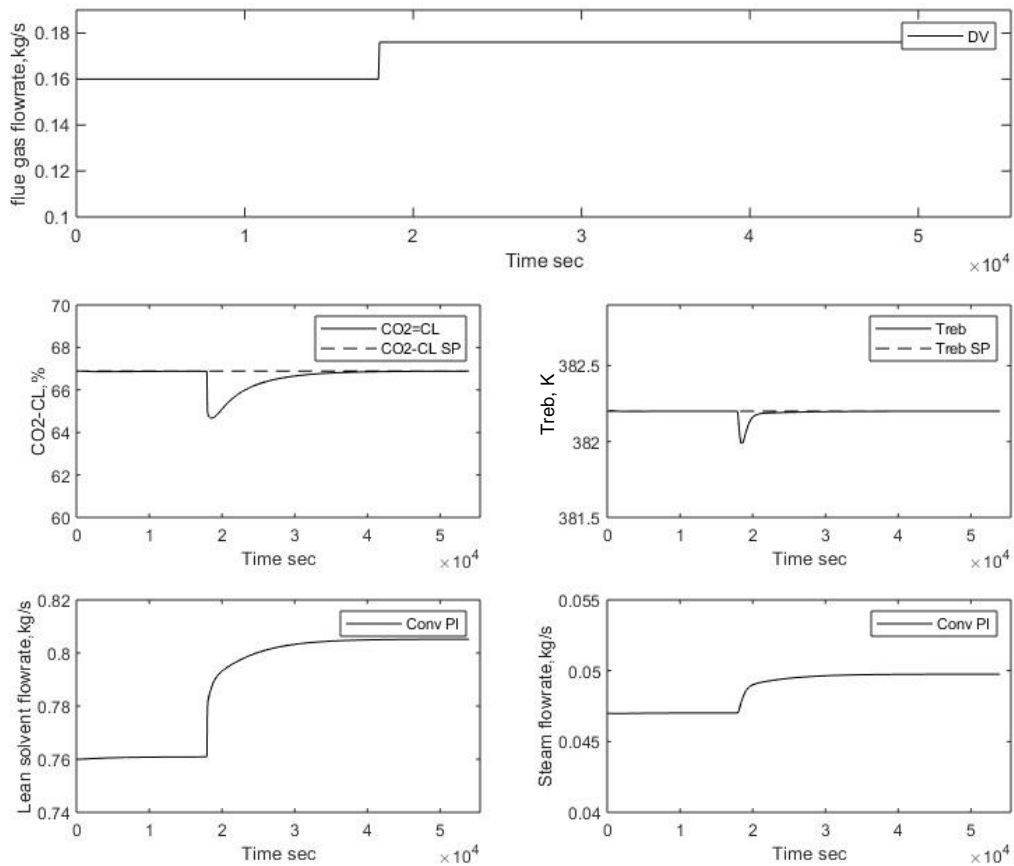


Figure 4-4 Close-loop capture model response, to a 10% step change in flue gas flowrate

Table 4-5 Performance evaluation of the conventional PI control scheme

| Scenarios | Controlled variables | | | |
|-----------|---|---------------|--|---------------|
| | CO ₂ capture level (CO ₂ -CL) | | Reboiler Temperature (T _{reb}) | |
| | ISE | Settling time | ISE | Settling time |
| 1 | 269.50 | 9hr | 0.684 | 0.52hr |
| 2 | 7499.71 | 8.75hr | 14.184 | 0.67hr |
| 3 | 1606.97 | > 10hr | 15.907 | 2.28hr |

4.5.2 Set-point tracking (Scenarios 2 &3)

This section evaluates the set-point tracking performance of the Decentralised control strategy. In this section, two (2) scenarios were considered;

4.5.2.1 Scenario 2

In this section, the CO₂ capture level (CO₂-CL) set point was increased from the nominal operating condition to 90%. The reboiler temperature (T_{reb}) setpoint is maintained at its nominal value. In this scenario, the CO₂ capture level set point was increased to 90% at a simulation time of 18000s (5hr) to the closed-loop system. This attained by using the step change in the CO₂ capture level set point. As shown in Figure 4-5 and Table 4-5, the conventional PI control scheme requires 8.75hr to achieve the new CO₂ capture level set point. Similar challenge as regards sluggish performance of the conventional PI control although the controlled variables attain their respective set-points. The increase in lean solvent flowrate to attain the new CO₂ capture level resulted in a reduction in the reboiler temperature (T_{reb}). However, the T_{reb} – SF loop was able to adequately offset and adjust the reboiler temperature (T_{reb}) controlled variable to its set point.

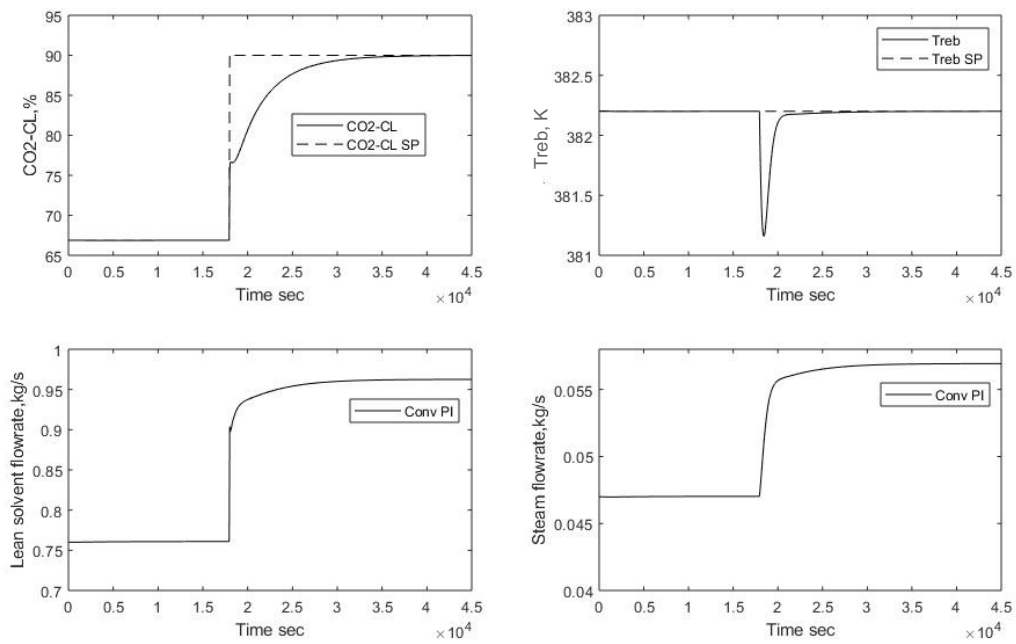


Figure 4-5 Closed-loop output responses to an increase in CO₂-CL (%)

4.5.2.2 Scenario 3

This scenario reviews the conventional PI control scheme closed-loop performance when the reboiler temperature (T_{reb}) set point was increased from its nominal operating point to 385K and CO₂-CL set point is maintaining at its nominal operational condition. This scenario was achieved by introducing a step increase in the reboiler temperature (T_{reb}) controlled variable at a simulation time of 18000s (5hr).

It can be observed from Fig 4-6 that the conventional PI control scheme was not able to meet all the control objectives (CO₂-CL). Although the new reboiler temperature (T_{reb}) set point was attained by manipulating the steam flowrate, an increase in steam flowrate resulted in a significant increase in CO₂ -CL controlled variable. The CO₂-CL -LSF loop was not able to adequately track CO₂ -CL to its set point.

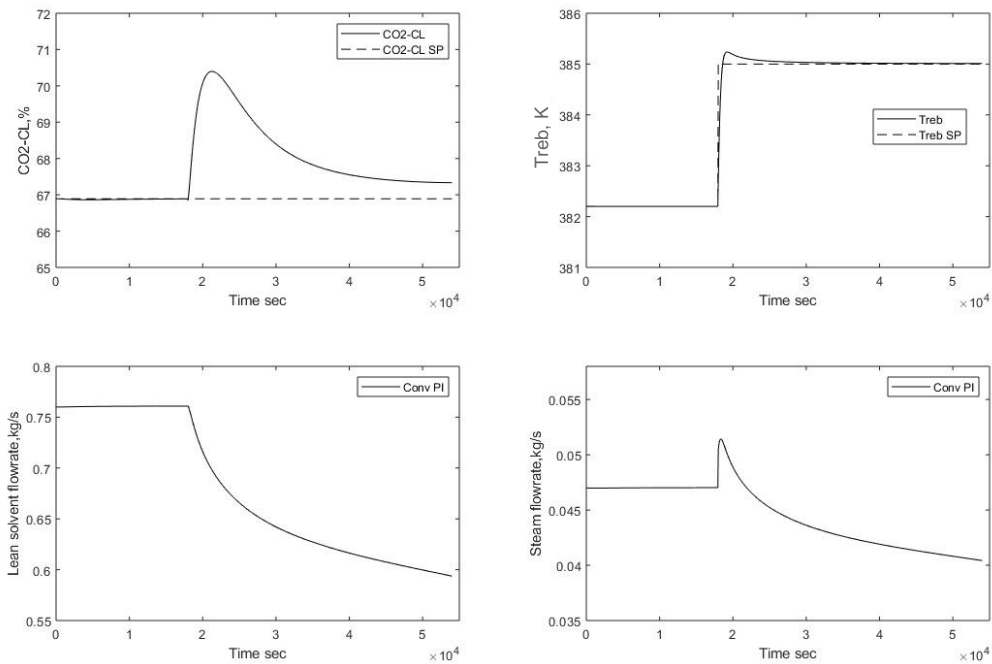


Figure 4-6 Closed-loop output responses to an increase in reboiler temperature (T_{reb})

4.6 Summary

In this Chapter, multivariable process control analysis and design of the solvent-based CO₂ capture process was carried out. This entails selecting an appropriate process control configuration and evaluating its performance under various scenarios. The identified nonlinear CO₂ capture model was adopted for the control analysis and implementation. The observable state-space realization of the nonlinear model was obtained for ease of control analysis. The following conclusions for this chapter are summarised as follows:

- RGA analysis was insufficient on the selection of an appropriate control configuration. The control configuration suggested by RGA analysis failed to meet the MIC criteria, which makes the closed-loop system unstable when the PI control is tuned.

- Process-oriented insight approach was adopted to select an appropriate control configuration (loop pairing). The loop pairing is shown below:

$$\text{CO}_2 - \text{CL} \rightarrow \text{LSF}$$

$$T_{reb} \rightarrow \text{SF}$$

A conventional PI control was design and implemented on the control scheme.

- The control scheme performance was evaluated under 3 scenarios based on ISE and settling for the controlled variable to attain steady-state condition.
- The conventional PI control scheme demonstrated a sluggish closed-loop performance under scenarios 1 and 2, although it was able to achieve its control objective. The settling time of the PI control under these scenarios was very large.
- The closed-loop performance of conventional PI control scheme under scenario 3 was weak due to its inability to deal with loop interactions within the capture model (i.e. maintaining CO₂-CL set-point). This call for the implementation of the model predictive control (MPC), which was implemented in the next Chapter

5 Linear model predictive control design and implementation on the solvent-based PCC process

5.1 Introduction

The chapter focuses on the design and implementation of a linear model predictive control (MPC) scheme on the solvent-based PCC process. As highlighted in the previous Chapter 4, the conventional PI control scheme gave a poor control performance based on its settling time and inability to handle loop interactions within the CO₂ capture process. The model predictive control (MPC) is a multivariable control scheme that has the advantage of being able to handle interactions within the process (Camacho & Alba, 2013). Thus, its implementation is becoming popular both in the industry and in academia (Zhang *et al.*, 2016; He *et al.*, 2016; Wu *et al.*, 2018). The MPC scheme uses a linear model to obtain control sequences that best achieve the desired output by optimizing the control objective function (Wu *et al.*, 2018; Camacho & Alba, 2013). MPC scheme performance was evaluated under different scenarios in comparison with the conventional PI-control scheme. Scenarios considered for control scheme performance in this chapter differs from what has been considered in chapter 4 as these scenarios are to reflect the flexible operation of solvent-based PCC process away from the nominal conditions (such as ramp change in flue gas flowrate , ramp change in CO₂-CL and variation of flue gas flowrate and CO₂-CL simultaneously).

In this chapter, section 5.2 describes the linearization of the solvent-based CO₂ capture model, while section 5.3 the MPC control scheme design for the capture process. The performance of the MPC scheme is evaluated in section 5.4.

5.2 Model Linearization

This section focuses on the linearization of the solvent-based PCC model developed via a nonlinear SI approach. The identified nonlinear model was represented as a Simulink model (see Figure 4-2). The nonlinear Simulink model was linearized around the operating point shown in Table 5-1 to obtain a discrete linear state-space model. This was carried out using the linear analysis toolbox in simulink.

Table 5-1 Linearization operating point

| | | |
|------------------|---|------------|
| Input variables | Flue gas flowrate | 0.16 kg/s |
| | Lean solvent flowrate | 0.76 kg/s |
| | Steam flowrate | 0.047 kg/s |
| Output variables | CO ₂ capture level (CO ₂ -CL) | 66.89 % |
| | Reboiler Temperature (T _{reb}) | 382.2 K |

The discrete linear state-space model obtained with a sampling period (T_s) of 60s is given below equation 5-1:

$$A = \begin{bmatrix} 0.9382 & 1 & 0 & 0 \\ 0.0284 & 0.2402 & 0 & 0 \\ 0 & 0 & 1.663 & 1 \\ 0 & 0 & -0.6834 & 0 \end{bmatrix}$$

$$B = \begin{bmatrix} -181.4 & 60.94 & -21.13 \\ -132.1 & -47.65 & 68.11 \\ 0 & -2.362 & 152.4 \\ -0.03549 & 1.446 & -135.7 \end{bmatrix} \quad 5-1$$

$$C = \begin{bmatrix} 1 & 0 & 0 & 0 \\ 0 & 0 & 1 & 0 \end{bmatrix}$$

$$D = \begin{bmatrix} 0 & 0 & 0 & 0 \\ 0 & 0 & 0 & 0 \end{bmatrix}$$

To ensure that the linear model capture the essential dynamics of the CO₂ capture process and is suitable for the MPC scheme, a step analysis was carried out. A step change of $\pm 10\%$ was applied to each input variable while the output response was observed. Figure 5-1 shows the normalised step responses.

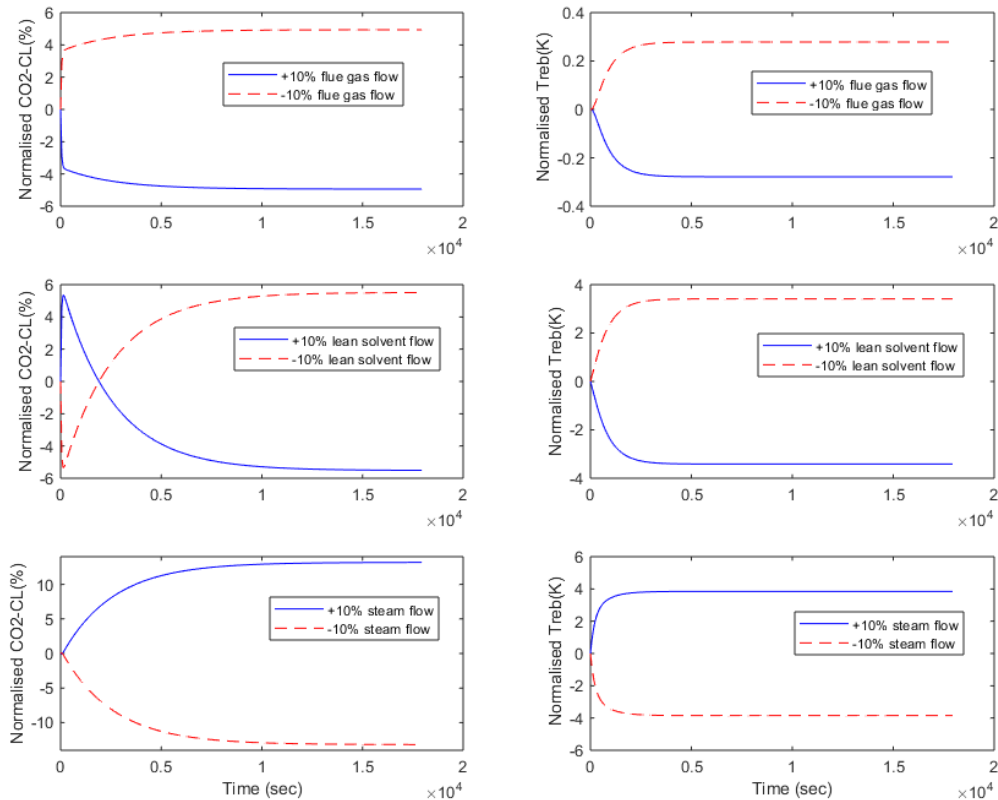


Figure 5-1 Step response plot of the discrete linear state-space model.

It was observed that the step response plot, shown in Figure 5-1, followed similar dynamic trends in response to step input change reported in literature (Wu *et al.*, 2019). This indicates that the linear discrete state-space model captures the essential dynamic trend of the CO₂ capture process. Hence, it is adopted as the prediction model for the implementation of the multivariable linear model predictive control (MPC) scheme.

5.3 Multivariable MPC Control scheme design

This section discusses the development of a multivariable MPC controller. This entails adopting a linear discrete state-space model as the prediction model, obtaining the objective function and control law.

A general formulation for a linear constrained multivariable MPC algorithm is as follows (Camacho & Alba, 2013):

$$\min_{\Delta \hat{u}_t, \dots, \Delta \hat{u}_{t+N_u-1}} \sum_{i=1}^{N_p} (\hat{y}_{t+i} - \hat{r}_{t+i})^T R (\hat{y}_{t+i} - \hat{r}_{t+i}) + \sum_{i=0}^{N_u} \Delta \hat{u}_{t+i}^T Q \Delta \hat{u}_{t+i}$$

Subject to:

$$\hat{x}_{t+1} = A \hat{x}_t + B \hat{u}_t$$

$$\hat{y}_t = C \hat{x}_t \tag{5-2}$$

$$\hat{y}_{min} \leq \hat{y}_t \leq \hat{y}_{max}$$

$$\hat{u}_{min} \leq \hat{u}_t \leq \hat{u}_{max}$$

$$\Delta \hat{u}_{min} \leq \Delta \hat{u}_t \leq \Delta \hat{u}_{max}$$

where \hat{y}_{t+i} represents the predicted outputs (CO₂–CL and T_{reb}) at $(t + i)$ th time instant and $\Delta \hat{u}_{(t+1)}^T$ represents the manipulated variables rate (lean solvent flowrate and steam flowrate) to achieve the targeted controlled variables close to the set-point condition $\hat{r}_{(t+1)}$ at $(t + i)$ th time instant. The upper and lower bounds for both controlled and manipulated variables are represented as $\hat{y}_{min}, \hat{y}_{max}, \hat{u}_{min}, \hat{u}_{max}$ respectively. The weights assigned to the manipulated and controlled variables were represented as Q and R respectively. Q and R were chosen to give a closed-loop performance based on robustness and stability. Q and R values are chosen such that the cost function is minimized. \hat{x}_t is the state vector of the linear state-space model of the CO₂ capture process at time instant t and A, B, C are the model matrices of the linear state space

prediction model. The state-space model is augmented by introducing an integrator (as differentiated state vectors) into the form below (Skogestad & Postlethwaite, 2007):

$$\begin{bmatrix} \Delta x_{(t+1)} \\ y_{(t+1)} \end{bmatrix} = \begin{bmatrix} A & o_{2 \times 4}^T \\ C & A \end{bmatrix} \begin{bmatrix} \Delta x_{(t)} \\ y_{(t)} \end{bmatrix} + \begin{bmatrix} B \\ C \end{bmatrix} \Delta u_{(t)} \quad 5-3$$

$$y_{(t)} = [o_{2 \times 4} \ I_{2 \times 2}] \begin{bmatrix} \Delta x_{(t)} \\ y_{(t)} \end{bmatrix}$$

Where $I_{2 \times 2}$ is an identity matrix with dimension corresponding to the number of output variables and o is a 2×4 zero matrix. The above equation can be re-written as:

$$\hat{x}_{(t+1)} = \hat{A}\hat{x}_{(t)} + \hat{B}\Delta\hat{u}_{(t)} \quad 5-4$$

$$y_{(t)} = \hat{C}\hat{x}_{(t)}$$

The state observer is used to estimate the state vector based on feedback principle to offset the state space error as shown below:

$$\hat{x}_{(t+1)} = A\hat{x}_{(t)} + B\Delta\hat{u}_{(t)} + K_{ob}(y_{(t)} - C\hat{x}_{(t)}) \quad 5-5$$

Where K_{ob} is the observer gain matrix adopted to offset the error between the measured and predicted output using the state estimate. N_p and N_u are the prediction and control horizons used to compute the predicted output variables and corresponding manipulated variables in the MPC framework. N_p and N_u were selected to satisfy the condition such that the difference between N_p and N_u is larger than the maximum total delay of the model.

5.3.1 MPC tuning design and Implementation

The MPC control strategy on the solvent-based CO₂ capture model was implemented in Simulink as shown in Figure 5-2.

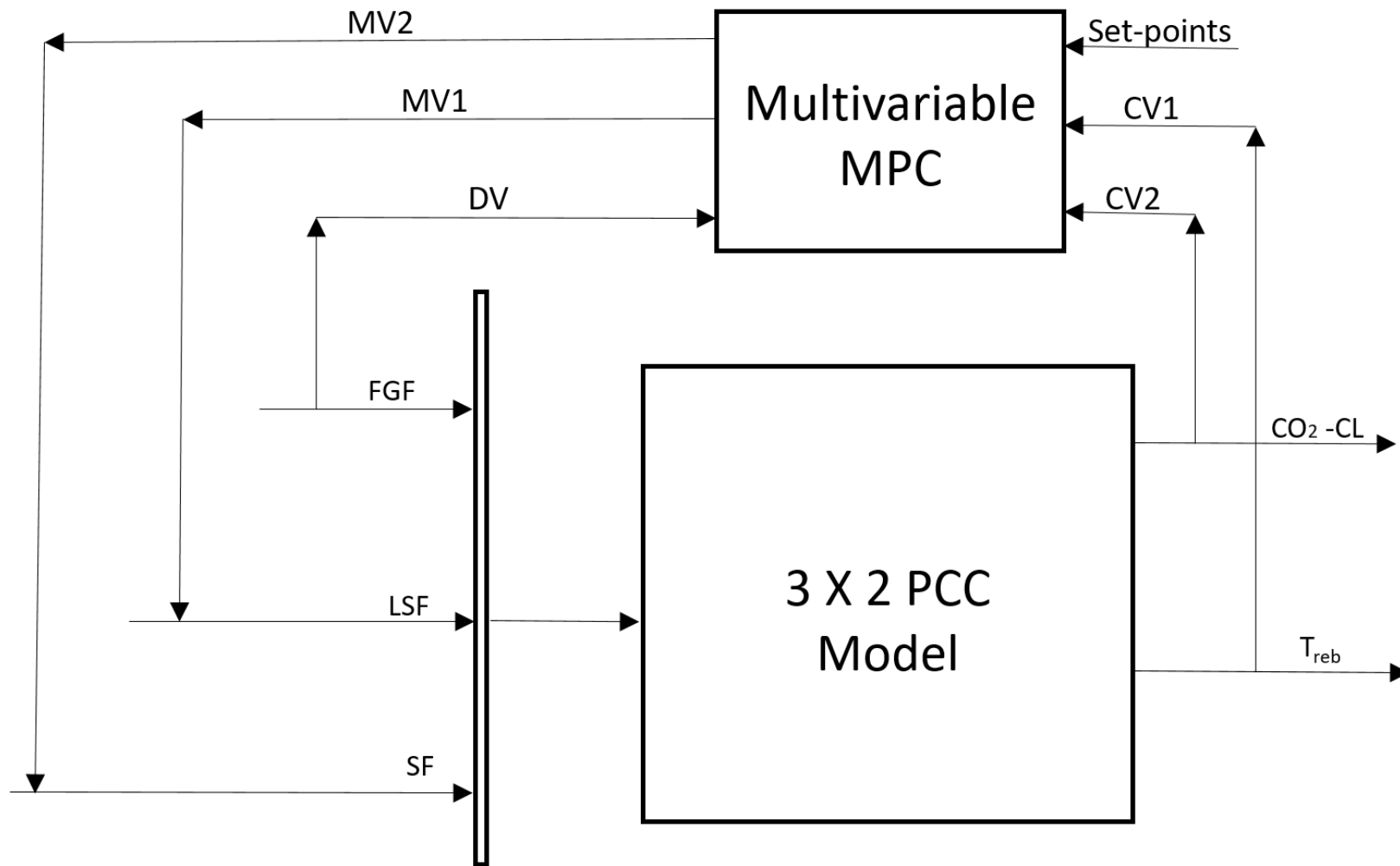


Figure 5-2 Implementation of MPC control strategy on the solvent-based PCC (identified) model; FGF-flue gas flowrate ; LSF- lean solvent flowrate; SF- steam flowrate; CO₂-CL – CO₂ capture level ; T_{reb} – Reboiler temperature; DV- disturbance variables; MV-manipulated variables; CV-controlled variables.

Tables 5-2, 5-3 and 5-4 show the nominal operating conditions, process constraints and tuning parameters in the MPC formulation. The sampling time was the same as the nonlinear model (60s). The horizon parameters and weights were selected such that the quadratic programming (QP) Hessian matrix is positive definite and the computational time is minimized.

Table 5-2 Nominal operating condition

| Operating conditions | Nominal value |
|--|---------------|
| CO ₂ capture rate (CO ₂ -CL) | 66.89% |
| Reboiler Temperature (T _{reb}) | 382.2K |
| Flue gas flowrate | 0.16 kg/s |
| Lean solvent flowrate | 0.76 kg/s |
| Steam flowrate | 0.047 kg/s |

Table 5-3 Process constraints

| Manipulated variables | \hat{u}_{min} | $\Delta\hat{u}_{min}$ | \hat{u}_{max} | $\Delta\hat{u}_{max}$ |
|--------------------------------------|-----------------|-----------------------|-----------------|-----------------------|
| Lean solvent flowrate (MV1) | 0.2 kg/s | -0.007kg/s | 1.0 kg/s | 0.007kg/s |
| Steam flowrate (MV2) | 0.01 kg/s | -0.001kg/s | 0.1 kg/s | 0.001kg/s |
| Controlled variables | \hat{y}_{min} | | \hat{y}_{max} | |
| CO ₂ capture level (CV1) | 30% | | 100% | |
| CO ₂ lean loading (CV2) | 370K | | 400k | |

Table 5-4 MPC control scheme-tuning parameters

| | | | |
|-------------|-----|-------------|-----|
| N_p | | 10 | |
| N_u | | 2 | |
| T_s | | 60s | |
| Weights (Q) | | Weights (R) | |
| MV1 rate | 0.1 | CV1 | 10 |
| MV2 rate | 0.1 | CV2 | 100 |

5.4 Performance Evaluation

The section discuss the performance evaluation of MPC strategy implemented on the solvent-based CO₂ capture model under various scenarios, which are listed as follows:

- Scenario 1: ramp change in the flue gas flowrate
- Scenario 2: ramp change in the CO₂ capture level
- Scenario 3: variation in the flue gas flowrate and CO₂ capture level

Performance evaluation under these scenarios 1 and 2 were carried out to assess the capability of the MPC for disturbance rejection (scenario 1) and set point tracking (scenario 2) in comparison with PI control scheme. Performance evaluation under scenario 3 was assess the capability of each control scheme to track the controlled variables effectively while there are changes in the flue gas flowrate simultaneously. The MPC control scheme performance was compared with the conventional PI control scheme based on integral square error (ISE) related to the controlled variables (CVs). However, it is essential to note that excessive changes in the manipulated variables to minimize the CVs performance measures is undesirable. Thus, each MV effort was evaluated based on the sum of squared deviation.

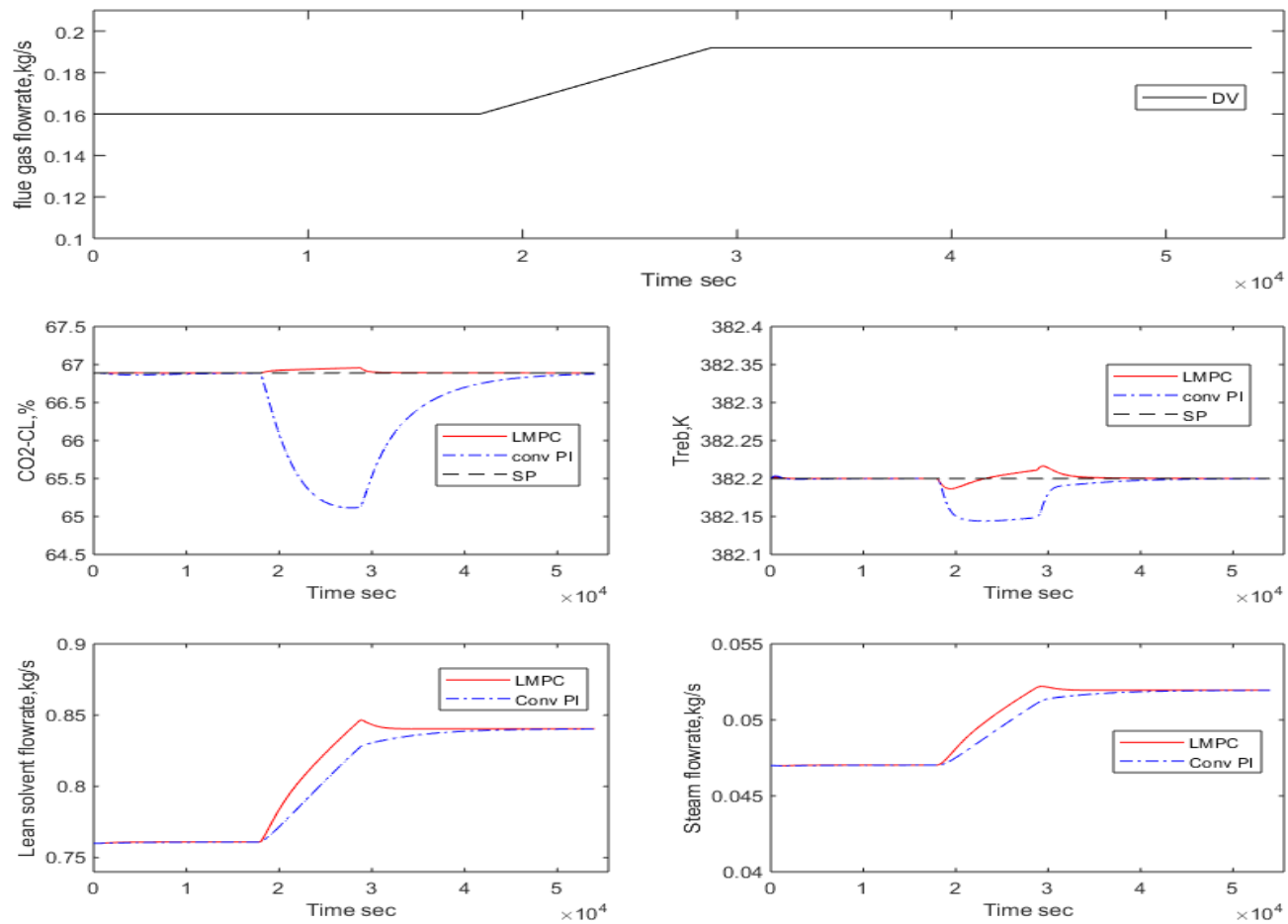


Figure 5-3 Closed-loop performance to a 20% ramp change in flue gas flowrate for 3hr (10800s). LMPC – linear model predictive control; conv PI – conventional PI control; SP – set point; DV – disturbance variable

5.4.1 Scenario 1

This section discusses the MPC control performance on the solvent-based CO₂ capture process under a ramp change in the flue gas flowrate. The controlled variables (CO₂-CL and T_{reb}) set point were maintained at the nominal operating condition (66.89% and 382.2K respectively). The variation in the flue gas flowrate reflects the variation in power plant load. For the scenario, a 20% increment in the flue gas flowrate was introduced at 5hr (18000s) simulation time for a period of 3hr (10800s) at a ramping rate of 0.1%/min.

Figure 5-3 showed that the MPC scheme was able to reject the effect of flue gas flowrate on the controlled variables (CO₂-CL and T_{reb}) faster than the conventional PI control scheme.

Also shown in Table 5-5, is the integral squared – error (ISE). This showed that the MPC scheme has a smaller deviation to the controlled variable set points compared with the convention PI control, indicating that the MPC scheme was able to effectively handle the interaction within the CO₂ capture process. As the flue gas flow rate increases, the MPC was able to estimate the disturbance variable effect and quickly activate the corresponding manipulated variables to offset its effect. As shown in Figure 5-3, with the use of MPC scheme on the solvent-based PCC model was able to run smoothly. The sum of squared deviation for each MVs shown in Table 5-6 revealed that MPC scheme requires more effort on the respective manipulated variables to attain the desired controlled variable set points compared with the PI control scheme. It should be noted that for the MPC, the MVs did not violate the deviation constraints shown in Table 5.3.

5.4.2 Scenario 2

For this scenario, the MPC control performance was considered when ramp change is introduced to the CO₂ capture level set point in comparison with the conventional PI control scheme. This scenario reflects the peak electricity price period, where more steam is needed for power generation and less CO₂ capture is required to be economical (Flø *et al*, 2016). At simulation time (5hr) 18000s, the CO₂ capture level set point was reduced from 66.89% to 61% at a ramping rate of 0.03%/min. under this scenario, the reboiler temperature set point is maintained at its nominal operating point (383.2K), while the flue gas flowrate is constant.

The plot shown in Figure 5-4 revealed that the MPC gave a better performance than the conventional PI control scheme for the scenario considered. The MPC scheme was able to achieve the control objective while the conventional PI control was unable to attain a suitable control performance. For the MPC control scheme, the respective manipulated variables (lean solvent flowrate and steam flowrate) were adequately adjusted to achieve the CO₂ capture level set point. Details of the performance evaluation parameter for this is given in Table 5-5. Similar trends as scenario 1 on the sum of squared deviation for MVs was observed in this scenario.

Table 5-5 summary of the closed-loop control performance evaluation for control schemes (MPC vs PI)

| Scenario | ISE | | | |
|------------|---------------------|------------------|---------------------|------------------|
| | MPC | | PI | |
| CVs | CO ₂ -CL | T _{reb} | CO ₂ -CL | T _{reb} |
| Scenario 1 | 0.4573 | 0.0187 | 488.0628 | 0.5054 |
| Scenario 2 | 0.7655 | 0.1842 | 600.1386 | 0.4669 |
| Scenario 3 | 20.1073 | 1.4205 | 4872.1123 | 5.3425 |

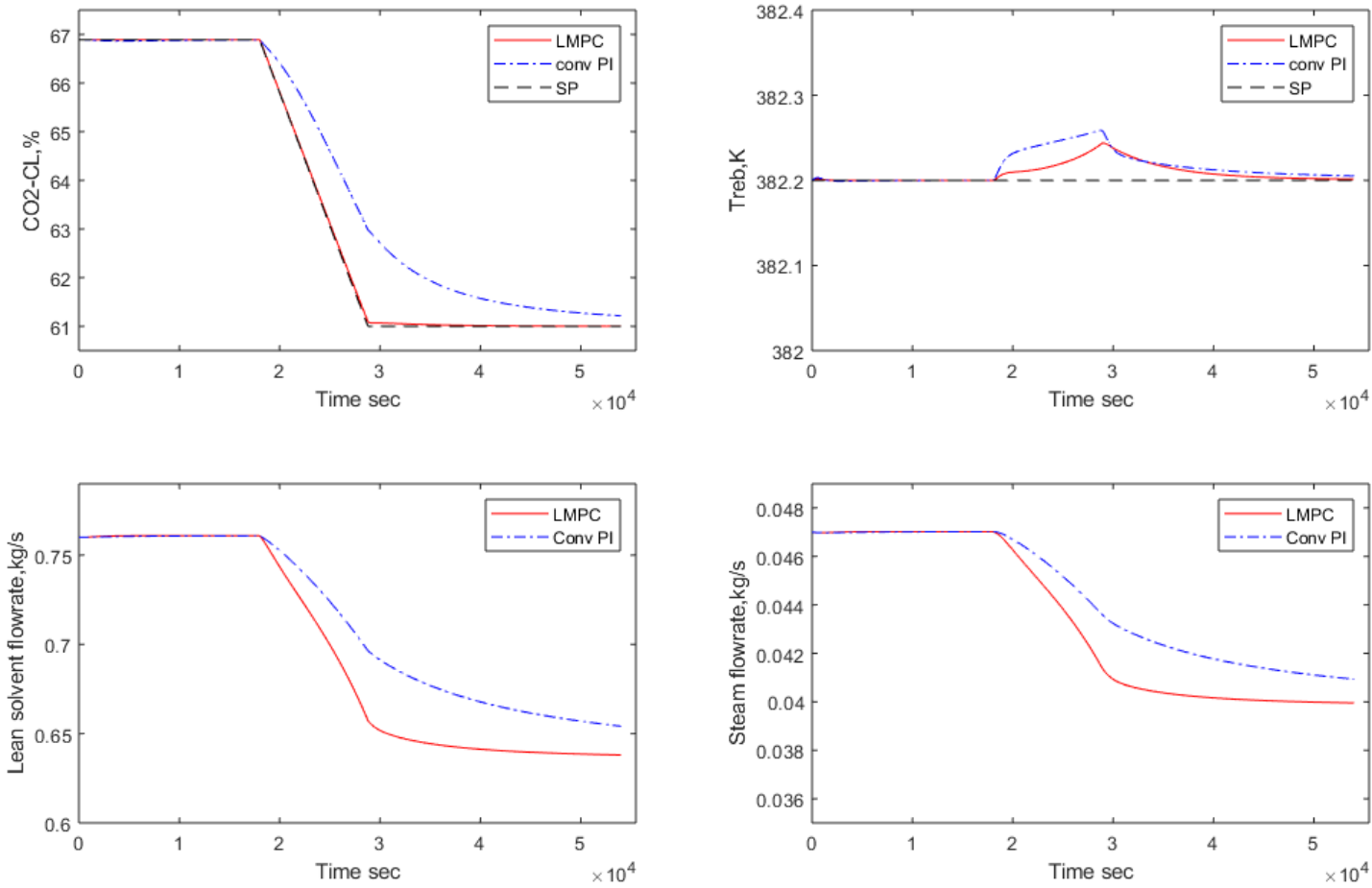


Figure 5-4 Closed-loop performance to a decrease in CO₂-CL for 3hr (10800s). LMPC – linear model predictive control; conv PI – conventional PI control; SP – set point; DV – disturbance variable

Table 5-6 sum of squared deviation of MVs for each control scheme (MPC vs PI)

| Scenario | Sum of squared deviation | | | |
|------------|--------------------------|----------|----------|----------|
| | MPC | | PI | |
| MVs | LSF | RSF | LSF | RSF |
| Scenario 1 | 4.45E-05 | 1.56E-07 | 4.19E-05 | 1.53E-07 |
| Scenario 2 | 6.35E-05 | 2.00E-07 | 2.97E-05 | 9.48E-08 |
| Scenario 3 | 2.06E-03 | 4.83E-06 | 8.17E-04 | 1.10E-06 |

5.4.3 Scenario 3

The final scenario considers the variation of the CO₂ capture level in accordance with the electricity price trends. This reflects the operation of the solvent-based CO₂ capture process to accommodate the flexible operation of the power plant (which includes off-peak and peak electricity periods). In this case study, the CO₂ capture level setpoint is varied between 61% and 90% as well as the flue gas flowrate (disturbance variable) (0.14kg/s – 0.19kg/s). Initially, the CO₂ capture level is maintained at the nominal operating point. The CO₂ capture level setpoint follows scheduling instructions at simulation time's t= 3hr (10800s), 11hr (39600s), 19hr (68400s) and 22hr (72260s). At simulation time 3hr, 11hr and 19hr, a ramp was introduced to CO₂-CL set point at a rate of 0.03%/min, 0.09%/min and 0.33%/min. at simulation time 22hr, a step change was introduced to the CO₂ level set point. During this case study (scenario), T_{reb} set point was maintained at its nominal operating point. As shown in Figure 5-5, the MPC gave a better control performance (see Table 5-5) in comparison to conventional PI control scheme when CO₂ capture level changes within the region 61% - 90%. However, both control schemes struggle to effectively maintain T_{reb} at its nominal operating condition. In addition, the MPC control

performance is depleted for a wide range of flexible operation (Wu *et al.*, 2018). This is because the wide range flexible operation induces the nonlinearity within the CO₂ capture process, which is not dynamically captured by the approximate linear model and thus cannot be appropriately handled by the MPC control scheme (Manaf *et al.*, 2016; Wu *et al.*, 2018). Hence, NMPC is required to be handled nonlinearities during the wide range of flexible operation given the large variation of the power plant operation as power generation from renewable energy sources are supplied to the Grid.

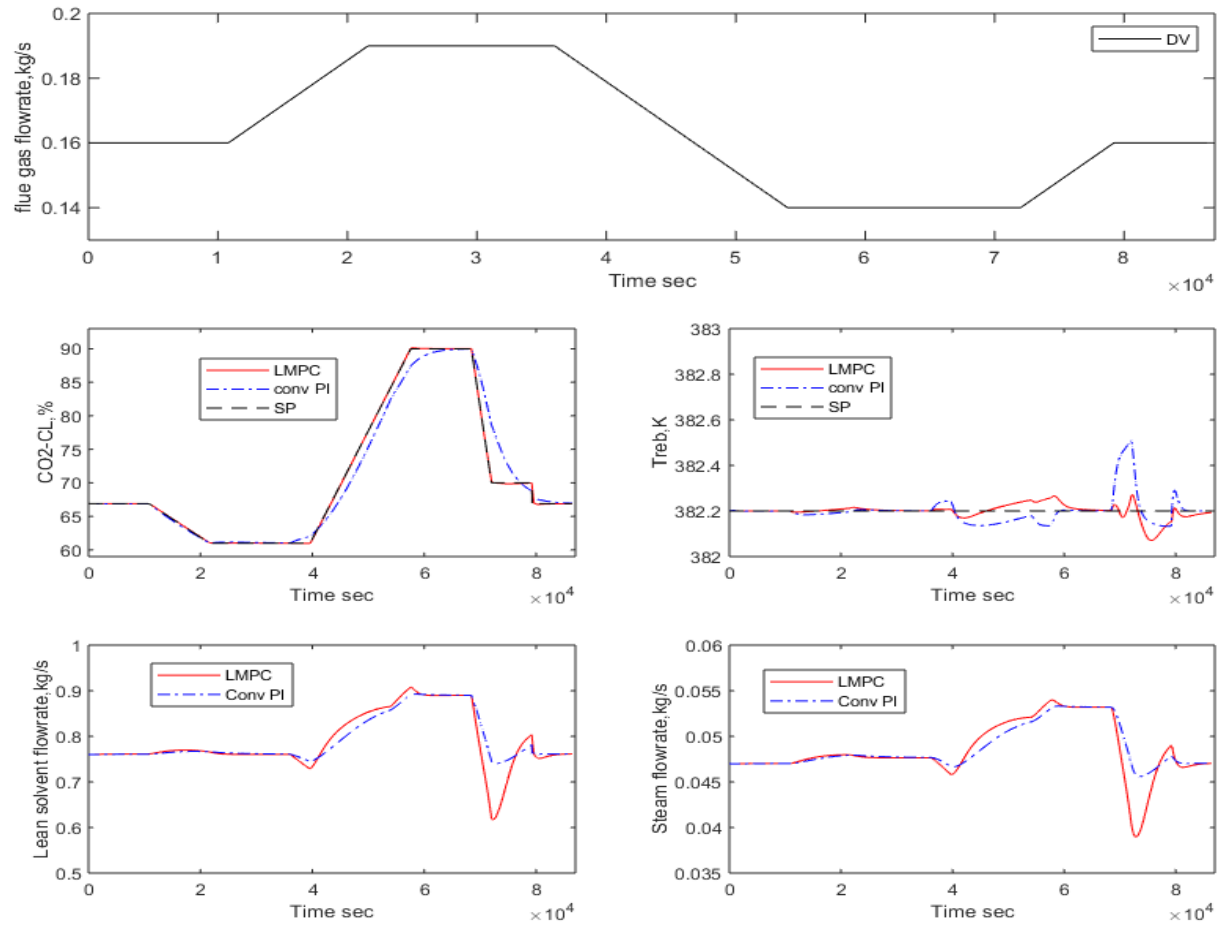


Figure 5-5 Closed-loop performance to a variation in CO₂-CL for 24hr (86400s). LMPC – linear model predictive control; conv PI – conventional PI control; SP – set point; DV – disturbance variable

5.5 Summary

This chapter focused on the design and implementation of a linear model predictive control (MPC) scheme on the solvent-based post-combustion CO₂ capture process. The MPC scheme uses a linear model, which captures the essential dynamics of the CO₂ capture process, for its implementation. The MPC scheme was evaluated in comparison with the conventional PI control scheme under three different scenarios (case studies). The conclusion is summarised as follows:

- For all scenarios considered in this chapter, the MPC scheme gave a better control performance compared to the conventional PI control scheme as it is able to handle the interactions within the process in comparison with the conventional PI control scheme. Thus, the MPC scheme avoids a sluggish response to the controlled variable setpoint changes.
- For all scenarios, MPC control scheme required more MV effort compared with PI control. Although the constraints on the deviation were not violated for both control schemes.
- For Scenario 3, the MPC scheme struggled to maintain the reboiler temperature (T_{reb}) at its set point. Major due to the inability to adequately handle the variation in the flue gas flowrate (disturbance variable) and CO₂ capture level set-point simultaneously.
- A wide flexible operation range triggers the nonlinearities within the CO₂ capture process and cannot be handled appropriately by the MPC scheme (Manaf *et al.*, 2016; Wu *et al.*, 2018). Hence, a NMPC is adopted to deal with the nonlinearity issues under a wide range of flexible operation.

6 Nonlinear model predictive control design for the solvent-based PCC process

6.1 Introduction

This chapter discusses the design and implementation of a nonlinear model predictive control (NMPC) in the solvent-based CO₂ capture process. The increased addition of renewable energy in the electricity generation mix (Mechleri *et al.*, 2017) is predicted to bring about more changes in power plant operation such as frequent ramps, shutdown and start-up operation (Mac Dowell & Staffell, 2015). As a result, it is important for the solvent-based CO₂ capture process to be operated flexibly in accordance with the host power plant load. This is achieved through the implementation of an appropriate control strategy (scheme) in the process. Previously, Chapters 4 and 5 focused on the implementation of a conventional PI control and MPC scheme. The MPC scheme gave a better performance. The MPC scheme, which is widely accepted in the industry, utilizes the linear model for its implementation. The MPC scheme works well within an operational range of the capture process where its nonlinearities are minimized. When a large disturbance (flue gas flowrate) is introduced to the capture process or the controlled variable set-points are varied within the flexible operation range where large nonlinearities are present, the MPC will be unable to effectively control the capture process, as the linear model is unable to capture the nonlinearity of the CO₂ capture process. Hence, NMPC scheme is adopted to handle nonlinearities of the solvent-based CO₂ capture process.

The NMPC utilizes the nonlinear model for its implementation on the solvent-based CO₂ capture process. It is important to note that the structure of the nonlinear model is important for the development of the NMPC scheme. In this chapter, NMPC scheme

utilizes the parsimonious NARX model developed via nonlinear SI in Chapter 3. The observable state-space representation of the NARX model was obtained in chapter 4. The control performance of the NMPC scheme was evaluated in comparison with MPC and conventional PI control schemes under different flexible operation scenarios.

6.2 Nonlinear model predictive control (NMPC) formulation

This section discusses the development of a multivariable NMPC Control strategy. The schematic diagram of the NMPC scheme on the solvent-based PCC process is shown in Figure 6-1. This entails adopting the nonlinear state-space model as the prediction model. NMPC adopts the standard cost function as the objective function. The constrained standard cost function is expressed below:

$$\min_{\Delta \hat{u}, \dots, \Delta \hat{u}_{t+N_u-1}} \sum_{i=1}^{N_p} (\hat{y}_{t+i} - \hat{r}_{t+i})^T Q (\hat{y}_{t+i} - \hat{r}_{t+i}) + \sum_{i=0}^{N_u} \Delta \hat{u}_{t+i}^T R \Delta \hat{u}_{t+i}$$

Subject to:

$$\hat{x}_{t+1} = f(\hat{x}_t, \hat{u}_t)$$

$$\hat{y}_{t+1} = g(\hat{x}_{t+1})$$

$$\hat{y}_{min} \leq \hat{y}_t \leq \hat{y}_{max}$$

$$\hat{u}_{min} \leq \hat{u}_t \leq \hat{u}_{max}$$

$$\Delta \hat{u}_{min} \leq \Delta \hat{u}_t \leq \Delta \hat{u}_{max}$$

6-1

where \hat{y}_{t+i} represents the predicted outputs (CO₂ capture level and reboiler temperature) at $(t + i)$ th time instant and $\Delta \hat{u}_{(t+1)}^T$ represents manipulated variable rates (lean solvent flowrate and steam flowrate) to achieve the target-controlled variables close to the set-point condition $\hat{r}_{(t+1)}$. The upper and lower bounds for both

manipulated and controlled variables are represented as $\hat{y}_{min}, \hat{y}_{max}, \hat{u}_{min}, \hat{u}_{max}$ respectively. The weights assigned to the controlled and manipulated variables rate were represented as Q and R respectively. \hat{x}_t represents the current state vector of the nonlinear state-space model of the solvent-based PCC process obtained as shown in equation 6-2. The tables below show the nominal operating condition, process constraints and NMPC formulation parameter respectively.

$$x_1(t+1) = x_2(t) + a1x_1(t) + b2u_3(t) + c1x_1(t)u_1(t) + b4u_2(t) + b5u_1(t) \\ + c6 u_1(t)u_2(t) + c10 u_2(t)u_3(t) + c11 x_1(t)u_3(t) + d$$

$$x_2(t+1) = a2 x_1(t) + b1 u_3(t) + b3 u_2(t) + b6 u_1(t) + c2 x_1(t)u_1(t) \\ + c4 u_2(t)u_3(t) + c7 u_1(t)u_2(t) + c6 x_1(t+1)u_1(t)$$

$$x_3(t+1) = x_4(t) + a11 x_3(t) + b11 u_3(t) + b31 u_2(t) + c31 u_3(t)u_3(t) + d1 \quad 6-2$$

$$x_4(t+1) = a21 x_3(t) + b21 u_3(t) + b41 u_2(t) + c21 u_3(t)u_3(t) \\ + c51 u_2(t)u_3(t) + b51u_1(t)$$

$$y_1(t) = x_1(t)$$

$$y_2(t) = x_3(t)$$

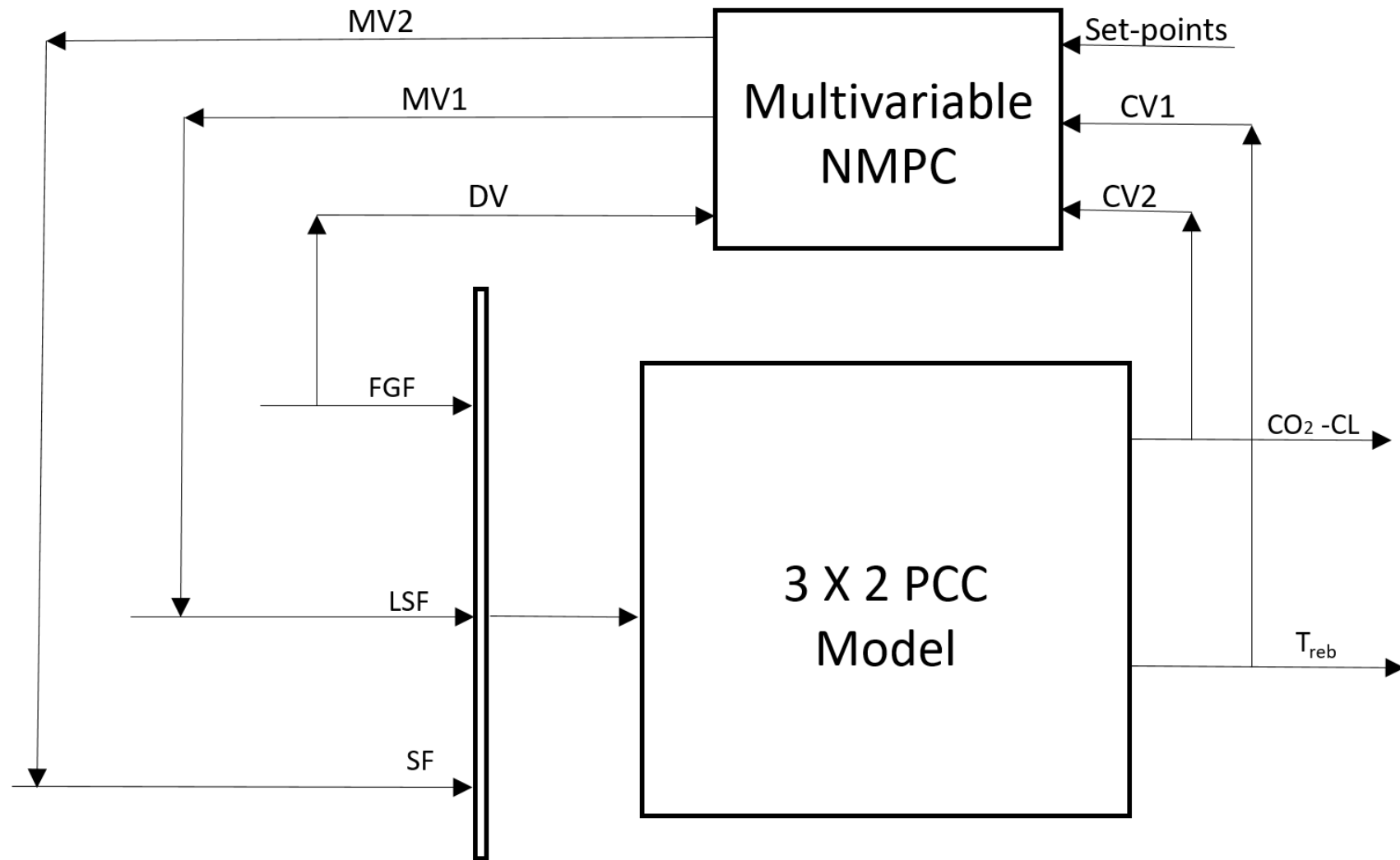


Figure 6-1 Schematic diagram of NMPC scheme on the solvent-based PCC model; FGF-flue gas flowrate ; LSF- lean solvent flowrate; SF- steam flowrate; CO₂-CL – CO₂ capture level ; T_{reb} – Reboiler temperature; DV- disturbance variables; MV-manipulated variables; CV-controlled variables.

where $y_1(t)$ and $y_2(t)$ represents CO₂ capture level and reboiler temperature respectively. $u_1(t)$, $u_2(t)$ and $u_3(t)$ represents flue gas flowrate (kg/s), lean solvent flowrate (kg/s) and steam flowrate (kg/s). Tables 6-1, 6-2 and 6-3 show the nominal operating conditions, Process constraints and NMPC formulation parameters. As explain in Chapter 5, the NMPC formulation parameter were selected to closed-loop performance based on robustness and stability.

Table 6-1 Nominal operating condition

| Operating conditions | Nominal value |
|---|--|
| Initial state condition (x_0) | [66.2302;0.574568; 380.2222;- 268.297] |
| Manipulated variables | |
| Lean solvent flowrate | 0.76 kg/s |
| Steam flowrate | 0.047 kg/s |
| Disturbance variable | |
| Flue gas flowrate | 0.16 kg/s |
| Output variables | |
| CO ₂ capture level (CO ₂ -CL) | 66.89 (%) |
| Reboiler Temperature (T_{reb}) | 382.22K |

Table 6-2 Process constraints

| Manipulated variables | \hat{u}_{min} | $\Delta\hat{u}_{min}$ | \hat{u}_{max} | $\Delta\hat{u}_{max}$ |
|-----------------------------|-----------------|-----------------------|-----------------|-----------------------|
| Lean solvent flowrate (MV1) | 0.2 kg/s | -0.007 kg/s | 1.0 kg/s | 0.007 kg/s |
| Steam flowrate (MV2) | 0.01 kg/s | -0.001 kg/s | 0.1 kg/s | 0.001 kg/s |
| Controlled variables | \hat{y}_{min} | | \hat{y}_{max} | |
| CO ₂ -CL (CV1) | 30 (%) | | 100 (%) | |
| T_{reb} (CV2) | 370 (K) | | 400 (K) | |

Table 6-3 NMPC formulation parameters

| | | | |
|-------------|-----|-------------|-----|
| N_p | | 10 | |
| N_u | | 2 | |
| Weights (Q) | | Weights (R) | |
| MV1 | 0.1 | CV1 | 10 |
| MV2 | 0.1 | CV2 | 100 |

6.3 Performance Evaluation

The section discuss the performance evaluation of NMPC strategy implemented on the solvent-based PCC model under various flexible operation scenarios, which are listed as follows:

- Scenario 1: variation in the flue gas flowrate
- Scenario 2: variation in the controlled variables ($\text{CO}_2\text{-CL}$ and T_{reb}) and flue gas flowrate simultaneously

6.3.1 Scenario 1

This section evaluates the control performance of NMPC strategy on the solvent-based CO_2 capture process in a scenario where there is fluctuation in the flue gas flowrate, which is recognised as a disturbance variable. This reflects the flexible operation of the power plant attached to the capture plant.

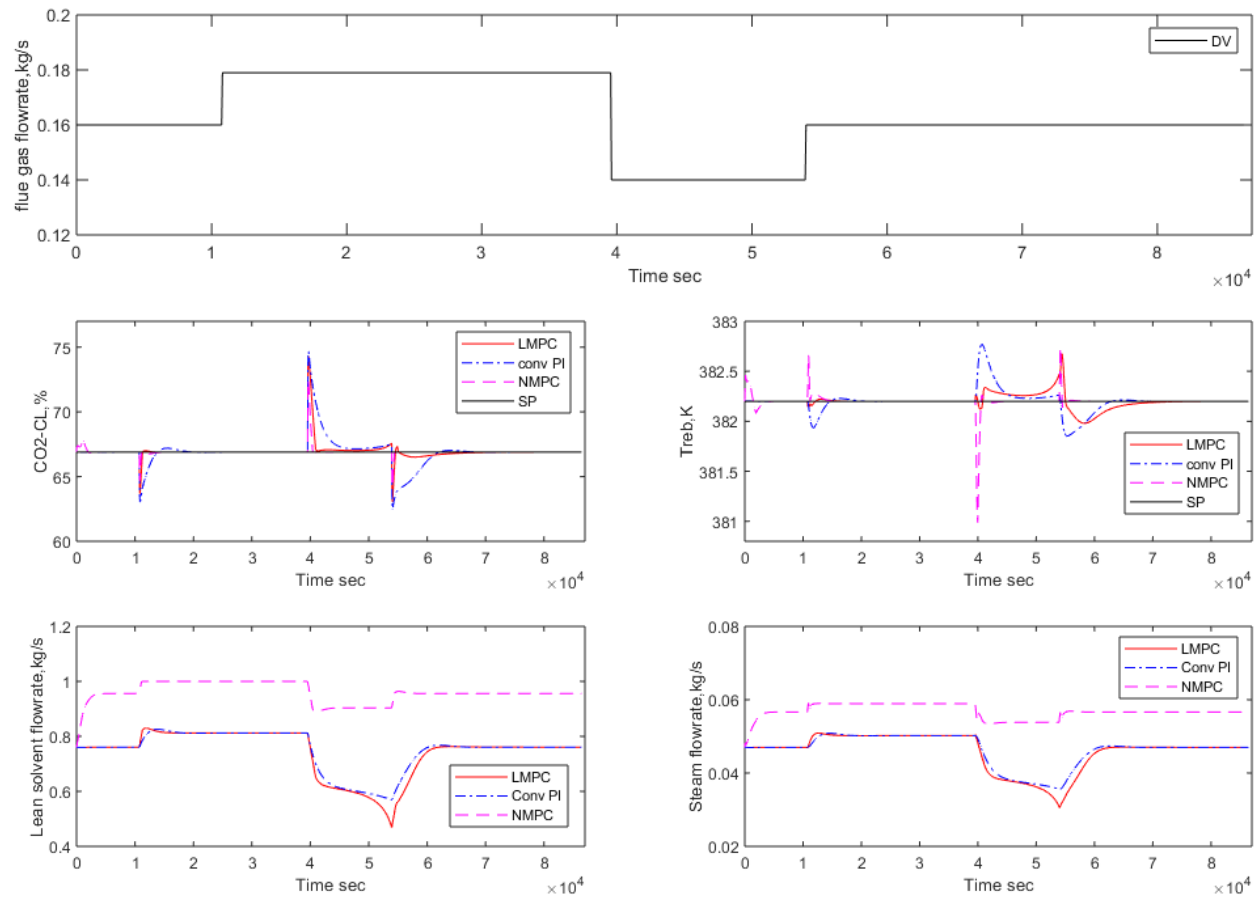


Figure 6-2 Closed-loop performance to a variation in flue gas flowrate for 24hr (86400s). LMPC – linear model predictive control; conv PI – conventional PI control; NMPC – nonlinear MPC; SP – set point; DV – disturbance variable

In this section, flue gas flowrate was varied as shown in Figure 6-2, while the controlled variable set points ($\text{CO}_2\text{-CL}$ and T_{reb}) were maintained at the nominal operating condition. The controlled variables were monitored to observe the disturbance rejection performance of the NMPC strategy in comparison with MPC and PI control scheme using the integral squared error (ISE) as a performance index. Given the strong variation in the flue gas flowrate, a large variation in the MVs to achieve to control is expected. Thus, to avoid excessive changes in the MVs (which can damage the action element in the control system), Process constraint was implemented on the deviation of each MVs as shown in Table 6.2.

The closed-loop control performance for the control strategies is shown in Figure 6-2. For CO_2 capture level control, the NMPC scheme gave a better control performance than the MPC and PI control scheme. The lowest ISE value for the NMPC strategy shown in Table 6-4 indicates the NMPC scheme deviation from the set-point compared to other control schemes (MPC and PI). The MPC gave a better performance than the conventional PI control scheme.

For the reboiler temperature control, the linear MPC and NMPC scheme gave a similar performance, which was better than the PI control scheme. Although MPC and NMPC scheme gave a similar performance, the smaller ISE value for the linear MPC indicates that it possesses a smaller deviation from the set point compared with the NMPC scheme. The significant overshoots observed in the NMPC scheme (Figure 6.2) reflects the larger ISE compared to MPC, although the NMPC settles faster compared MPC. The NMPC scheme gave a better overall control performance on the solvent-based CO_2 capture process.

Table 6-4 Summary of the closed-loop control performance evaluation for control schemes (NMPC vs MPC vs PI)

| Scenario | ISE | | | | | |
|------------|---------------------|------------------|---------------------|------------------|---------------------|------------------|
| | NMPC | | MPC | | PI | |
| CVs | CO ₂ -CL | T _{reb} | CO ₂ -CL | T _{reb} | CO ₂ -CL | T _{reb} |
| Scenario 1 | 207.393 | 10.756 | 621.315 | 7.678 | 1761.070 | 18.743 |
| Scenario 2 | 1.11E+04 | 105.005 | 1.33E+07 | 2.17E+03 | 6.21E+07 | 2.47E+05 |

6.3.2 Scenario 2

This scenario focuses on the control system performance under strong variation in the operation of controlled variables (especially CO₂ -CL) as well as the variation in the flue gas flowrate. This scenario reflects the penetration of renewable energy sources into the grid, where the solvent-based CO₂ capture process is required to accommodate the flexible operation of the power plant in response to stringent demand of the Grid.

Along with the same disturbance (i.e. flue gas flowrate variation) in scenario 1, the CO₂ capture level set point was varied at time $t = 10800s$ from 66.89% to 45%, $t = 36000s$ from 45% to 60%, $t = 48000s$ from 60% to 80%, $t = 57000s$ from 80% to 90% and $t = 75600s$ from 90% to 95%. In addition, the reboiler temperature set point was varied from 382.2K to 387K and to 389K at time $t = 46800s$, $t = 57000s$ and $t = 75600s$ respectively as shown in Figure 6-3.

The MPC and PI control scheme were not able to achieve the control objective under this scenario as shown in Figure 6.3 and Table 6.4. This is attributed to large nonlinearity triggered within process due to a wide and frequent variation in the controlled variables set point (CO₂-CL and T_{reb}) and disturbance variable (flue gas flowrate). This brought about severe degradation and instability in the closed-loop

performance for both PI control and MPC. On the other hand, results shown in Figure 6.3 and Table 6.4 demonstrated that NMPC scheme is able to handle wide variation in the flue gas flowrate while effectively tracking the controlled variables set point effectively.

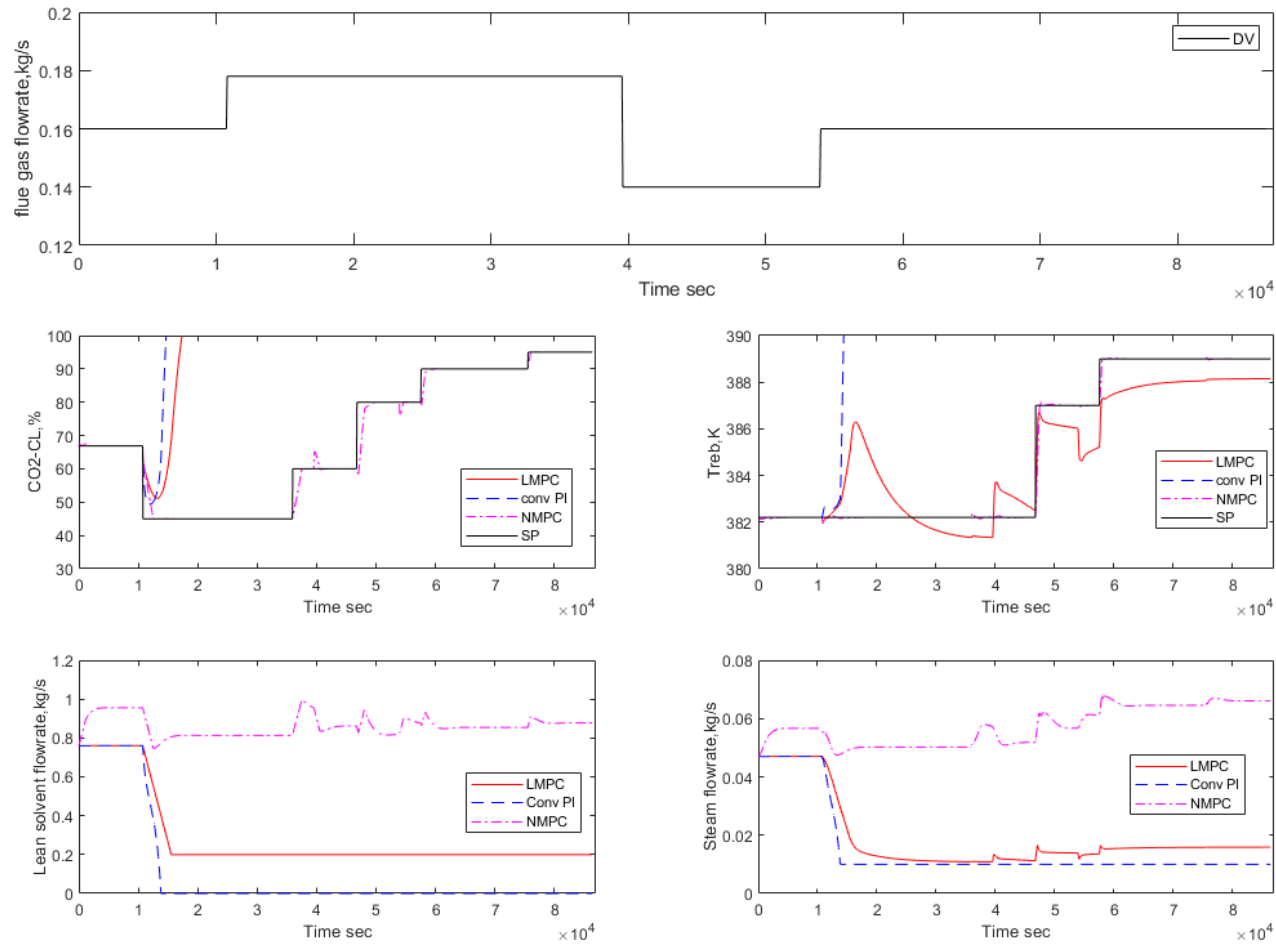


Figure 6-3 NMPC closed-loop performance to a variation in CO₂-CL and flue gas flowrate for 24hr (86400s). LMPC – linear model predictive control; conv PI – conventional PI control; NMPC – nonlinear MPC; SP – set point; DV – disturbance variable

6.4 Summary

This chapter focused on the design and implementation of a nonlinear model predictive control (NMPC) scheme on the solvent-based post-combustion CO₂ capture process. The large load variation in the power plant operation due to the increased penetration of electricity generated by renewable sources supplied to the Grid has resulted in the need for the NMPC scheme. The NMPC scheme adopted the nonlinear model for its implementation. The NMPC scheme was evaluated under two (2) different scenarios (case studies).

The MPC and PI control scheme gave a poor control performance for a large variation in the controlled variable set-points, as they are unable to handle the nonlinearities triggered within the CO₂ capture model at the large flexible operation region. The NMPC scheme gave a good control performance, as it is able to handle the nonlinearities within the solvent-based PCC process.

7 Conclusion and Recommendation

7.1 Conclusion

In this thesis, non-linear model predictive control (NMPC) system was developed for a solvent-based PCC process using an identified model derived based on the FROLS-ERR algorithm. From an extensive literature review, presented in Chapter 2, it was found that:

- Existing SI studies for solvent-based PCC process are based on linear models. As the process is strongly nonlinear, these identified models could fail to capture the process dynamics accurately under wide load varying scenario.
- Nonlinear SI application in solvent-based PCC process are often based on the assumption of the model order. This approach could result in the inclusion of irrelevant model terms, making the model unnecessarily complex.
- The FROLS-ERR algorithm can determine the model terms in a stepwise manner, based on their significance. This algorithm have not been explored for solvent-based PCC process.
- Study on NMPC scheme on the solvent-based PCC process to handle process interactions in response to large load variation during flexible operation is essential due to high penetration of power generation from renewable energy source to the national grid and stringent environmental regulations.
- Comparison between linear controllers (e.g. PI and MPC) and nonlinear controller (NMPC) using model developed through FROLS-ERR algorithm has not been performed.

Based on the conclusions from the literature review, the research was divided into different tasks. Key conclusions from these tasks are presented in section 7.1.1 – 7.1.4.

7.1.1 Nonlinear SI of the solvent-based PCC process

In contrast to existing studies, a parsimonious polynomial NARX model was developed to predict the dynamic responses of an amine-based PCC plant (3-inputs and 2-outputs) using the FROLS-ERR algorithm. The process operating data used for the model development was obtained through model simulation using a first principles model implemented in gPROMS model by Lawal *et al.*,(2010). The FROLS-ERR algorithm proved to be a powerful tool in selecting the most significant model terms for representing and predicting the response variables ($\text{CO}_2\text{-CL}$ and T_{reb}). These model terms were ranked based on ERR. This gives a simple and transparent mathematical representation of the systems where we can clearly know how the system outputs depend on the variables and their interactions. Prediction efficiency evaluation as well as process dynamic analysis of identified NARX models developed in comparison with the first principles (gPROMS®) model were carried out successfully. It was concluded that the identified model captures the underlying dynamics of the capture process.

7.1.2 Multivariable conventional PI control scheme

Chapter 4 presented the multivariable process control analysis and PI control design of the solvent-based CO_2 capture process. The identified nonlinear PCC model was adopted for the multivariable control analysis and PI control implementation. The observable state-space realization of the nonlinear model was obtained for ease of control analysis. The appropriate control configuration (loop pairing) based on the multivariable control configuration analysis was selected to be CO_2 capture level

controlled by manipulating the lean solvent flowrate ($\text{CO}_2\text{-CL-LSF}$) and reboiler temperature controlled by manipulated by steam flowrate to the reboiler ($T_{\text{reb}} - \text{SF}$).

The conventional PI control scheme demonstrated a sluggish closed-loop performance under scenarios 1 and 2, although it was able to achieve the respective set-points. The settling time of the PI control under these scenarios was large. For scenario 3, the PI control scheme had complications with handling loop interactions within the capture model.

7.1.3 MPC scheme

Chapter 5 presented the linear model predictive control (MPC) scheme design and implementation on the solvent-based PCC process. The MPC scheme was evaluated in comparison with the conventional PI control scheme under 3 different scenarios (case studies). For all scenarios considered, the MPC scheme gave a better control performance compared to the conventional PI control scheme, as it is able to handle the interactions within the process in comparison with the conventional PI control scheme. Thus, the MPC scheme avoids a sluggish response to the controlled variable set-point changes. However, the incapability of the MPC scheme to adequately control the capture model for a wide range flexible operation mode was highlighted due to the inability of the linear model to capture the accurate process dynamics of the wide flexible operating mode.

7.1.4 NMPC scheme

The design and implementation of a nonlinear model predictive control (NMPC) scheme on the solvent-based post-combustion CO_2 capture process was presented in Chapter 6. The NMPC scheme was evaluated under 2 different scenarios (case studies). Performance evaluation of the NMPC scheme in comparison with

conventional PI and MPC revealed it was capable of handling interactions within the capture process at wide (large disturbance and frequent set-point change) flexible operation.

7.2 Recommendation for future study

The following areas are recommended for further research on the nonlinear SI and control of solvent-based PCC process.

- The data-driven model development of the solvent-based PCC process through nonlinear SI utilizes data obtained from the detailed rate-based PCC model by developed Lawal et al., 2010. In the rate-based model, CO₂ kinetics was assumed to attain equilibrium. This does not reflect what is obtainable in a real plant. Thus, it will be interesting to utilize data obtained from pilot-scale PCC plant (like the UKCCSRC PACT facilities) for data-driven model development via nonlinear SI.
- In This thesis, Identified nonlinear model was developed representing the solvent-based PCC process as 2 sub-systems with 3 inputs and 2 outputs. While the model developed cannot be applied for more than 3 inputs and 2 outputs, the model building method and associated (FROLS) algorithms are not restricted to the small number of input and output variables and can be easily extended to many input and output variables to represent the power plant integrated with solvent-based PCC process. Although the interaction with the power plant is reflected in the variation of flue gas flowrate and steam flowrate, further research on the data-driven model development of the power plant integrated with the capture process via nonlinear SI technique based on FROLS algorithms.

- Further investigation to demonstrate real-time implementation of the NMPC on an industrial scale solvent-based PCC process utilizing nonlinear model developed via FROLS algorithms should be carried out. This is to ascertain the reliable use of NMPC as the control performance of the NMPC can be erratic mainly due to the nonlinear model mismatch with the industrial scale capture process. The ease of been able to update the model developed based on FROLS algorithm using the plant data, it will to investigate how the reliability of the NMPC real time performance on an industrial scale solvent-based PCC plant is improved.
- As the world is shifting to the application of Artificial intelligence and with the advancement of software and algorithm, it will be interesting to explore the application of AI in model development and process control of the solvent-based CO₂ capture process. An interesting area is the use of machine learning tools for uncertainty quantification of the data-driven model developed to represent the solvent-based CO₂ capture process.

References

- Abdul Manaf, N., Cousins, A., Feron, P. & Abbas, A. (2016). Dynamic Modelling, Identification and Preliminary Control Analysis of an Amine-Based Post-Combustion CO₂ Capture Pilot Plant. *Journal of Cleaner Production*, 113, 635–653.
- Abu-Zahra, M. R. M., Niederer, J. P. M., Feron, P. H. M. & Versteeg, G. F. (2007). CO₂ Capture from Power Plants: Part II. A Parametric Study of the Economical Performance Based on Mono-Ethanolamine. *International Journal of Greenhouse Gas Control*, 1(2), 135–142.
- Abu-Zahra, M. R. M., Schneiders, L. H. J., Niederer, J. P. M., Feron, P. H. M. & Versteeg, G. F. (2007). CO₂ Capture from Power Plants: Part I. A Parametric Study of the Technical Performance Based on Monoethanolamine. *International Journal of Greenhouse gas control*, 1(1), 37–46.
- Agbonghae, E. O., Hughes, K. J., Ingham, D. B., Ma, L. & Pourkashanian, M. (2014). Optimal Process Design of Commercial-Scale Amine-Based CO₂ Capture Plants. *Industrial & Engineering Chemistry Research*, 53(38), 14815–14829.
- Ahn, H., Luberti, M., Liu, Z. & Brandani, S. (2013). Process Configuration Studies of the Amine Capture Process for Coal-Fired Power Plants. *International Journal of Greenhouse Gas Control*, 16, 29–40.
- Åkesson, J., Laird, C. D., Lavedan, G., Prölb, K., Tummescheit, H., Velut, S. & Zhu, Y. (2012). Nonlinear Model Predictive Control of a CO₂ Post-Combustion Absorption Unit. *Chemical Engineering and Technology*, 35(3), 445–454.
- Akinola, T. E., Oko, E., Gu, Y., Wei, H.-L. & Wang, M. (2019). Non-Linear System Identification of Solvent-Based Post-Combustion CO₂ Capture Process. *Fuel*, 239, 1213–1223.
- Akinola, T. E., Oko, E. & Wang, M. (2019). Study of CO₂ Removal in Natural Gas Process Using Mixture of Ionic Liquid and MEA through Process Simulation. *Fuel*, 236, 135–146.
- Al-Gherwi, W., Budman, H. & Elkamel, A. (2011). Robust Distributed Model Predictive Control: A Review and Recent Developments. *Canadian Journal of Chemical Engineering*, 89(5), 1176–1190.
- Alcaráz-Calderon, A. M., González-Díaz, M. O., Mendez, Á., González-Santaló, J. M. & González-Díaz, A. (2019). Natural Gas Combined Cycle with Exhaust Gas Recirculation and CO₂ Capture at Part-Load Operation. *Journal of the Energy Institute*, 92(2), 370–381.
- Álvarez-Gutiérrez, N., Rubiera, F., Pevida, C., Jin, Y., Bae, J. & Su, S. (2017). Adsorption Performance Indicator to Screen Carbon Adsorbents for Post-Combustion CO₂ Capture. *Energy Procedia*, 114, 2362–2371.
- Arce, A., Mac Dowell, N., Shah, N. & Vega, L. F. (2012). Flexible Operation of Solvent Regeneration Systems for CO₂ Capture Processes Using Advanced Control Techniques: Towards Operational Cost Minimisation. *International Journal of Greenhouse Gas Control*, 11, 236–250.
- Aroonwilas, A. & Veawab, A. (2007). Integration of CO₂ Capture Unit Using Single-

- and Blended-Amines into Supercritical Coal-Fired Power Plants: Implications for Emission and Energy Management. *International Journal of Greenhouse Gas Control*, 1(2), 143–150.
- Aroonwilas, A. & Veawab, A. (2009). Integration of CO₂ Capture Unit Using Blended MEA–AMP Solution into Coal-Fired Power Plants. *Energy Procedia*, 1(1), 4315–4321.
- Aroonwilas, A. & Veawab, A. (2016). Mass Transfer in Amine-Based CO₂ Absorption Process: Theory and Its Applications to Plant Design and Operation, in: *Carbon Dioxide Capture: Processes, Technology and Environmental Implications*, (pp. 69–94).
- Asif, M., Suleman, M., Haq, I. & Jamal, S. A. (2018). Post-Combustion CO₂ Capture with Chemical Absorption and Hybrid System: Current Status and Challenges. *Greenhouse Gases: Science and Technology*, 8(6), 998–1031.
- Bandrés, I., Royo, F. M., Gascón, I., Castro, M. & Lafuente, C. (2010). Anion Influence on Thermophysical Properties of Ionic Liquids: 1-Butylpyridinium Tetrafluoroborate and 1-Butylpyridinium Triflate. *The Journal of Physical Chemistry B*, 114(10), 3601–3607.
- Belaissaoui, B., Le Moullec, Y., Willson, D. & Favre, E. (2012). Hybrid Membrane Cryogenic Process for Post-Combustion CO₂ Capture. *Journal of Membrane Science*, 415–416, 424–434.
- Bequette, B. W. (2007). Non-Linear Model Predictive Control: A Personal Retrospective. *Canadian Journal of Chemical Engineering*, 85(4), 408–415.
- Biliyok, C., Lawal, A., Wang, M. & Seibert, F. (2012b). Dynamic Modelling, Validation and Analysis of Post-Combustion Chemical Absorption CO₂ Capture Plant. *International Journal of Greenhouse Gas Control*, 9, 428–445.
- Biliyok, C., Lawal, A., Wang, M. & Seibert, F. (2012a). Dynamic Validation of Model for Post-Combustion Chemical Absorption CO₂ Capture Plant. *Computer Aided Chemical Engineering*, 30, 807–811.
- Billings, S. A. (2013). *Nonlinear System Identification: NARMAX Methods in the Time, Frequency, and Spatio-Temporal Domains*. University of Sheffield, United Kingdom: wiley.
- Billings, S. A., Chen, S. & Korenbergs, M. J. (1989). Identification of MIMO Non-Linear Systems Using a Forward-Regression Orthogonal Estimator. *International Journal of Control*, 49(6), 2157–2189.
- Billings, S. A., Korenberg, M. J. & Chen, S. (1988). Identification of Non-Linear Output-Affine Systems Using an Orthogonal Least-Squares Algorithm. *International Journal of Systems Science*, 19(8), 1559–1568.
- Billings, S. A. & Leontaritis, I. J. (1981). Identification of nonlinear systems using parameter estimation techniques. *IEE Conference Publication*, (194), 183–187.
- Billings, S. A. & Wei, H.-L. (2005). A New Class of Wavelet Networks for Nonlinear System Identification. *IEEE Transactions on neural networks*, 16(4), 862–874.
- Billings, S. A. & Zhu, Q. M. (1991). Rational Model Identification Using an Extended Least-Squares Algorithm. *International Journal of Control*, 54(3), 529–546.
- Billings, S. A. & Zhu, Q. M. (1994). A Structure Detection Algorithm for Nonlinear

- Dynamic Rational Models. *International Journal of Control*, 59(6), 1439–1463.
- Bui, M., Gunawan, I., Verheyen, V., Artanto, Y., Meuleman, E. & Feron, P. (2013). Dynamic Modeling and Validation of Post-Combustion CO₂ Capture Plants in Australian Coal-Fired Power Stations, in: *Energy Procedia*, (pp. 2694–2702).
- Bui, M., Gunawan, I., Verheyen, V., Feron, P. & Meuleman, E. (2016). Flexible Operation of CSIRO's Post-Combustion CO₂ Capture Pilot Plant at the AGL Loy Yang Power Station. *International Journal of Greenhouse Gas Control*, 48, 188–203.
- Bui, M., Gunawan, I., Verheyen, V., Feron, P., Meuleman, E. & Adeloju, S. (2014). Dynamic Modelling and Optimisation of Flexible Operation in Post-Combustion CO₂ Capture Plants—A Review. *Computers & Chemical Engineering*, 61, 245–265.
- Burt, S. S., Baxter, A., Bence, C. & Baxter, L. L. (2010). Cryogenic CO₂ Capture for Improved Efficiency at Reduced Cost, in: *Proceedings of the AIChE 2010 annual meeting*.
- Cadena, C., Anthony, J. L., Shah, J. K., Morrow, T. I., Brennecke, J. F. & Maginn, E. J. (2004). Why Is CO₂ so Soluble in Imidazolium-Based Ionic Liquids? *Journal of the American Chemical Society*, 126(16), 5300–5308.
- Camacho, E. F. & Alba, C. B. (2013). *Model Predictive Control*. Springer Science & Business Media.
- Camacho, E. F. & Bordons, C. (2007). Nonlinear Model Predictive Control: An Introductory Review. *Lecture Notes in Control and Information Sciences*, 358(1), 1–16.
- Camacho, E. F. & Bordons, C. (2012). *Model Predictive Control in the Process Industry*. Springer Science & Business Media.
- Canepa, R., Wang, M., Biliyok, C. & Satta, A. (2013). Thermodynamic Analysis of Combined Cycle Gas Turbine Power Plant with Post-Combustion CO₂ Capture and Exhaust Gas Recirculation. *Proceedings of the Institution of Mechanical Engineers, Part E: Journal of Process Mechanical Engineering*, 227(2), 89–105.
- CCS, M. (2016). Jilin Fact. Retrieved September 10, 2019, from <http://sequestration.mit.edu/tools/projects/jilin.html>
- Chalmers, H., Lucquiaud, M., Gibbins, J. & Leach, M. (2009). Flexible Operation of Coal Fired Power Plants with Postcombustion Capture of Carbon Dioxide. *Journal of Environmental Engineering*, 135(6), 449–458.
- Chen, S., Billings, S. A. & Luo, W. (1989). Orthogonal Least Squares Methods and Their Application to Non-Linear System Identification. *International Journal of Control*, 50(5), 1873–1896.
- Chi, S. & Rochelle, G. T. (2002). Oxidative Degradation of Monoethanolamine. *Industrial & engineering chemistry research*, 41(17), 4178–4186.
- Coent, L. (2017). The IEA energy data collection and CO₂ Estimates: an Overview. *IEA Energy Data center*. Available from https://www.transparency-partnership.net/sites/default/files/u2620/the_iea_energy_data_collection_and_co2_estimates_an_overview_iea_coent.pdf [Accessed on Retrieved September 23, 2019]

- Cohen, S. M., Rochelle, G. T. & Webber, M. E. (2011). Optimal Operation of Flexible Post-Combustion CO₂ Capture in Response to Volatile Electricity Prices. *Energy Procedia*, 4, 2604–2611.
- Cottrell, A. & Feron, P. H. M. (2011). Experience from Post-Combustion Capture Pilot Plant Operations in Australia, in: *1st Post Combustion Capture Conference*, (pp. 17–19).
- Cousins, A., Wardhaugh, L. T. & Feron, P. H. M. (2011). A Survey of Process Flow Sheet Modifications for Energy Efficient CO₂ Capture from Flue Gases Using Chemical Absorption. *International Journal of Greenhouse Gas Control*, 5(4), 605–619.
- Dantas, T. S. S., Franco, I. C., Fileti, A. M. F. & Da Silva, F. V. (2016). Nonlinear System Identification of a Refrigeration System. *International Journal of Air-Conditioning and Refrigeration*, 24(4).
- Davis, J. & Rochelle, G. (2009). Thermal Degradation of Monoethanolamine at Stripper Conditions. *Energy Procedia*, 1(1), 327–333.
- Mac Dowell, N., Samsatli, N. J. & Shah, N. (2013). Dynamic Modelling and Analysis of an Amine-Based Post-Combustion CO₂ Capture Absorption Column. *International Journal of Greenhouse Gas Control*, 12, 247–258.
- Mac Dowell, N. & Shah, N. (2013). Identification of the Cost-Optimal Degree of CO₂ Capture: An Optimisation Study Using Dynamic Process Models. *International Journal of Greenhouse Gas Control*, 13, 44–58.
- Mac Dowell, N. & Shah, N. (2014). Dynamic Modelling and Analysis of a Coal-Fired Power Plant Integrated with a Novel Split-Flow Configuration Post-Combustion CO₂ Capture Process. *International Journal of Greenhouse Gas Control*, 27, 103–119.
- Mac Dowell, N. & Staffell, I. (2015). The Role of Flexible CCS in the UK's Future Energy System. *International Journal of Greenhouse Gas Control*, 48, 327–344
- Drax. (2019). BECCS Pilot Project. Available on https://www.drax.com/press_release/world-first-co2-beccs-ccus/ [Accessed on Retrieved September 10, 2019]
- Dugas, R. E. (2006). Pilot Plant Study of Carbon Dioxide Capture by Aqueous Monoethanolamine. *MSE Thesis, University of Texas at Austin*.
- Dunia, R., Rochelle, G. T. & Qin, S. J. (2011). Subspace System Identification for CO₂ Recovery Processes, in: *Proceedings of the IEEE International Symposium on Computer-Aided Control System Design*. Department of Chemical Engineering, University of Texas, Austin, TX 78712, United States, Department of Chemical Engineering and Material Sciences, University of Southern California, CA 90089, United States, pp. 846–851.
- Enaasen Flø, N., Knuutila, H., Kvamsdal, H. M. & Hillestad, M. (2015). Dynamic Model Validation of the Post-Combustion CO₂ Absorption Process. *International Journal of Greenhouse Gas Control*, 41, 127–141.
- Enaasen, N., Tobiesen, A., Kvamsdal, H. M. & Hillestad, M. (2013). Dynamic Modeling of the Solvent Regeneration Part of a CO₂ Capture Plant, in: *Energy Procedia*,

(pp. 2058–2065).

- Enerdata. (2019). Global Energy Statistical Yearbook 2019. 1. Available on <https://yearbook.enerdata.net/electricity/electricity-domestic-consumption-data.html> [Accessed on September 5, 2019]
- Faber, R., Köpcke, M., Biede, O., Knudsen, J. N. & Andersen, J. (2011). Open-Loop Step Responses for the MEA Post-Combustion Capture Process: Experimental Results from the Esbjerg Pilot Plant, in: *Energy Procedia*, 4, 1427–1434).
- Fan, Z., Liu, K., Qi, G., Frimpong, R. & Nikolic, H. (2015). Aspen Modeling for MEA-CO₂ Loop: Dynamic Gridding for Accurate Column Profile. *International Journal of Greenhouse Gas Control*, 37, 318–324.
- Findeisen, R. & Allgöwer, F. (2002). An Introduction to Nonlinear Model Predictive Control, in: *21st Benelux meeting on systems and control*, (pp. 119–141). Technische Universiteit Eindhoven Veldhoven Eindhoven, The Netherlands.
- Flø, N. E., Kvamsdal, H. M. & Hillestad, M. (2016). Dynamic Simulation of Post-Combustion CO₂ Capture for Flexible Operation of the Brindisi Pilot Plant. *International Journal of Greenhouse Gas Control*, 48, 204–215.
- Gardarsdóttir, S. Ó., Normann, F., Andersson, K., Prölb, K., Emilsdóttir, S. & Johnsson, F. (2015). Post-Combustion CO₂ Capture Applied to a State-of-the-Art Coal-Fired Power Plant-The Influence of Dynamic Process Conditions. *International Journal of Greenhouse Gas Control*, 33, 51–62. R
- Garriga, J. L. & Soroush, M. (2010). Model Predictive Control Tuning Methods: A Review. *Industrial and Engineering Chemistry Research*, 49(8), 3505–3515.
- Gaspar, J. & Cormos, A.-M. (2012). Dynamic Modeling and Absorption Capacity Assessment of CO₂ Capture Process. *International Journal of Greenhouse Gas Control*, 8, 45–55.
- Gáspár, J. & Cornoş, A. M. (2011). Dynamic Modeling and Validation of Absorber and Desorber Columns for Post-Combustion CO₂ Capture. *Computers and Chemical Engineering*, 35(10), 2044–2052.
- Gaspar, J., Gladis, A., Jørgensen, J. B., Thomsen, K., von Solms, N. & Fosbøl, P. L. (2016). Dynamic Operation and Simulation of Post-Combustion CO₂ Capture. *Energy Procedia*, 86, 205–214.
- Gaspar, J., Ricardez-Sandoval, L., Jørgensen, J. B. & Fosbøl, P. L. (2016). Controllability and Flexibility Analysis of CO₂ Post-Combustion Capture Using Piperazine and MEA. *International Journal of Greenhouse Gas Control*, 51, 276–289.
- Global CCS Institute. (2017). The Global Status of CCS. *Global CCS Institute*. Available on <https://www.globalccsinstitute.com/wp-content/uploads/2018/12/2017-Global-Status-Report.pdf> [Accessed on September 23, 2019]
- Global CCS Institute. (2019). CO₂RE Facilities Data. Available on <https://co2re.co/FacilityData> [Accessed on September 20, 2019]
- Goto, K., Yogo, K. & Higashii, T. (2013). A Review of Efficiency Penalty in a Coal-Fired Power Plant with Post-Combustion CO₂ Capture. *Applied Energy*, 111, 710–720.
- GPSA, G. (2004). Engineering Data Book. *Gas Processors Suppliers Association*, 2,

16–24.

- Grancharova, A. & Johansen, T. A. (2004). Explicit Approaches to Constrained Model Predictive Control: A Survey. *Modeling, Identification and Control*, 25(3), 131–157.
- Grande, C. A. & Rodrigues, A. E. (2008). Electric Swing Adsorption for CO₂ Removal from Flue Gases. *International Journal of Greenhouse Gas Control*, 2(2), 194–202.
- Greer, T., Bedelbayev, A., Igreja, J. M., Gomes, J. F. & Lie, B. (2010). A Simulation Study on the Abatement of CO₂ Emissions by de-Absorption with Monoethanolamine. *Environmental Technology*, 31(1), 107–115.
- Hägglom, K. E. & Böling, J. M. (1998). Multimodel Identification for Control of an Ill-Conditioned Distillation Column. *Journal of Process Control*, 8(3), 209–218.
- Harun, N., Douglas, P. L., Ricardez-Sandoval, L. & Croiset, E. (2011). Dynamic Simulation of MEA Absorption Processes for CO₂ Capture from Fossil Fuel Power Plant, in: *Energy Procedia*, 4, 1478–1485.
- Han, K., Ahn, C. K., Lee, M. S., Rhee, C. H., Kim, J. Y. & Chun, H. D. (2013). Current Status and Challenges of the Ammonia-Based CO₂ Capture Technologies toward Commercialization. *International Journal of Greenhouse Gas Control*, 14, 270–281.
- Hasan, M. M. F., Baliban, R. C., Elia, J. A. & Floudas, C. A. (2012). Modeling, Simulation, and Optimization of Postcombustion CO₂ Capture for Variable Feed Concentration and Flow Rate. 2. Pressure Swing Adsorption and Vacuum Swing Adsorption Processes. *Industrial & Engineering Chemistry Research*, 51(48), 15665–15682.
- Hauger, S. O., Flø, N. E., Kvamsdal, H., Gjertsen, F., Mejdell, T. & Hillestad, M. (2019). Demonstration of Non-Linear Model Predictive Control of Post-Combustion CO₂ Capture Processes. *Computers and Chemical Engineering*, 123, 184–195.
- He, Z., Sahraei, M. H. & Ricardez-Sandoval, L. A. (2016). Flexible Operation and Simultaneous Scheduling and Control of a CO₂ Capture Plant Using Model Predictive Control. *International Journal of Greenhouse Gas Control*, 48, 300–311.
- Hirata, T., Nagayasu, H., Yonekawa, T., Inui, M., Kamijo, T., Kubota, Y., Tsujiuchi, T., Shimada, D., Wall, T. & Thomas, J. (2014). Current Status of MHI CO₂ Capture Plant Technology, 500 TPD CCS Demonstration of Test Results and Reliable Technologies Applied to Coal Fired Flue Gas. *Energy Procedia*, 63, 6120–6128.
- Hosseini Sahraei, M. & Ricardez-Sandoval, L. A. (2014). Controllability and Optimal Scheduling of a CO₂ Capture Plant Using Model Predictive Control. *International Journal of Greenhouse Gas Control*, 30, 58–71.
- Huaman, R. N. E. & Jun, T. X. (2014). Energy Related CO₂ Emissions and the Progress on CCS Projects: A Review. *Renewable and Sustainable Energy Reviews*, 31, 368–385.
- Huang, Y., Zhang, X., Zhang, X., Dong, H. & Zhang, S. (2014). Thermodynamic Modeling and Assessment of Ionic Liquid-Based CO₂ Capture Processes. *Industrial & Engineering Chemistry Research*, 53(29), 11805–11817.

- Ishibashi, M., Ota, H., Akutsu, N., Umeda, S., Tajika, M., Izumi, J., Yasutake, A., Kabata, T. & Kageyama, Y. (1996). Technology for Removing Carbon Dioxide from Power Plant Flue Gas by the Physical Adsorption Method. *Energy Conversion and Management*, 37(6–8), 929–933.
- Jayarathna, S. A., Lie, B. & Melaaen, M. C. (2013). Dynamic Modelling of the Absorber of a Post-Combustion CO₂ Capture Plant: Modelling and Simulations. *Computers & Chemical Engineering*, 53, 178–189.
- Joel, A. S., Wang, M., Ramshaw, C. & Oko, E. (2014). Process Analysis of Intensified Absorber for Post-Combustion CO₂ Capture through Modelling and Simulation. *International Journal of Greenhouse Gas Control*, 21, 91–100.
- Jones, K. O. & Hengue, W. (2009). Limitations of Multivariable Controller Tuning Using Genetic Algorithms, in: *Proceedings of the International Conference on Computer Systems and Technologies and Workshop for PhD Students in Computing*, (p. 46). ACM.
- Karimi, M., Hillestad, M. & Svendsen, H. F. (2011). Capital Costs and Energy Considerations of Different Alternative Stripper Configurations for Post Combustion CO₂ Capture. *Chemical Engineering Research and Design*, 89(8), 1229–1236.
- Kenig, E. Y., Schneider, R. & Górak, A. (2001). Reactive Absorption: Optimal Process Design via Optimal Modelling. *Chemical Engineering Science*, 56(2), 343–350.
- Khare, Y. B. & Singh, Y. (2010). PID Control of Heat Exchanger System. *International Journal of Computer Applications*, 8(6), 975–8887.
- Kidnay, A. J., Parrish, W. R. & McCartney, D. G. (2011). *Fundamentals of Natural Gas Processing*. CRC Press.
- Kotta, Ü. & Sadegh, N. (2002). Two Approaches for State Space Realization of Narma Models: Bridging the Gap. *Mathematical and Computer Modelling of Dynamical Systems*, 8(1), 21–32.
- Kvamsdal, H. M., Jakobsen, J. P. & Hoff, K. A. (2009). Dynamic Modeling and Simulation of a CO₂ Absorber Column for Post-Combustion CO₂ Capture. *Chemical Engineering and Processing: Process Intensification*, 48(1), 135–144.
- Larsson, T. & Skogestad, S. (2000). Plantwide Control - a Review and a New Design Procedure. *Modeling, Identification and Control*, 21(4), 209–240.
- Lawal, A., Wang, M., Stephenson, P., Koumpouras, G. & Yeung, H. (2010). Dynamic Modelling and Analysis of Post-Combustion CO₂ Chemical Absorption Process for Coal-Fired Power Plants. *Fuel*, 89(10), 2791–2801.
- Lawal, A., Wang, M., Stephenson, P. & Obi, O. (2012). Demonstrating Full-Scale Post-Combustion CO₂ Capture for Coal-Fired Power Plants through Dynamic Modelling and Simulation. *Fuel*, 101, 115–128.
- Lawal, A., Wang, M., Stephenson, P. & Yeung, H. (2009). Dynamic Modelling of CO₂ Absorption for Post Combustion Capture in Coal-Fired Power Plants. *Fuel*, 88(12), 2455–2462.
- Lee, J. & Edgar, T. F. (2005). Continuation Method for the Modified Ziegler-Nichols Tuning of Multiloop Control Systems. *Industrial & engineering chemistry research*,

44(19), 7428–7434.

- Lee, J. H., Kwak, N. S., Lee, I. Y., Jang, K. R., Lee, D. W., Jang, S. G., Kim, B. K. & Shim, J.-G. (2015). Performance and Economic Analysis of Commercial-Scale Coal-Fired Power Plant with Post-Combustion CO₂ Capture. *Korean Journal of Chemical Engineering*, 32(5), 800–807.
- Lee, S.-Y. & Park, S.-J. (2015). A Review on Solid Adsorbents for Carbon Dioxide Capture. *Journal of Industrial and Engineering Chemistry*, 23, 1–11.
- Leontaritis, I. J. & Billings, S. A. (1985). Input-Output Parametric Models for Non-Linear Systems Part I: Deterministic Non-Linear Systems. *International Journal of Control*, 41(2), 303–328.
- Lepaumier, H., Da Silva, E. F., Einbu, A., Grimstvedt, A., Knudsen, J. N., Zahlsen, K. & Svendsen, H. F. (2011). Comparison of MEA Degradation in Pilot-Scale with Lab-Scale Experiments, in: *Energy Procedia*, 4, 1652–1659.
- Leung, D. Y. C., Caramanna, G. & Maroto-Valer, M. M. (2014). An Overview of Current Status of Carbon Dioxide Capture and Storage Technologies. *Renewable and Sustainable Energy Reviews*, 39, 426–443.
- Levin, A. U. & Narendra, K. S. (1993). Control of Nonlinear Dynamical Systems Using Neural Networks: Controllability and Stabilization. *IEEE Transactions on neural networks*, 4(2), 192–206.
- Li, F., Zhang, J., Oko, E. & Wang, M. (2015). Modelling of a Post-Combustion CO₂ Capture Process Using Neural Networks. *Fuel*, 151, 156–163.
- Li, F., Zhang, J., Oko, E. & Wang, M. (2017). Modelling of a Post-Combustion CO₂ Capture Process Using Extreme Learning Machine. *International Journal of Coal Science and Technology*, 4(1), 33–40.
- Li, P., Wei, H.-L., Billings, S. A., Balikhin, M. A. & Boynton, R. (2013). Nonlinear Model Identification from Multiple Data Sets Using an Orthogonal Forward Search Algorithm. *Journal of Computational and Nonlinear Dynamics*, 8(4), 41001.
- Lin, Y. J., Pan, T. H., Wong, D. S. H., Jang, S. S., Chi, Y. W. & Yeh, C. H. (2011). Plantwide Control of CO₂ Capture by Absorption and Stripping Using Monoethanolamine Solution. *Industrial and Engineering Chemistry Research*, 50(3), 1338–1345.
- Lin, Y. J., Wong, D. S. H., Jang, S. S. & Ou, J. J. (2012). Control Strategies for Flexible Operation of Power Plant with CO₂ Capture Plant. *AIChE Journal*, 58(9), 2697–2704.
- Lindsey, R. (2019). Climate Change: Atmospheric Carbon Dioxide. NOAA *Climate.gov*. Available on <https://www.climate.gov/news-features/understanding-climate/climate-change-atmospheric-carbon-dioxide> [Accessed on September 23, 2019]
- Liu, X., Chen, J., Luo, X., Wang, M. & Meng, H. (2015). Study on Heat Integration of Supercritical Coal-Fired Power Plant with Post-Combustion CO₂ Capture Process through Process Simulation. *Fuel*, 158, 625–633.
- Ljung, L. (1987). System Identification: Theory for the User. New Jersey: *Englewood Cliffs*.
- Llovel, F., Marcos, R. M., MacDowell, N. & Vega, L. F. (2012). Modeling the

- Absorption of Weak Electrolytes and Acid Gases with Ionic Liquids Using the Soft-SAFT Approach. *Journal of Physical Chemistry B*, 116(26), 7709–7718.
- Lucquiaud, M. & Gibbins, J. (2011). Effective Retrofitting of Post-Combustion CO₂ Capture to Coal-Fired Power Plants and Insensitivity of CO₂ Abatement Costs to Base Plant Efficiency. *International Journal of Greenhouse Gas Control*, 5(3), 427–438.
- Luo, X. & Wang, M. (2017). Improving Prediction Accuracy of a Rate-Based Model of an MEA-Based Carbon Capture Process for Large-Scale Commercial Deployment. *Engineering*, 3(2), 232–243.
- Luo, X., Wang, M. & Chen, J. (2015). Heat Integration of Natural Gas Combined Cycle Power Plant Integrated with Post-Combustion CO₂ Capture and Compression. *Fuel*, 151, 110–117.
- Luu, M. T., Abdul Manaf, N. & Abbas, A. (2015). Dynamic Modelling and Control Strategies for Flexible Operation of Amine-Based Post-Combustion CO₂ Capture Systems. *International Journal of Greenhouse Gas Control*, 39, 377–389.
- Luyben, M. L., Tyreus, B. D. & Luyben, W. L. (1997). Plantwide Control Design Procedure. *AIChE Journal*, 43(12), 3161–3174.
- Luyben, W. L. (1986). Simple Method for Tuning SISO Controllers in Multivariable Systems. *Industrial & Engineering Chemistry Process Design and Development*, 25(3), 654–660.
- Macedo, M. M. G., Takimura, C. K., Lemos, P. A. & Gutierrez, M. A. (2015). An Automatic Labeling Bifurcation Method for Intracoronary Optical Coherence Tomography Images, in: *Progress in Biomedical Optics and Imaging - Proceedings of SPIE*, vol. 9417.
- Mansourizadeh, A. & Ismail, A. F. (2009). Hollow Fiber Gas–liquid Membrane Contactors for Acid Gas Capture: A Review. *Journal of Hazardous Materials*, 171(1), 38–53.
- Mantripragada, H. C., Zhai, H. & Rubin, E. S. (2019). Boundary Dam or Petra Nova – Which Is a Better Model for CCS Energy Supply? *International Journal of Greenhouse Gas Control*, 82, 59–68.
- Di Marco, R., Semino, D. & Brambilla, A. (1997). From Linear to Nonlinear Model Predictive Control: Comparison of Different Algorithms. *Industrial and Engineering Chemistry Research*, 36(5), 1708–1716.
- Mathworks, C. (2019). MATLAB and Optimization Toolbox™ Release R2019a. USA
- MathWorks, M. (2015). SIMULINK for Technical Computing. Available on <http://www.mathworks.com>. [Accessed on September 9, 2019].
- Mechleri, E., Lawal, A., Ramos, A., Davison, J. & Dowell, N. Mac. (2017). Process Control Strategies for Flexible Operation of Post-Combustion CO₂ Capture Plants. *International Journal of Greenhouse Gas Control*, 57, 14–25.
- Mehler, E. D., Dowell, N. M. & Thornhill, N. F. (2015). Model Predictive Control of Post-Combustion CO₂ Capture Process Integrated with a Power Plant. *Computer Aided Chemical Engineering*, 37, 161–166.
- Mehler, E. D., Mac Dowell, N. & Thornhill, N. F. Model Predictive Control of Post-Combustion CO₂ Capture Process Integrated with a Gas-Fired Power Plant.

- Mokhtarani, B., Sharifi, A., Mortaheb, H. R., Mirzaei, M., Mafi, M. & Sadeghian, F. (2009). Density and Viscosity of Pyridinium-Based Ionic Liquids and Their Binary Mixtures with Water at Several Temperatures. *The Journal of Chemical Thermodynamics*, 41(3), 323–329.
- Mumford, K. A., Wu, Y., Smith, K. H. & Stevens, G. W. (2015). Review of Solvent Based Carbon-Dioxide Capture Technologies. *Frontiers of Chemical Science and Engineering*, 9(2), 125–141.
- Nittaya, T., Douglas, P. L., Croiset, E. & Ricardez-Sandoval, L. A. (2014a). Dynamic Modelling and Control of MEA Absorption Processes for CO₂ Capture from Power Plants. *Fuel*, 116, 672–691.
- Nittaya, T., Douglas, P. L., Croiset, E. & Ricardez-Sandoval, L. A. (2014b). Dynamic Modelling and Controllability Studies of a Commercial-Scale MEA Absorption Processes for CO₂ Capture from Coal-Fired Power Plants. *12th International Conference on Greenhouse Gas Control Technologies, GHGT-12*, 63, 1595–1600.
- Norquay, S. J., Palazoglu, A. & Romagnoli, J. (1998). Model Predictive Control Based on Wiener Models. *Chemical Engineering Science*, 53(1), 75–84.
- Ohashi, Y., Ogawa, T. & Egami, N. (2011). Development of Carbon Dioxide Removal System from the Flue Gas of Coal Fired Power Plant. *Energy Procedia*, 4, 29–34.
- Oko, E. (2015). Study of Power Plant, Carbon Capture and Transport Network through Dynamic Modelling and Simulation. PhD Thesis. The University of Hull, United Kingdom.
- Oko, E., Wang, M. & Joel, A. S. (2017). Current Status and Future Development of Solvent-Based Carbon Capture. *International Journal of Coal Science & Technology*, 4(1), 5–14.
- Oko, E., Wang, M. & Olaleye, A. K. (2015). Simplification of Detailed Rate-Based Model of Post-Combustion CO₂ Capture for Full Chain CCS Integration Studies. *Fuel*, 142, 87–93.
- Olajire, A. A. (2010). CO₂ Capture and Separation Technologies for End-of-Pipe Applications—a Review. *Energy*, 35(6), 2610–2628.
- Onda, K., Takeuchi, H. & Okumoto, Y. (1968). Mass Transfer Coefficients between Gas and Liquid Phases in Packed Columns. *Journal of chemical engineering of Japan*, 1(1), 56–62.
- Panahi, M. & Skogestad, S. (2011). Economically Efficient Operation of CO₂ Capturing Process Part I: Self-Optimizing Procedure for Selecting the Best Controlled Variables. *Chemical Engineering and Processing: Process Intensification*, 50(3), 247–253.
- Panahi, M. & Skogestad, S. (2012). Economically Efficient Operation of CO₂ Capturing Process. Part II. Design of Control Layer. *Chemical Engineering and Processing: Process Intensification*, 52, 112–124.
- Peng, J., Edgar, T. F. & Eldridge, R. B. (2003). Dynamic Rate-Based and Equilibrium Models for a Packed Reactive Distillation Column. *Chemical Engineering Science*, 58(12), 2671–2680.

- Pirngruber, G. D., Guillou, F., Gomez, A. & Clause, M. (2013). A Theoretical Analysis of the Energy Consumption of Post-Combustion CO₂ Capture Processes by Temperature Swing Adsorption Using Solid Sorbents. *International Journal of Greenhouse Gas Control*, 14, 74–83.
- Poorani, V. J. & Anand, L. D. V. (2013). Comparison of PID Controller and Smith Predictor Controller for Heat Exchanger, in: *2013 IEEE International Conference ON Emerging Trends in Computing, Communication and Nanotechnology (ICECCN)*, (pp. 217–221).
- Posch, S. & Haider, M. (2013). Dynamic Modeling of CO₂ Absorption from Coal-Fired Power Plants into an Aqueous Monoethanolamine Solution. *Chemical Engineering Research and Design*, 91(6), 977–987.
- Proß, K., Tummescheit, H., Velut, S. & Åkesson, J. (2011). Dynamic Model of a Post-Combustion Absorption Unit for Use in a Non-Linear Model Predictive Control Scheme. *Energy Procedia*, 4, 2620–2627.
- Pröll, K., Tummescheit, H., Velut, S. & Åkesson, J. (2011). Dynamic Model of a Post-Combustion Absorption Unit for Use in a Non-Linear Model Predictive Control Scheme. *Energy Procedia*, 4, 2620–2627.
- Rabensteiner, M., King, G., Koller, M. & Hochenauer, C. (2014). Three Years of Working Experience with Different Solvents at a Realistic Post Combustion Capture Pilot Plant, in: *Energy Procedia*, 63, 1578–1584.
- Radgen, P., Rode, H., Reddy, S. & Yonkoski, J. (2014). Lessons Learned from the Operation of a 70 Tonne per Day Post Combustion Pilot Plant at the Coal Fired Power Plant in Wilhelmshaven, Germany. *Energy Procedia*, 63, 1585–1594.
- Rahimpour, M. R. & Kashkooli, A. Z. (2004). Enhanced Carbon Dioxide Removal by Promoted Hot Potassium Carbonate in a Split-Flow Absorber. *Chemical Engineering and Processing: Process Intensification*, 43(7), 857–865.
- Roberts, P. D. (2000). A Brief Overview of Model Predictive Control. *Elektron*, 17(2), 46–47.
- Sadegh, N. (2001). Minimal Realization of Nonlinear Systems Described by Input-Output Difference Equations. *IEEE Transactions on Automatic control*, 46(5), 698–710.
- Sadegh, N. & Maqueira, B. (1994). Output Control of Discrete-Time Nonlinear Systems, in: *Proceedings of 1994 American Control Conference-ACC'94*, 2, 2175–2179.
- Samanta, A., Zhao, A., Shimizu, G. K. H., Sarkar, P. & Gupta, R. (2012). Post-Combustion CO₂ Capture Using Solid Sorbents: A Review. *Industrial & Engineering Chemistry Research*, 51(4), 1438–1463.
- Seibert, F., Chen, E., Perry, M., Briggs, S., Montgomery, R. & Rochelle, G. (2011). UT/SRP CO₂ Capture Pilot Plant - Operating Experience and Procedures, in: *Energy Procedia*, (pp. 1616–1623).
- Da Silva, E. F. & Svendsen, H. F. (2005). The Chemistry of CO₂ Absorption in Amine Solutions Studied by Computational Chemistry, in: *Greenhouse Gas Control Technologies*, 2, 1891–1895.
- Van Sint Annaland, M., Tuinier, M. J. & Gallucci, F. (2015). Cryogenic CO₂ Capture,

- in: *Process Intensification for Sustainable Energy Conversion*, 7–52.
- Sipöcz, N., Tobiesen, F. A. & Assadi, M. (2011). The Use of Artificial Neural Network Models for CO₂ Capture Plants. *Applied Energy*, 88(7), 2368–2376.
- Skogestad, S. (2004). Control Structure Design for Complete Chemical Plants. *Computers & Chemical Engineering*, 28(1–2), 219–234.
- Skogestad, S. & Postlethwaite, I. (2007). *Multivariable Feedback Control: Analysis and Design*. Wiley New York.
- Skorek-Osikowska, A., Kotowicz, J. & Janusz-Szymańska, K. (2012). Comparison of the Energy Intensity of the Selected CO₂-Capture Methods Applied in the Ultra-Supercritical Coal Power Plants. *Energy and Fuels*, 26(11), 6509–6517.
- Solomatine, D. P. & Ostfeld, A. (2008). Data-Driven Modelling: Some Past Experiences and New Approaches. *Journal of hydroinformatics*, 10(1), 3–22.
- Stec, M., Tatarczuk, A., Więclaw-Solny, L., Krótki, A., Spietz, T., Wilk, A. & Piewak, D. (2016). Demonstration of a Post-Combustion Carbon Capture Pilot Plant Using Amine-Based Solvents at the Łaziska Power Plant in Poland. *Clean Technologies and Environmental Policy*, 18(1), 151–160.
- Stephanopoulos, G. (1984). *Chemical Process Control: An Introduction to Theory and Practice*. New Jersey: Englewood Cliffs.
- Supasitmongkol, S. & Styring, P. (2010). High CO₂ Solubility in Ionic Liquids and a Tetraalkylammonium- Based Poly(Ionic Liquid). *Energy and Environmental Science*, 3(12), 1961–1972.
- Tanaka, Y., Abe, M., Sawada, Y., Tanase, D., Ito, T. & Kasukawa, T. (2014). Tomakomai CCS Demonstration Project in Japan, 2014 Update. *Energy Procedia*, 63, 6111–6119.
- Thimsen, D., Maxson, A., Smith, V., Cents, T., Falk-Pedersen, O., Gorset, O. & Hamborg, E. S. (2014). Results from MEA Testing at the CO₂ Technology Centre Mongstad. Part I: Post-Combustion CO₂ Capture Testing Methodology. *Energy Procedia*, 63, 5938–5958.
- Tlili, N., Grévilot, G. & Vallières, C. (2009). Carbon Dioxide Capture and Recovery by Means of TSA and/or VSA. *International Journal of Greenhouse Gas Control*, 3(5), 519–527.
- Tomida, D., Kenmochi, S., Qiao, K., Tsukada, T. & Yokoyama, C. (2013). Densities and Thermal Conductivities of N-Alkylpyridinium Tetrafluoroborates at High Pressure. *Fluid Phase Equilibria*, 340, 31–36.
- Vu, T. N. L. & Lee, M. (2010). Multi-Loop PI Controller Design Based on the Direct Synthesis for Interacting Multi-Time Delay Processes. *ISA transactions*, 49(1), 79–86.
- Wall, T. F. (2007). Combustion Processes for Carbon Capture. *Proceedings of the combustion institute*, 31(1), 31–47.
- Walters, M. S., Edgar, T. F. & Rochelle, G. T. (2016). Dynamic Modeling and Control of an Intercooled Absorber for Post-Combustion CO₂ Capture. *Chemical Engineering and Processing: Process Intensification*, 107, 1–10.
- Wang, J. & Xu, S. (2014). CO₂ Capture RD&D Proceedings in China Huaneng Group.

- International Journal of Coal Science & Technology*, 1(1), 129–134.
- Wang, M., Lawal, A., Stephenson, P., Sidders, J. & Ramshaw, C. (2011). Post-Combustion CO₂ Capture with Chemical Absorption: A State-of-the-Art Review. *Chemical Engineering Research and Design*, 89(9), 1609–1624.
- Wang, Y., Zhao, L., Otto, A., Robinius, M. & Stolten, D. (2017). A Review of Post-Combustion CO₂ Capture Technologies from Coal-Fired Power Plants. *Energy Procedia*, 114, 650–665.
- Wei, H. L. & Billings, S. A. (2008). Model Structure Selection Using an Integrated Forward Orthogonal Search Algorithm Assisted by Squared Correlation and Mutual Information. *International Journal of Modelling, Identification and Control*, 3(4), 341–356.
- Wei, H. L. & Billings, S. A. (2009). Improved Model Identification for Non-Linear Systems Using a Random Subsampling and Multifold Modelling (RSMM) Approach. *International Journal of Control*, 82(1), 27–42.
- Wei, H. L., Billings, S. A. & Liu, J. (2004). Term and Variable Selection for Non-Linear System Identification. *International Journal of Control*, 77(1), 86–110.
- Wiley, D. E., Ho, M. T. & Donde, L. (2011). Technical and Economic Opportunities for Flexible CO₂ Capture at Australian Black Coal Fired Power Plants. *Energy Procedia*, 4, 1893–1900.
- Wu, X. D., Yang, Q., Chen, G. Q., Hayat, T. & Alsaedi, A. (2016). Progress and Prospect of CCS in China: Using Learning Curve to Assess the Cost-Viability of a 2x600MW Retrofitted Oxyfuel Power Plant as a Case Study. *Renewable and Sustainable Energy Reviews*, 60, 1274–1285.
- Wu, X., Shen, J., Li, Y., Wang, M. & Lawal, A. (2018). Flexible Operation of Post-Combustion Solvent-Based Carbon Capture for Coal-Fired Power Plants Using Multi-Model Predictive Control: A Simulation Study. *Fuel*, 220, 931–941.
- Wu, X., Shen, J., Li, Y., Wang, M., Lawal, A. & Lee, K. Y. (2019). Dynamic Behavior Investigations and Disturbance Rejection Predictive Control of Solvent-Based Post-Combustion CO₂ Capture Process. *Fuel*, 242, 624–637.
- Wu, Y., Zhou, Q. & Chan, C. W. (2010). A Comparison of Two Data Analysis Techniques and Their Applications for Modeling the Carbon Dioxide Capture Process. *Engineering Applications of Artificial Intelligence*, 23(8), 1265–1276
- Zhang, L., Qu, R., Sha, Y., Wang, X. & Yang, L. (2015). Membrane Gas Absorption for CO₂ Capture from Flue Gas Containing Fine Particles and Gaseous Contaminants. *International Journal of Greenhouse Gas Control*, 33, 10–17.
- Zhang, Q., Turton, R. & Bhattacharyya, D. (2016). Development of Model and Model-Predictive Control of an MEA-Based Postcombustion CO₂ Capture Process. *Industrial and Engineering Chemistry Research*, 55(5), 1292–1308.
- Zhang, Q., Turton, R. & Bhattacharyya, D. (2018). Nonlinear Model Predictive Control and H_∞ Robust Control for a Post-Combustion CO₂ Capture Process. *International Journal of Greenhouse Gas Control*, 70, 105–116.
- Zhang, Y., Chen, H., Chen, C.-C., Plaza, J. M., Dugas, R. & Rochelle, G. T. (2009). Rate-Based Process Modeling Study of CO₂ Capture with Aqueous Monoethanolamine Solution. *Industrial and Engineering Chemistry Research*,

48(20), 9233–9246.

- Zhao, S., Feron, P. H. M., Deng, L., Favre, E., Chabanon, E., Yan, S., Hou, J., Chen, V. & Qi, H. (2016). Status and Progress of Membrane Contactors in Post-Combustion Carbon Capture: A State-of-the-Art Review of New Developments. *Journal of Membrane Science*, 511, 180–206.
- Zhou, Q., Wu, Y., Chan, C. W., Tontiwachwuthikul, P., Idem, R. O. & Gelowitz, D. (2012). Part 4b: Application of Data Modeling and Analysis Techniques to the CO₂ Capture Process System. *Carbon Management*, 3(1), 81–94.
- Zhou, S., Chen, X., Nguyen, T., Voice, A. K. & Rochelle, G. T. (2010). Aqueous Ethylenediamine for CO₂ Capture. *ChemSusChem*, 3(8), 913–918.
- Zhu, Q. (2019). Developments on CO₂-Utilization Technologies. *Clean Energy*, 3(2), 85–100.
- Zhou, Q., Chan, C. W. & Tontiwachiwuthikul, P. (2008). Regression Analysis Study on the Carbon Dioxide Capture Process. *Industrial and Engineering Chemistry Research*, 47(14), 4937–4943
- Zhu, Y. (2001). *Multivariable System Identification for Process Control*. Elsevier.
- Zhu, Y. (2006). System identification for process control: recent experience and outlook. *IFAC Proceedings Volumes*, 39(1), 20–32.
- Ziaii Fashami, S. (2012). Dynamic Modeling, Optimization, and Control of Monoethanolamine Scrubbing for CO₂ Capture.
- Ziaii, S., Rochelle, G. T. & Edgar, T. F. (2009). Dynamic Modeling to Minimize Energy Use for CO₂ Capture in Power Plants by Aqueous Monoethanolamine. *Industrial and Engineering Chemistry Research*, 48(13), 6105–6111.